AD-A173 617 EFFECTS OF 30 MEV ELECTRON IRRADIATION ON INGAASP LEDS (LIGHT EMITTING DIODES) AND INGAAS PHOTODIODES(U) NAVAL POSTGRADUATE SCHOOL MONTEREY CA P J O'REILLY JUN 86 1/2

UNCLASSIFIED F/G 20/12 NL

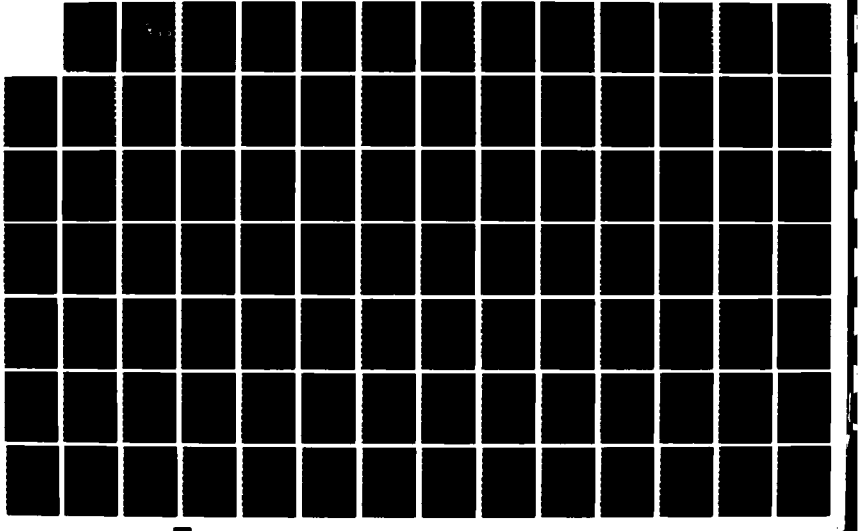

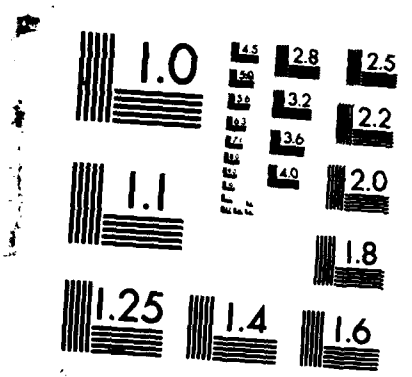

NAVAL POSTGRADUATE SCHOOL
Monterey, California

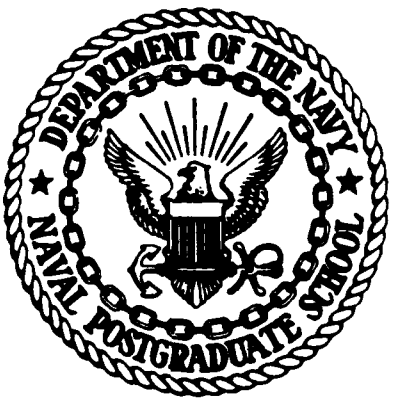

THESIS

EFFECTS OF 30 Mev ELECTRON IRRADIATION ON InGaAsP LEDS AND InGaAs PHOTODIODES

by

Patrick James O'Reilly

June 1986

Thesis Advisor: K.C. Dimiduk

Approved for public release; distribution is unlimited

SECURITY CLASSIFICATION OF THIS PAGE AD-A173617

REPORT DOCUMENTATION PAGE

1a. REPORT SECURITY CLASSIFICATION UNCLASSIFIED	1b. RESTRICTIVE MARKINGS
2a. SECURITY CLASSIFICATION AUTHORITY	3. DISTRIBUTION/AVAILABILITY OF REPORT DISTRIBUTION STATEMENT A Approved for public release Distribution Unlimited
2b. DECLASSIFICATION / DOWNGRADING SCHEDULE	
4. PERFORMING ORGANIZATION REPORT NUMBER(S)	5. MONITORING ORGANIZATION REPORT NUMBER(S)
6a. NAME OF PERFORMING ORGANIZATION Naval Postgraduate School 6b. OFFICE SYMBOL (If applicable) Dept 33	7a. NAME OF MONITORING ORGANIZATION Naval Postgraduate School
6c. ADDRESS (City, State, and ZIP Code) Monterey, California 93943-5100	7b. ADDRESS (City, State, and ZIP Code) Monterey, California 93943-5100
8a. NAME OF FUNDING / SPONSORING ORGANIZATION 8b. OFFICE SYMBOL (If applicable)	9. PROCUREMENT INSTRUMENT IDENTIFICATION NUMBER
8c. ADDRESS (City, State, and ZIP Code)	10. SOURCE OF FUNDING NUMBERS PROGRAM ELEMENT NO. / PROJECT NO. / TASK NO. / WORK UNIT ACCESSION NO.

11. TITLE (Include Security Classification)
EFFECTS OF 30 MEV ELECTRON IRRADIATION ON InGaAsP LEDS AND InGaAs PHOTODIODES

12 PERSONAL AUTHOR(S)
O'Reilly, Patrick J.

13a. TYPE OF REPORT	13b. TIME COVERED	14. DATE OF REPORT (Year, Month, Day)	15. PAGE COUNT
Master's Thesis	FROM _____ TO _____	1986 June	191

16. SUPPLEMENTARY NOTATION

17 COSATI CODES			18. SUBJECT TERMS (Continue on reverse if necessary and identify by block number)
FIELD	GROUP	SUB-GROUP	electron irradiation, light emitting diodes, LEDs, radiation effects, photodiodes, InGaAsP, InGaAs

19. ABSTRACT (Continue on reverse if necessary and identify by block number)

InGaAsP LEDs and InGaAs photodiodes were irradiated with a 30 MEV electron beam. The rate of performance degradation and the effects of the increase in temperature during irradiations were studied. Simple models for LED and photodiode current controlling mechanisms and for a phenomenological radiation damage constant are presented. The dominant current controlling mechanisms and the peak wavelength of the LEDs and photodiodes did not change during irradiation. The light output of the InGaAsP LED decreased 63% and current output increased 8% at 10^{14}e/cm^2. Although the lifetime-damage constant product ($t_oK=1.5x10^{-14}$cm^2/e sec) was of the same order of hardness as found for other III-V compound LEDs, this t_oK was considered very hard for a high radiance LED. The responsivity of the InGaAs photodiode degraded 54% and the dark current increased by more than 84 times at $3x10^{14}$e/cm^2. The effect of radiation was greater when

20 DISTRIBUTION / AVAILABILITY OF ABSTRACT ☒ UNCLASSIFIED/UNLIMITED ☐ SAME AS RPT. ☐ DTIC USERS	21. ABSTRACT SECURITY CLASSIFICATION unclassified
22a NAME OF RESPONSIBLE INDIVIDUAL Dr. K.C. Dimiduk	22b. TELEPHONE (Include Area Code) 408-646-2116 22c. OFFICE SYMBOL 61DM

DD FORM 1473, 84 MAR 83 APR edition may be used until exhausted. All other editions are obsolete.

SECURITY CLASSIFICATION OF THIS PAGE

19. (Continued)

the devices were not operated during irradiation. Annealing was observed for both devices. The method used to calculate irradiation fluence at the Naval Postgraduate School's LINAC was refined (which increased previous fluence calculations by four times).

Appproved for public release; distribution is unlimited

Effects of 30 Mev Electron Irradiation on InGaAsP LEDs and InGaAs Photodiodes

by

Patrick James O'Reilly
Captain, United States Army
B.S., United States Military Academy, 1978

Submitted in partial fulfillment of the
requirements for the degree of

MASTER OF SCIENCE IN PHYSICS

from the

NAVAL POSTGRADUATE SCHOOL
June 1986

Author: Patrick J. O'Reilly
Patrick James O'Reilly

Approved by: Kathryn C. Dimiduk
K. C. Dimiduk, Thesis Advisor

K. E. Woehler
K. E. Woehler, Second Reader

G. E. Schacher
G. E. Schacher, Chairman,
Department of Physics

J. N. Dyer
J. N. Dyer, Dean of Science and Engineering

ABSTRACT

InGaAsP LEDs and InGaAs photodiodes were irradiated with a 30 Mev electron beam. The rate of performance degradation and the effects of the increase in temperature during irradiations were studied. Simple models for LED and photodiode current controlling mechanisms and for a phenomenological radiation damage constant are presented. The dominant current controlling mechanisms and the peak wavelength of the LEDs and photodiodes did not change during irradiation. The light output of the InGaAsP LED decreased 63% and current output increased 8% at 10^{14} e/cm^2. Although the lifetime-damage constant product ($t_oK=1.5x10^{-14}$ cm^2/e sec) was of the same order of hardness as found for other III-V compound LEDs, this t_oK was considered very hard for a high radiance LED. The responsivity of the InGaAs photodiode degraded 54% and the dark current increased by more than 84 times at $3x10^{14}$ e/cm^2. The effect of radiation was greater when the devices were not operated during irradiation. Annealing was observed for both devices. The method used to calculate irradiation fluence at the Naval Postgraduate School's LINAC was refined (which increased previous fluence calculations by four times).

TABLE OF CONTENTS

I. INTRODUCTION..... 10

A. THE REASON FOR THIS INVESTIGATION..... 10

1. Overview..... 10

2. Background..... 11

B. SOURCES OF RADIATION..... 15

C. PREVIOUS WORK..... 18

D. ORGANIZATION OF THIS PAPER..... 20

II. THEORY..... 22

A. BASIC SEMICONDUCTOR PHYSICS..... 22

1. Energy Bands..... 22

2. Doping..... 24

3. Compound Semiconductor Materials..... 24

B. CURRENT CONTROLLING MECHANISMS..... 25

1. the Conduction of Current in Semiconductors..... 25

2. the Conduction of Current Across p-n Junctions..... 28

3. the Equation for the Current Conducted Across p-n Junctions..... 30

C. RADIATIVE TRANSISTIONS..... 32

D. PRINCIPLES OF LED OPERATION..... 34

1. the Quantum Efficiency of LEDs..... 35

2. the Loss Mechanisms of Radiated Light in LEDs..... 35

3. Materials Used in Manufacturing LEDs..... 36

4. LED Configurations..... 37

E. TEMPERATURE EFFECTS ON LED PERFORMANCE..... 38

1. Temperature Effects on Current..... 38

2. Other Temperature Effects..... 40

3. Temperature Effects on III-V Compounds..... 40

F. THE GENERAL CHARACTERISTICS OF RADIATION DAMAGE IN SEMICONDUCTORS..... 41

1. Displacement Damage..... 41

2. Ionization Damage..... 43

3. Electron Radiation Damage..... 43

G. LIFETIME-DAMAGE CONSTANT PRODUCTS FOR LEDS..... 46

1. the Effect of Radiation on Carrier Lifetimes and the Derivation of Damage Constants..... 46

2. Measurement of Lifetime-damage Constant Products.... 48

3. the Validity of Damage Constants..... 50

4. the Radiation Hardness of III-V Compounds..... 52

H. PRINCIPLES OF PHOTODIODE OPERATION..... 53

1. Photocurrent Generation..... 53

2. PIN Photodiodes..... 55

3. Responsivity of Photodiodes..... 56

4. the Dark Current..... 57

5. III-V Compound Photodiodes..... 58

I. RADIATION DAMAGE TO PHOTODIODES..... 59

1. Radiation Damage Mechanisms in Photodiodes..... 59

2. Radiation Hardness of III-V Compound Photodiodes.... 60

3. The Theorectical Radiation Hardness of the InGaAs Photodiode..... 61

III. EXPERIMENTAL PROCEDURE..... 63

A. THE InGaAsP LED MEASUREMENTS..... 64

1. Characteristics of the InGaAsP LED..... 64

2. Measurement of Radiation Effects on the Glass Cap..... 66

3. Before and After Irradiation LED Preformance Measurements..... 67

4. Measurement of Temperature Effects on Device Performance:..... 70

5. The Irradiation Procedure..... 72

6. During Irradiation LED Performance Measurements..... 80

B. THE InGaAs PHOTODIODE MEASUREMENTS..... 83

1. Characteristics Of The InGaAs Photodiode..... 83

2. Before and After Irradiation Photodiode Performance Measurements..... 84

3. During Irradiation Photodiode Performance Measurements..... 86

IV. RESULTS 89

A. THE RESULTS OF THE InGaAsP LED MEASUREMENTS..... 89

1. LED Performance During Irradiation..... 89

2. LED Performance Before And After Irradiation..... 105

B. RESULTS OF THE InGaAs PHOTODIODE MEASUREMENTS..... 117

1. Photodiode Performance During Irradiation..... 117

2. Photodiode Performance Before and After Irradiation. 124

DISCUSSION..... 134

A. THE RADIATION HARDNESS OF THE InGaAsP LED..... 134

1. Comparison of the Results with the Theory and Previous Research..... 134

2. Lifetime-damage Constant Product Calculations..... 142

B. THE RADIATION HARDNESS OF THE InGaAs PHOTODIODE..... 147

1. Responsivity Degradation..... 148

2. Increase in the Dark Current..... 149

C. THE RADIATION HARDNESS OF A SYSTEM COMPRISED OF THE InGaAsP LED AND THE InGaAs PHOTODIODE..... 150

VI. CONCLUSIONS AND RECOMMENDATIONS FOR FUTURE WORK..... 154

A. CONCLUSIONS..... 154

B. RECOMMENDATIONS FOR FUTURE WORK..... 156

APPENDIX A: MEASUREMENT OF RADIATION EFFECTS ON THE GLASS CAP.... 158

APPENDIX B: RESULTS OF MEASURING THE ELECTRON BEAM FLUENCE..... 162

APPENDIX C: COMPUTER PROGRAM USED FOR LED CURRENT AND LIGHT OUTPUT VERSUS FORWARD BIAS MEASUREMENTS..... 172

APPENDIX D: COMPUTER PROGRAM USED FOR LED CURRENT AND LIGHT OUTPUT VERSUS FLUENCE MEASUREMENTS..... 177

APPENDIX E: COMPUTER PROGRAM USED FOR PHOTODIODE CURRENT VERSUS FORWARD BIAS MEASUREMENTS..... 181

APPENDIX F: COMPUTER PROGRAM USED FOR PHOTODIODE CURRENT VERSUS FLUENCE MEASUREMENTS..... 184

LIST OF REFERENCES..... 187

INITIAL DISTRIBUTION LIST..... 190

ACKNOWLEDGEMENT

I wish to express my sincere appreciation to Dr. Kathryn C. Dimiduk for the essential guidance and conscientious review that she contributed to this thesis. Her expertise and previous experience in this area of research made her advice invaluable during all phases of this work. I am very appreciative of her effort to ensure her easy accessibility after she departed the Naval Postgraduate School and continued to advise me.

My special gratitude goes to Don Snyder whose advice and "can do" attidude greatly exceeded his responsibilities of operating the LINAC. His assistance in the design of the experimental equipment configuration and his willingness to share his vast experience with research using the LINAC was instrumental in the successful completion of this work. I would also like to thank Bob Sanders for his ideas and technical expertise in utilizing lab equipment. Finally, I would like to thank Professors K. Woehler and H. Handler whose review of my work and excellent teaching assured the quality of this thesis.

I. INTRODUCTION

A. THE REASON FOR THIS INVESTIGATION

1. Overview

Since the first successful experiments of generating light by passing electric current through a crystal in 1907, scientists have gained much insight into the phenomenon of electroluminescence [Ref.1]. During the past two decades the knowledge of electroluminescence and it's applications in optoelectronic devices has increased substantially. An important application of this knowledge is the manufacture of light emmiting diodes (LEDs) and photodiodes. Today, these devices are extensively utilized in civilian and military applications such as fiber optic communication systems, night vision devices, opto-isolaters, console displays and in other optoelectronic circuits.

Due to the current utilization of optoelectronic devices in satellites and military combat systems, the reliability of LEDs and photodiodes when exposed to the typical radiation of a space or nuclear weapons effects environment is important. Previous investigations of the survivability of LEDs and photodiodes when exposed to radiation indicate that optoelectronic devices manufactured from compounds comprised of elements having constituent atoms with

three or five valence electrons (referred to as III-V compounds) display particular resistance to radiation effects [Ref.2].

This paper reports the results of my investigation into the effects of 30 million electron volt (MeV) electron radiation on two optoelectronic devices manufactured using III-V compounds. An LED manufactured from Indium Gallium Arsenide Phosphide (InGaAsP) and a photodiode made using Indium Gallium Arsenide (InGaAs) were studied. Both the InGaAsP LED and the InGaAs photodiode operate in the near infrared wavelength region. At these wavelengths, fiber optic communication systems have the greatest reliability during exposure to radiation.

2. Background

Electroluminescence is the emission of light by the excitation of electrons in a material when an electric current is applied. Light emitting diodes are designed to maximize the electroluminescent properties of semiconductor materials for specific applications. These devices provide compact and reliable light sources in control panels in aircraft, computers, automobiles and common home appliances. Conversely, a photodiode is an electronic device that absorbs light (photons) which then excite electrons and cause a current to flow. Several applications are dicussed below.

When an LED is connected to a photodiode by an optical fiber, a lightweight and efficient communications system is formed, capable

of replacing the much larger and heavier conventional communication wires. When an input signal current is received by the LED, light is radiated. The photodector detects this light and converts it into an electrical current. Information is transmitted in coded signals by flashing the LED on and off. The weight advanatage of optoelectronic communications systems is extensively utilized in the design of aircraft and spacecraft. Additionally, fiber optic communication systems have the advantages of a wider bandwidth and no susceptibilty to interference from an electromagnetic pulse. Also, since no electric current is transmitted, these systems do not emit electromagnetic radiation. Thus, fiber optic communication systems are more secure than conventional communication systems.

Another very effective application of LEDs and photodiodes is in opto-isolators. Figure one is a schematic diagram of a typical opto-isolator circuit. Opto-isolators use LEDs and specially matched photodiodes to provide information transfer without a direct electrical connection [Ref.3]. The input current required to send an optical signal to a detector is a small fraction of the current rquired to send the same signal over conventional wires to a receiver.

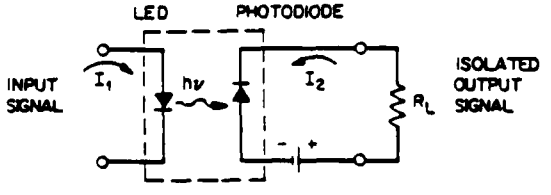

Figure 1. An Opto-isolator Circuit [Ref.3]

The typical current transfer ratio between the input current of the LED and the output current of the photodiode is on the order of 10^{-3}. Therefore, this system allows the transmission of information while conserving power.

Recently, photodiodes have been extensively used in the design of night vision devices. By controlling the growth and composition of the crystals used during their manufacture, LEDs and photodiodes can be made to emit or absorb specific ranges of wavelengths. Thus LEDs and photodiodes can be tailored to meet the requirements of specific applications. Figure two shows the electromagnetic spectrum and the corresponding wavelengths delineating the regions of the spectrum. The wavelength requirements for most optoelectronic applications extend from the near infrared (approximately 1.5 micrometers) to the ultraviolet (approximately .03 micrometers).

The use of optoelectronic devices in spacecraft and military equipment makes them vulnerable to exposure to various types of radiation. In the previously discussed applications, the reliable operation of these electronic systems depend upon the survivability of LEDs and photodiodes during and after their exposure to radiation. Therefore, research and development projects involving space and military applications have established radiation hardness assurance programs [Ref.4]. Due to these requirements, much research has been conducted on the reliability of electronic systems when exposed to radiation.

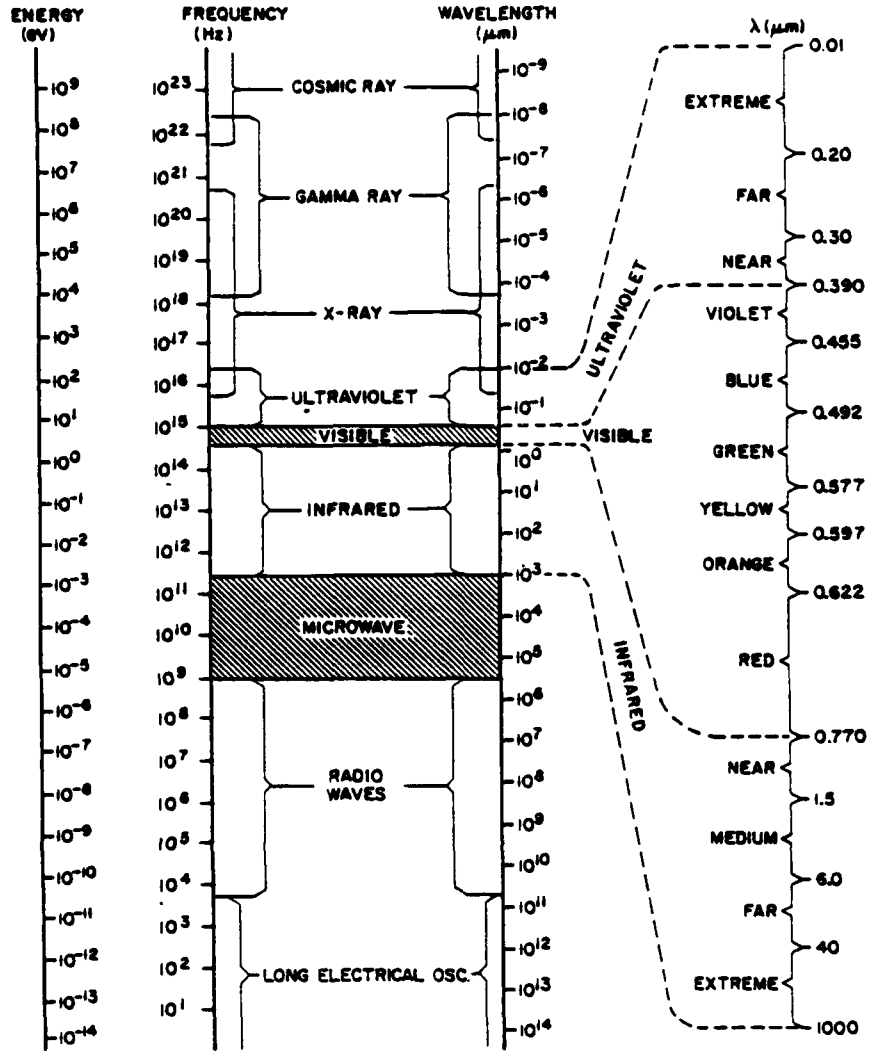

Figure 2. The Electromagnetic Spectrum [Ref.3]

Research has revealed that optical fibers have low attenuation and dispersion properties in the near infrared wavelength region of the electromagnetic spectrum. Figure three shows that the attenuation of light for a silica optical fiber is lowest near 1.3 micrometer wavelengths. Furthermore, radiation effects studies on silica fibers

reveal that radiation induced attenuation losses decrease with increasing wavelength [Ref. 5]. Because of the increased efficiency of optical fibers in the near infrared wavelength region and for reasons to be discussed later in this paper, optoelectronic device designers have become very interested in the radiation hardness of LEDs and photodiodes which operate in the near infrared wavelength region. Both the InGaAsP LED and the InGaAs photodiode studied in this investigation either absorb or emit light in this wavelength region.

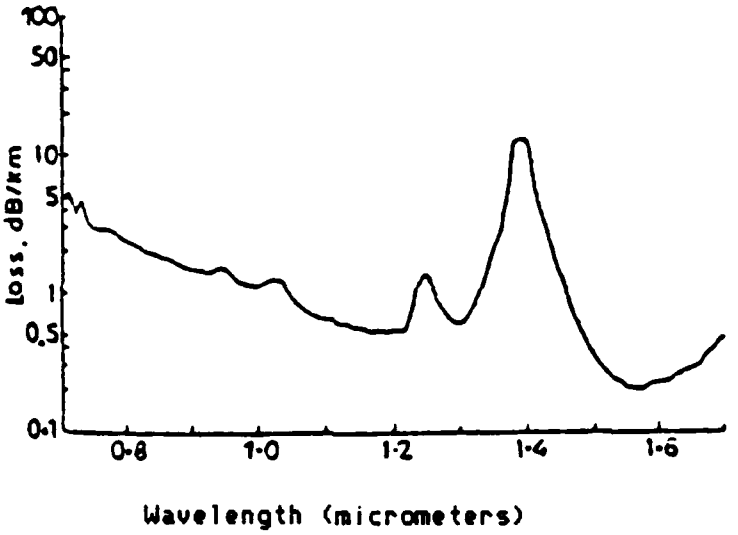

Figure 3. Attenuation Spectrum of a Silica Optical Fiber [Ref.4]

B. SOURCES OF RADIATION

There exists three primary sources of radiation that an LED or a photodetector could be exposed to: nuclear power plants, space environments or a nuclear weapon detonation. When located on the

surface of the earth, nuclear power plants have most of the operating equipment located with the reactor in a large containment building [Ref. 6]. Under normal operating conditions, electronic devices are not exposed to any threatening radiation. However, if an accident occurs, such as the loss of coolant, the coolant water could become contaminated with radioactive elements resulting in radiation exposure to electronic equipment located inside the containment building. The primary types of radiation resulting from such an accident would be gamma emission and beta decay. Beta decay is a process where a positive or negative electron is emitted from the nucleus [Ref.7]. The nucleus captures an orbiting electron which results in the emission of an antineutrino or neutrino. Reactors used in outer space pose a much more severe radiation threat to electronic devices. Weight and size limitations cause the designs of space reactors to have only small amounts of shielding to protect the electronic circuits that control the reactor.

The types and magnitudes of the radiation that a spacecraft is exposed to in a natural space environment varies widely and is dependent upon recent natural events and the specific spacecraft's orbit [Ref.8]. The solar wind is a low temperature, low density plasma that has little effect on spacecraft electronic systems. Cosmic rays also constitute low energy radiation; however, their effect on photodiodes causes frequent unwanted background noise. Other types of space radiation are energetic protons and electrons

emitted from the sun. A solar flare can produce a 5 MeV proton flux of greater than $10^5/cm^2$ sec steradian. Electrons emitted from the sun have less energy than the protons but their fluxes are still significant. Within the earth's magnetosphere, trapped electrons, protons and ions constitute a continuous radiation threat to orbiting electronic systems. The fluxes and kinetic energies of these particles vary tremendously with location and occurances of magnetic storms. Trapped electrons having kinetic energies of several Mev and protons having kinetic energies of 700 Mev have been observed [Ref.9]. The Van Allen radiation belt is composed primarily of protons near the earth and electrons at higher orbits extending to 35,000 miles above the earth's surface. Additionally, electrons, neutrons and other products from a high altitude detonation of a nuclear weapon can form an additional radiation belt for an extended period of time. For a more detailed discussion, Garrett and Pike provide a thorough description of the radiation environment in space [Ref.10].

The detonation of a nuclear weapon causes the release of a tremendous amount of energy over a very short period of time. Neutrons and gamma rays produced from the fission and fussion of nuclei causes the medium surrounding the weapon to be heated to extremely high temperatures [Ref.6]. This hot medium emits a complicated spectrum of energy in the X-ray wavelength region. The fission process and the inelastic scattering of fusion neutrons by the surrounding medium produces neutrons with a wide spectrum of energies.

The inelastic scattering of neutrons and the fission proccess also produces gamma rays whose spectrum depend on the medium surrounding the nuclear weapon. Additionally, a nuclear explosion emits photons which interact with air to produce Compton electrons and photoelectrons. For a more detailed discussion, Glasstone and Dolan provide an excellent description of the radiation produced by a nuclear weapon [Ref.11].

C. PREVIOUS WORK

Most of the previous research on the effects of radiation on optoelectronic devices was concentrated on LEDs and photodiodes that were manufactured from silicon, germanium or gallium arsenide. Some studies which contributed to the basic understanding of radiation induced performance degradation mechanisms are listed in Table one. (In addition, Table one includes two studies by Ness and Foley which were conducted at the Naval Postgraduate school using experimental procedures that were similar to my investigation.) Barnes [Ref.2] wrote an excellent summary of radiation damage mechanisms in optoelectronic devices. Early research revealed that LEDs and photodiodes manufactured using III-V compounds will emit and absorb infrared light and will exhibit good radiation hardness. A discussion of the results of this early research is included in Chapter four of this thesis.

III-V compounds are still the subject of considerable research. Specifically, although InGaAsP LEDs and InGaAs photodiodes are now commercially available, only preliminary research has been completed on the radiation effects on LEDs and photodiodes manufactured using

TABLE 1: PREVIOUS RADIATION STUDIES ON OPTOELECTRONIC DEVICES

Author(s)	Year	Device	Material	Type Radiation	Ref.
Aukerman, Millea, McColl	1966	LED	GaAs	2 Mev Electrons	12
Stanley	1970	LED	GaAs,GaP GaAsP	2.0 - 2.5 Mev Electrons	13
Mitchell	1977	Photodectors	Si,GaAsSb InP,GaAs	Gamma	14
Hardwick, Kalma	1979	LED, Photodectors Optical Fibers	GaAlAs Si	1 Mev Electrons, 30 Mev Protons, gamma	15
Wiczer, Dawson, Barnes	1981	Photodectors	AlGaAs, AlGaSb, InGaAsP	X-ray (1.55 to 2.5 Mev Photons)	16
Rose, Barnes	1981	LED	InGaAsP GaAlAs,GaAs	16 Mev Protons	17
Wiczer, Dawson, Osbourn, Barnes	1982	Photodectors	Si, AlGaAs/GaAs	Gamma	18
Ness	1984	LED	GaAs,GaP GaAsP	30 Mev Electrons	19
Foley	1985	LED	GaAsP	30 Mev Electrons	20

III-V ternary (consisting of three elements) and quarternary (consisting of four elements) compounds. Early research and design of these ternary and quarternary LEDs and photodiodes was conducted at Bell Laboratories [Ref.21] and at Rockwell International Electronics Research Center [Ref.22]. Table two lists the completed studies on radiation damage to LEDs and photodiodes made with InGaAsP and InGaAs materials (performed at Sandia National Laboratories).

TABLE 2: PREVIOUS RADIATION STUDIES ON InGaAsP AND InGaAs MATERIALS

Author(s)	Compound	Device	Radiation Type	Ref
Barnes	InGaAs	LED	Gamma, Neutrons	5
Rose, Barnes	InGaAsP	LED	16 Mev Protons	17
Wiczer, Dawson, Barnes	InGaAsP	Photodiode	.15-2.5 Mev X-ray	16

D. ORGANIZATION OF THIS PAPER

The subjects discussed in this paper are presented in the following order. In Chapter two the operating mechanisms of LEDs and photodiodes are explained. The effects of temperature and radiation damage are also discussed. Additionally, quantitative methods of characterizing the phenomenological effects of radiation damage to LEDs and photodiodes are presented. In Chapter three, the procedures used to irradiate the LEDs and photodiodes are described. The methods used to characterize the devices before and after irradiation are also discussed. Furthermore, the techniques used in measuring the device's

performance during irradiation are presented. The results of all measurements made in this study are presented in Chapter four. Chapter five is a comparision of my experimental results with theory and with previous research. Chapter six presents my conclusions fro the results of the experiments and a discussion of recommended experiments to be performed in the future. Appendix A describes the results of the investigation of the effects of radiation on the glass cap of the LED and photodiode. Appendix B is a discussion of the systematic errors in the fluence calculations used in this investigation. An estimation of the magnitudes of the errors is derived. Appendix C, D, E and F are the computer programs which performed the light and current measurements before, during and after irradiation of the LEDs and photodiodes.

II. THEORY

This chapter covers basic semiconductor physics and the physics of radiation damage in semiconductors. It includes a discussion of the current controlling mechanisms and the radiative carrier recombination processes that occur in LEDs and photodiodes. The basic principles of LED operation and the effects of temperature on LED performance are then presented. Then the radiation effects on semiconductors in general is followed by a discussion of the specific mechanisms of electron interaction with LEDs. Next, a quantitative method of characterizing the sensitivity of LEDs to radiation hardness is given. The operation of photodiodes and methods of characterizing their radiation damage is then presented. Finally, the theoretical radiation hardness of LEDs and photodiodes manufactured from III-V compounds is explained.

A. BASIC SEMICONDUCTOR PHYSICS

1. Energy Bands

Semiconductor physics is based on the concept that the energy of the electrons belonging to the atoms that comprise a crystal are allowed to exist only in certain bands of energy levels. Between these bands of allowed energies are energy levels that electrons theoretically cannot occupy. These nonallowed regions of energy

levels are called bandgaps. In a semiconductor material, the band of energies below the forbidden gap on an energy diagram, called the valence band, is usually almost completely full of electrons. The region above the forbidden gap, called the conduction band, is typically almost free of electrons. This simple model incorporates most of the results of solid state physics needed for a basic understanding of semiconductors.

Once in the conduction band, electrons can freely move to other locations in the band and thus move a negative charge. The vacant space that was once occupied by the electron in the valence band (called a hole) can be thought of as moving inside the valence band and thus moving a positive charge. Free electrons and holes are called charge carriers. The carrier with the greater concentration is called the majority carrier and the carrier with the lesser concentration is called the minority carrier. The process in which electron-hole pairs are created is called generation. The process by which electrons return to the valence band (thus annihilating electron-hole pairs) is called recombination. In a crystal free of impurities (called an intrinsic crystal) at zero energy, there exists an equal number of holes and free electrons. The population of electrons at the various energy levels is governed by the Fermi-Dirac distribution function [Ref.23]. The lower the energy level, the greater the probability that that level is occupied by an electron.

The Fermi level is the energy level at which the probability of ocupancy is fifty percent.

2. Doping

Imperfections in a crystal lattice change the density of carriers and affect the location of allowed energy levels. An impurity atom which has more valence electrons than the original lattice atom it replaced gives up an electron to the conduction band and is called a donor. An impurity atom with fewer valence electrons than the original atom takes an electron from the valence band leaving a hole and is called an acceptor. The process of adding acceptor or donor impurity atoms is called doping. In addition, donor or acceptor atoms have different allowed energy levels than the original atoms that comprise a crystal. Thus, a crystal that has been doped has allowed energy levels existing in the original crystal's band gap [Ref.4]. These new energy levels act as traps or recombination centers for electrons or holes moving between the valence and conduction bands.

3. Compound Semiconductor Materials

Crystals can be comprised of atoms of different elements. In these crystals, neighboring atoms share electrons resulting in each atom having eight valence electrons bonded with the neighboring lattice atoms. By selecting the elements used in the manufacture of a

crystal, the band gap and other properties can be controlled. Crystals made from atoms of two different elements with three and five valence electrons respectively are common semiconductor materials. Recently, the improved manufacturing processes of crystals comprised of three or four different III-V elements allow manufacturers a great amount of control over the properties of the crystals. The exact properties that these crystals have is also dependent on the ratio of the concentration of each element in the crystal. The InGaAsP and the InGaAs crystals used in this investigation were manufactured specifically to absorb or emit light of 1.3 micrometer wavelenth. A more detailed discussion of basic semiconductor physics is provided by Sze [Ref.3].

B. CURRENT CONTROLLING MECHANISMS

1. The Conduction of Current in Semiconductors

Two types of current are conducted in semiconductors: drift current and diffusion current. Drift current is the movement of charged carriers due to the influence of an applied electric field. Diffusion current is the movement of charged carriers due to the spatial variation in carrier densities.

Drift current is considered first. Since conduction band electrons are not associated with any particular atom, they are considered "free". The electrons are accelerated in the direction of

an electric field until they collide with a lattice atom. The average velocity of these electrons is derived using the relationship between the impulse applied by the electric field during the time between collisions and the momentum gained by the electrons. The current density (J) is the average velocity times the charge density of the carriers. Muller and Kamins [Ref.23] perform this derivation and show that the electron current density due to the applied electric field can be expressed as:

$$J = nq\mu E \qquad (1)$$

where n is the electron concentration, q is the charge of an electron, μ is carrier mobility and E is the applied electric field. The current due to the movement of holes is given by a similar relationship.

Current is also conducted in bulk semiconductor materials by the diffusion of charged carriers. If there exists a spatial variation in carrier densities, carriers having random thermal energies will move from regions of higher density to lower density. Muller and Kamins show that the current density due to electron diffusion is

$$J = qD_n \, dn/dx \qquad (2)$$

where D_n is the electron diffusion constant and dn/dx is the spatial rate of change of the electron concentration [Ref.23]. By combining the expressions for the drift and diffusion currents for electrons and holes, the total current density for bulk semiconductor material is

$$J = nq\mu E + qD_n dn/dx + pq\mu E - qD_p dp/dx \qquad (3)$$

For a typical semiconductor application, the concentration of one type of charged carrier is usually many orders of magnitude greater than the opposite type of carrier. Therefore, only the current due to the majority carrier is considered.

Additional current mechanisms exist if impurity atoms or defects exist in the crystal lattice. Only electrons and holes having sufficient energy can move directly between the conduction and valence bands. However, the presence of impurities and lattice defects allow carriers with less energy to move completely across the forbidden gap by first moving to a impurity energy level (referred to as a trap or recombination center). While the carrier is occcupying the impurity energy level it will either recombine with an opposite carrier type, lose energy and return to it's original band, or it will gain enough energy to complete the move to the opposite band.

The carrier lifetime is the average time that an electron exists in the conduction band or that a hole exists in the valence band before recombining with the opposite type carrier. Quantitative descriptions of carrier generation and recombination at recombination centers were derived by Shockley, Read and Hall [Ref.24]. An approximate but useful expression for minority carrier lifetime is

$$t = 1/(n_t v_{th} \sigma) \qquad (4)$$

where n_t is the density of recombination centers, v_{th} is the thermal velocity of the carriers and σ is the recombination center's capture

cross-section for holes and electrons. Since recombination requires both types of charge carriers to be present at the recombination center, the concentration of the minority carrier limits the recombination rate. Therefore, the electron-hole pair recombination rate is porportional to the reciprocal of the minority carrier lifetime. Furthermore, the rate of recombination increases with the density of recombination centers [Ref.24].

2. The Conduction of Current Across p-n Junctions

When a semiconductor material having electrons as the majority charge carrier (referred to as a n type material) is connected to a semiconductor material having holes as the majority charge carrier (referred to as a p type material) a p-n junction is formed. The regions of material on either side of the p-n junction are referred to as the bulk semiconductor regions. The majority carriers initially on either side of the junction diffuse across the junction to regions of lesser concentration. The p-n junction is assumed to be depleted of charge carriers; therefore, it is referred to as the depletion region. As the carriers diffuse, uncompensated impurity ions remain behind. The charge of the impurity ions creates an electrostatic field which opposes futher carrier diffusion [Ref.23]. Equilibrium is achieved when the "potential barrier" of the electric field prevents further carrier diffusion.

When a voltage from an external power source is applied across the p-n junction, the magnitude of the potential barrier can be controlled. The p-n junction is called forward biased when the potential barrier is decreased. Figure four shows the potential barrier of a p-n junction.

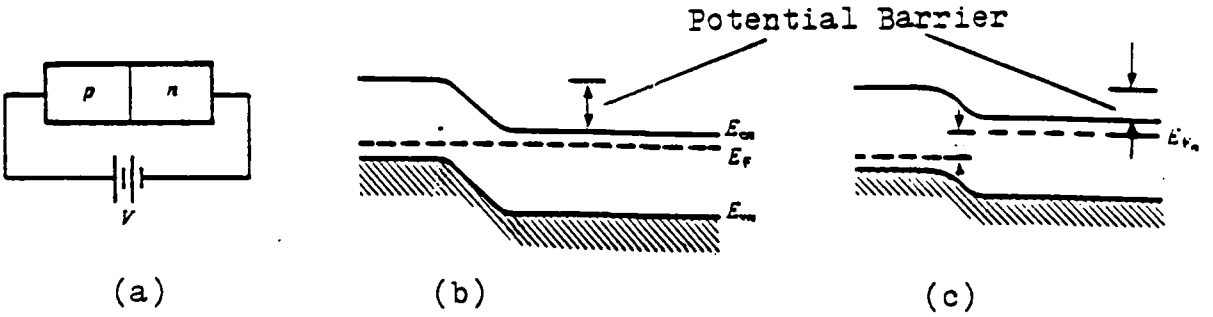

Figure 4. (a) p-n Junction Under Forward Bias (b) Energy Level Diagram for No Applied Bias and (c) for Forward Bias [Ref.25]

Under forward bias, the majority carriers are allowed to diffuse (sometimes referred to as injected) into the opposite side of the junction where they become the minority carriers (see Figure five). These "excess" minority carriers quickly recombine with the majority carriers. The majority carriers that were annihilated by recombining with the excess minority carriers are replaced by additional majority carriers. The additional majority carriers enter the bulk regions through the ohmic contacts that connect the semiconductor to an electrical circuit. The combination of the flow of minority and majority carriers in the semiconductor material comprises the flow of the total current.

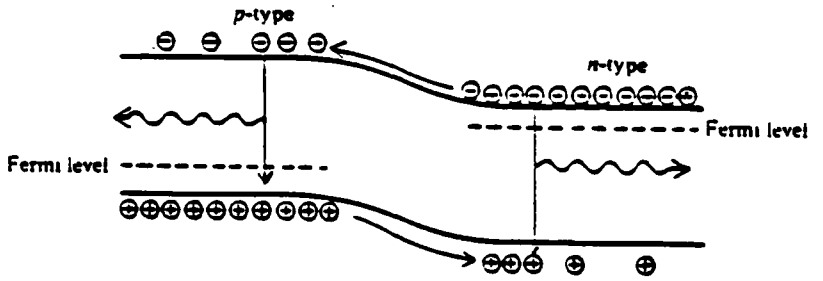

Figure 5. Injection of Carriers Across p-n Junction [Ref.25]

3. The Equation for the Current Conducted Across p-n Junctions

To derive an expression for the current conducted across the p-n junction the continuity equations for the majority and minority carrier densities in the bulk regions must be solved. Simplified solutions of the continuity equations require that several assumptions be made. The first assumption is that the voltage applied to the semiconductor material is sustained primarily across the p-n junction. This would result in a constant majority carrier density across the bulk semiconductor regions. Second, it is assumed that no generation or recombination occurs as the charge carriers are injected across the p-n junction. A thorough analysis of the solutions to the continuity equations is presented by Muller and Kamins [Ref.23]. Using these assumptions, they derive the relationship between current and voltage for a semiconductor :

$$I = I_o[\exp(qv/KT)-1] \qquad (5)$$

where v is the applied bias, q is the charge of an electron, K is Boltzmann's constant, T is the absolute temperature and I_o is the

saturation current obtained when a negative bias of a few kT/q volts is applied.

The first assumption in the preceding derivation (that all the applied voltage is dropped across the p-n junction) is valid for typical biases. However, the second assumption (that little generation or recombination occurs in the depletion region) is not valid for small forward bias voltages. Carrier recombination and generation (and the current caused by it) does occur in the depletion region. Muller and Kamins show that the current generated in the depletion region is proportional to exp(qv/2kT) [Ref.23]. However, at large biases (usually greater than 0.5 volts) the amount of current generated in the depletion region is negligible compared to the amount of current controlled by the diffusion and subsequent recombination of minority carriers in the bulk regions.

The type of current controlling mechanism that dominates in a semiconductor at a specific bias can be identified by the slope of it's current versus bias voltage curve. As shown above, the current controlled by minority charge carrier diffusion and recombination in the bulk regions is proportional to exp(qv/kT) and the current controlled by charge carrier generation and recombination in the depletion region is proportional to exp(qv/2kT). Therefore the slope of the logarithm of the current versus bias voltage curve indicates the dominant current controlling mechanism of a semiconductor over a specific range of biases [Ref.18].

C. RADIATIVE TRANSISTIONS

When an electron moves from a higher to lower energy level and subsequently recombines with a hole, energy is released. The energy released is equal to the difference between the two energy levels. The energy is released through one of three processes. First, the energy may be released in the form of phonons (heat). Second, the energy may be released to a third carrier (called Auger recombination) [Ref.25]. Third, the energy may be released in the form of a photon by a process called radiative recombination. The wavelength (λ) of the emitted photon is related to the released energy by

$$\lambda = 1240/E \text{ nanometers} \qquad (6)$$

where E is the released energy in electron volts. Figure six illustrates radiative and nonradiative recombinations.

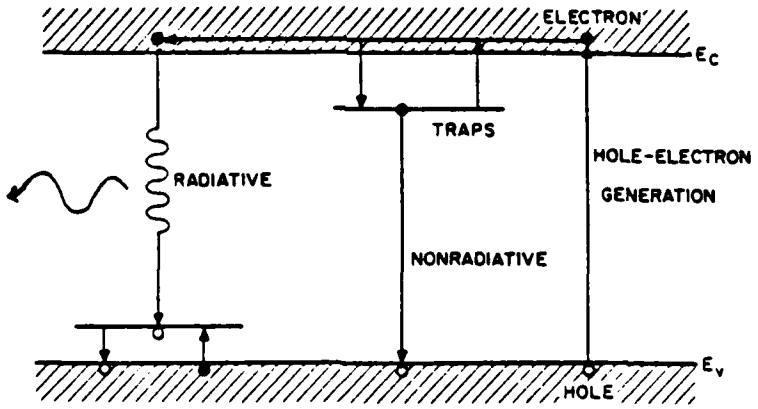

Figure 6. Electron-hole Generation and Recombination [Ref.25]

Radiative recombination processes can occur either by direct bandgap recombination or indirect bandgap recombination [Ref.25].

Direct bandgap recombination occurs when the electrons in the conduction band combine directly with the holes in the valence band. Materials that exhibit this type of recombination are called direct bandgap materials. In indirect bandgap materials, electron-hole recombination requires an interaction with a phonon as described below.

Examples of direct and indirect bandgap recombinations on an energy versus momentum diagram are illustrated in Figure seven. Since momentum must be conserved during recombination, the momentum of the electrons and holes must be equivalent for a direct bandgap recombination to occur [Ref.24]. In indirect bandgap materials the holes and electrons have different momenta. Therefore, the excess momentum must be transfered away from the hole-electron pair during the recombination in the form of a phonon (thus conserving momentum). Since direct recombination involves one electron-hole pair and indirect recombination involves an electron-hole pair and a phonon, the probablility of direct recombination occuring (if allowed) is considerably greater [Ref.25]. Which type of recombination is allowed is determined by the energy momentum diagram (as in Figure seven) for each crystal material.

A third radiative recombination process, called exciton recombination, is caused by exciton energy states that exist in the bandgap of all crystalline materials. Exciton states are characterized by weakly bound hole-electron pairs that orbit their

common center of gravity. If the exciton state becomes localized, the electron and hole may recombine directly across the bandgap even in indirect bandgap semiconductor materials [Ref.25].

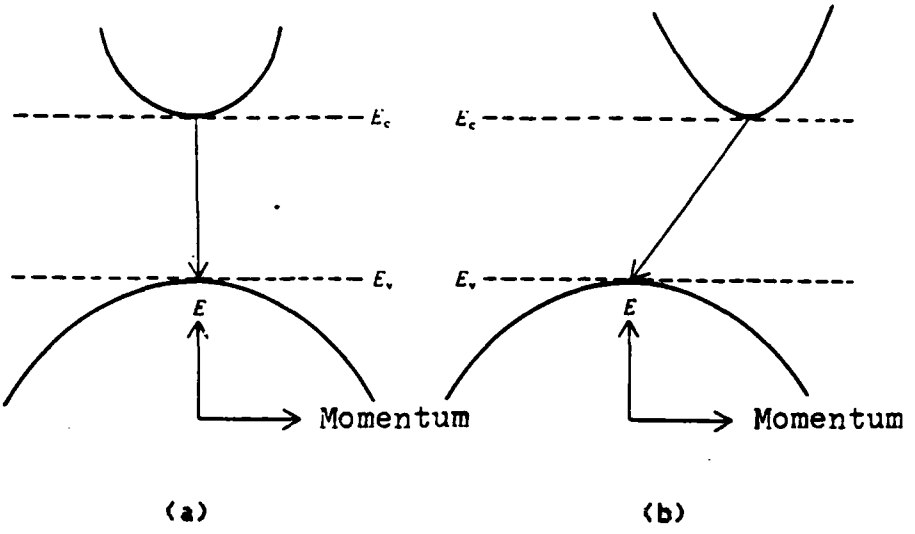

Figure 7. (a) Direct, (b) Indirect Bandgap Recombination [Ref.2]

D. PRINCIPLES OF LED OPERATION

A simple LED consists of a p-n junction with a forward bias applied. As carriers are injected across the p-n junction they either recombine in the depletion region or they diffuse away from the junction and recombine with the majority carriers in the bulk regions. In both the depletion region and the bulk regions the radiative and the non-radiative recombination processes compete. In materials used in the manufacture of LEDs radiative recombinations dominate the other recombination processes. The radiative output of an LED depends upon

the design and materials used in it's manufacture and the radiative loss mechanisms which affect it.

1. The Quantum Efficiency of LEDs

Quantum efficiency is a figure of merit for the efficiency of photon emission due to a current supplied across the p-n junction. Quantum efficiency is defined as the ratio of the number of injected carriers that recombine radiatively to the total number of carriers injected across the junction [Ref.3]. Using the reciprocal relationship between the recombination rate and the minority carrier lifetime, the quantum efficiency (η) can be alternatively expressed as

$$\eta = t_{onr} / (t_{onr} + t_{or}) \qquad (7)$$

where t_{onr} is the mean non-radiative lifetime and t_{or} is the mean radiative lifetime of the *minority carriers*. Thus semiconductor materials with high quantum efficiencies have small radiative lifetimes.

2. The Loss Mechanisms of Radiated Light in LEDs

Not all photons generated by radiative recombination are emitted from an LED. Radiated photon loss in LEDs is primarily due to photon absorbtion in the material, Fresnel loss and critical angle loss [Ref.24]. Absorbtion loss occurs because the photons emitted during an electron-hole radiative recombination can later be absorbed and create another electron-hole pair at a different lattice site. Fresnel loss occurs because the index of refraction of a semiconductor

material is greater than that of air. Therefore, some of the photons will be reflected at the LED-air interface. Fresnel loss can be reduced by coating the LED surface with quarter wavelength films [Ref.25].

Critical angle loss is explained by Snell's Law:

$$n_1 \sin \theta_1 = n_2 \sin \theta_2 \qquad (8)$$

where n_1 is the index of refraction of the semiconductor material, n_2 is the index of refraction of air, θ_1 is the angle of incidence and θ_2 is the angle of refraction. If n_2 is greater than n_1 a critical incident angle (θ_c) exists where photons incident to the air-semiconductor surface are totally reflected back into the semiconductor [Ref.3]. Most III-V compounds have a large index of refraction which results in small critical angles. The loss due to small critical angles can be reduced by shaping the surface of LEDs into hemispheres. [Ref.25].

3. Materials Used in Manufacturing LEDs

Wilson and Hawkes state that materials used in making LEDs should have large band gaps, exist in both p and n type forms, have low resistivity and have efficient pathways for which radiative transitions can occur [Ref.25]. Additional requirements depend on the intended use of the LED. III-V compounds are particularly versatile LED materials since they can perform as indirect or direct band gap materials depending on the specific elements that comprise the

compounds and the dopant levels of the impurities. By adjusting the composition of a semiconductor material during the crystal growth process, semiconductor materials can be tailored to emit photons of specific wavelengths. The InGaAsP crystals studied in this investigation were manufactured to emit 1.36 micrometer wavelength light.

4. LED Configurations

LEDs are designed to optimize the radiation of light of a specific wavelength while minimizing the impact of the nonradiative loss mechanisms. Figure eight shows a typical LED configuration. When materials surrounding the radiative recombination region of an LED absorb the generated photons, little light is emitted from it's surface. To minimize this internal absorption, LEDs are manufactured using heterojunctions (a junction between two different semiconductor materials). Material where radiative recombinations occur is placed

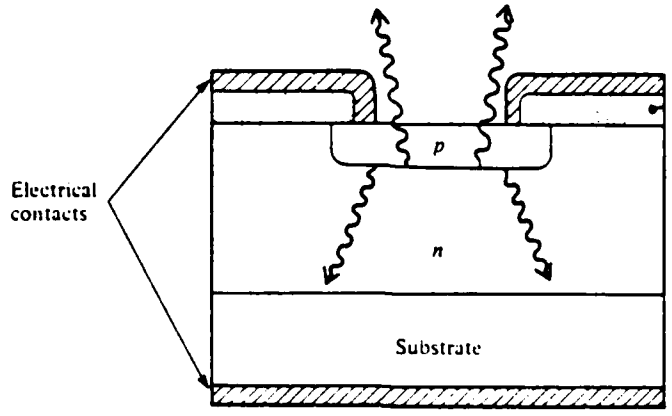

Figure 8. Typical LED (arrows indicate emitted light) [Ref.25]

between materials with larger bandgaps. Since the emitted photons do not have sufficient energy to be absorbed by the materials with the larger bandgaps, a larger emitted light output results [Ref.3]. For example, InGaAsP LEDs are usually grown on an InP substrate since InP readily transmits infrared light. These compounds have typical quantum efficiencies between 55% and 70% [Ref.3]

E. TEMPERATURE EFFECTS ON LED PERFORMANCE

1. Temperature Effects on Current

Several aspects of an LED's performance are temperature dependent. First, the conduction of current across a p-n junction, which results in radiative recombinations, decreases as the temperature of a semiconductor increases. This temperature dependence is apparent in equation five (repeated here):

$$I = I_0(T)[\exp(qv/kT - 1)] \qquad (5)$$

where $I_0(T)$ indicates that the saturation current is also temperature dependant. The saturation current's temperature dependance is due to the dependance of carrier mobility and carrier density on temperature. The relationship between the saturation current, the carrrier mobilities and the carrier densities depends on parameters which are specific to a particular device. Muller and Kamins provide a detailed discussion of this relationship [Ref.23].

The dependence of carrier mobility on temperature is determined by whether dopant impurities or defects exist in the lattice. In an intrinsic crystal, the movement of charge carriers is impeded by the scattering caused by the vibrating lattice. As the temperature of a lattice increases, the amplitudes of the vibrations increase resulting in an increase in lattice scattering and a decrease in carrier mobility [Ref.3]. However, in a crystal where the scattering from ionized impurities or defects dominate, the carrier mobility increases with temperature. This is due to the carriers moving faster at increased temperatures, thus reducing the amount of time that the carriers are close to the impurity atoms [Ref.23]. The scattering becomes less effective and the carrier mobility increases.

The saturation current is also dependent on the carrier density. Muller and Kamins show that the relationship between carrier densities and temperature is porportional to exp(qv/nkT) where n is a material dependant property [Ref.23]. At temperatures above 150°K the electrons in most dopant atoms are thermally excited into the conduction band. However, at temperatures above 400°K the electrons from the intrinsic material are also excited into the conduction band (allowing the ionized intrinsic atoms to recombine with the dopant electrons). Thus, the dopant carrier density, and the saturation current, is decreased in extrinsic semiconductors [Ref.23].

2. Other Temperature Effects

Temperature also affects the peak wavelength of emitted photons and the quantum efficiency of LEDs. In direct band gap materials the peak wavelength of emitted photons increases because the bandgap decreases with temperature [Ref.3]. Equation six shows that the reduction of released energy causes the wavelength to increase. If the increase with temperature of radiative carrier lifetimes is greater than the increase of nonradiative lifetimes, then the quantum efficiency of an LED decreases. This relationship can be seen in equation seven.

3. Temperature Effects on III-V Compounds

Research is currently being done on quantizing the effects of temperature on III-V compounds [Ref.27 and 28]. The temperature dependence of the light output of LEDs manufactured from III-V compounds varies widely in magnitude depending on the configuration of the elements comprising the LED's crystal. Some InGaAsP LEDs have demonstrated a large light output degradation at temperatures above 313°K. At this temperature, these LEDs have shown a significant increase in non-radiative impurity center recombinations and Auger recombinations [Ref.28]. Thus, the nonradiative carrier lifetimes decrease causing the quantum efficiency of these InGaAsP LEDs to decrease (see equation seven). In contrast, InGaAsP/InP (this notation indicates that the InGaAsP crystal layer was grown on top of

InP crystal) LEDs have been operated over 14,000 hours at 343°K without any indication of performance degradation [Ref.27]. (An InGaAsP/InP LED was studied in this investigation.)

F. THE GENERAL CHARACTERISTICS OF RADIATION DAMAGE IN SEMICONDUCTORS

There are four principle types of radiation which affect the performance of semiconductors: proton, electron, neutron and photon (gamma ray and x-ray) radiation. All four types of radiation cause two fundamental types of damage to semiconductor materials: displacement damage and ionization damage [Ref.24]. Displacement damage is the displacement of atoms from their lattice sites. Ionization damage is the removal of orbital electrons from lattice atoms creating conduction electrons and ions. Displacement damage is usually permanent while ionization damage usually causes only temporary changes in the electrical properties of bulk semiconductor material. Therefore, ionization effects are also referred to as transient effects. However, ionization can cause long term effects in the oxides that are usually on the surface of semiconductor materials in devices [Ref.24].

1. Displacement Damage

Displacement damage occurs when an irradiating particle (such as a neutron, proton, electron, etc.) collides with a lattice atom. The recoiling atom is displaced to a new location between other

lattice atoms, hence becoming an interstitial atom. Both the interstitial atom and the vacant lattice site, created by the atom's displacement, can act as nonradiative recombination centers (referred to as defect sites or defects) [Ref.3]. (In optical materials such as glass these defects are referred to as color centers.) Like impurity recombination centers, defect sites allow energy states to exist in the band gap of semiconductor materials. When only one atom is displaced, the defect is called a simple or Frenkel defect. Electrons and gamma rays usually cause Frenkel defects. Defects caused by the displacemenet of hundreds of lattice atoms (typical of high energy neutron damage) are called defect clusters.

By acting as additional recombination centers, defects change the carrier densities in a semiconductor material. Thus, the conductivity and resistivity of the material is changed [Ref.4]. At a given input current in the bulk regions, the increase in the number of nonradiative recombination centers causes an increase in the nonradiative current and a decrease in the radiative current. Barnes [Ref.2] states that in the depletion region, displacement damage has little effect on the recombination rate since the recombination rate at a particular type of recombination center is governed by the Fermi level. Previous research has shown that the Fermi levels do not change with irradiation unless the majority carrier densities in the bulk semiconductor regions are significantly reduced [Ref.2]. To a lesser extent, a reduction in the carrier mobility also reduces LED

light output. The lattice defects decrease the length of the mean free path of carriers between Rutherford scatterings, thus reducing the carrier mobility. Therefore, for most LEDs, light output degrades due to the addition of defects.

It is usual for some interstitial atoms to diffuse to vacant lattice sites after displacement damage occurs. This process is referred to as annealing. The magnitude of the annealing is material dependent. Annealing usually begins to occur within a few seconds after irradiation and is enhanced by high temperatures [Ref.24].

2. Ionization Damage

Ionizing radiation temporarily increases the density of charge carriers. This usually results in a current pulse that can disrupt or destroy electronic circuits. Additionally, ionizing radiation can cause echemical effects, trapped charges and the generation of electromagnetic fields [Ref.5]. Research conducted by Barnes has revealed that ionizing radiation poses no severe problem to LED applications [Ref.2]. This is primarily due to the absence of insulating oxide layers in the design of LEDs.

3. Electron Radiation Damage

Electron irradiation of a semiconductor causes both ionization and displacement damage in a semiconductor material. An electron can interact with a semiconductor material through inelastic and elastic

collisions with the electrons or nuclei of the lattice atoms [Ref.4]. Inelastic collisions are usually the dominate energy loss mechanism. An incident electron transfers energy to a lattice atom by colliding with the nucleus. The maximum kinetic energy (T) that can be transferred from an incident electron to a lattice atom during an inelastic collision is

$$T = 2(E + 2mC^2)/MC^2 \qquad (9)$$

where E is the electron's energy, m is the electron's mass, M is the atom's mass and C is the speed of light in a vacuum [Ref.4]. If the transferred energy is larger than the molecular binding energy of the lattice atom, the atom is displaced. Elastic collisions occur when an irradiating electron interacts with the electric field of a lattice atom's nucleus. Energy is transferred from the electron to the nucleus and the electron is scattered. This process is referred to as Coulomb scattering.

An irradiating electron can also interact with the electron cloud of a lattice atom through elastic or inelastic collisions. The energy transferred from the irradiating electron to a valence electron can excite the lattice atom's electrons into higher energy levels. If the transferred energy is greater than the electron binding energy the lattice atom's electron can be removed from the atom (ionization).

Usually, an irradiating electron loses energy to a lattice atom through both ionization and displacement mechanisms. The dominant radiation damage mechanism depends on the atomic number of

each element in the semiconductor material and the energy of the irradiating electron. If the energy of an irradiating electron is greater than a certain critical energy (T_c), displacement damage dominates, otherwise, ionization damage dominates. An approximate expression for this critical energy is

$$T_c = 800/(1.2 + Z) \text{ Mev} \qquad (10)$$

where T_c is the critical energy and Z is the atomic number of each element in the semiconductor [Ref.4]. Table three shows the critical energies for each element in the LED and photodiode studied in this investigation.

Table 3. Critical Energies

Element	Z	T_c (Mev)	Dominating damage mechanism for 30 Mev electrons
In	49	16	ionizing
Ga	31	25	ionizing
As	33	24	ionizing
P	15	50	displacement

Since 30 Mev electrons were used in the irradiations performed in this study, both ionizing damage and displacement damage dominated elements exsisted in the LED. Since the manufacturer would not reveal the ratio of the concentration of the constituent elements (for proprietary reasons), it is uncertain which mechanism overall dominated. However, extensive prior research by Barnes (see Tables

one and two) indicates that the primary damage mechanism in LEDs is the displacement of lattice atoms in the crystal [Ref.4].

G. LIFETIME-DAMAGE CONSTANT PRODUCTS FOR LEDS

Lifetime-damage constant products are extensively used by researchers to indicate the relative immunity of LEDs to radiation damage. The analysis of lifetime-damage constant products of LEDs provides insight into the desired characteristics for radiation hardened optoelectronic divides. In this section the theory, the techniques of measurement and the validity of lifetime-damage constant products are discussed.

1. The Effect of Radiation on Carrier Lifetimes and the Derivation of the Damage Constant

As discussed previously, nonradiative and radiative recombination are competing mechanisms in the electron-hole recombination process of most LEDs. The before irradiation carrier lifetime for radiative recombination (t_{or}) is expressed as

$$t_{or} = 1/\sigma_r \, v_{th} N_r \qquad (11)$$

where N_r is the radiative recombination center density, σ_r is the radiative capture cross-section and v_{th} is the thermal velocity of the carriers [Ref.17]. Likewise, the before irradiation carrier lifetime for nonradiative recombinations (t_{onr}) is expressed as

$$t_{onr} = 1/\sigma_{nr} v_{th} N_{nr} \qquad (12)$$

where N_{nr} is the nonradiative recombination center density and σ_{nr} is the nonradiative capture cross-section. The reciprocal of the total minority carrier lifetime (t_o) is the sum of the reciprocal of the radiative and nonradiative lifetimes:

$$1/t_o = 1/t_{or} + 1/t_{onr}. \qquad (13)$$

During irradiation nonradiative defect sites are usually created; thus they decrease the nonradiative lifetime as shown in the expression

$$t_{onr} = 1/\sigma_{nr} v_{th} N_{nr} + 1/\sigma_{nri} v_{th} N_{nri} \qquad (14)$$

where σ_{nri} is the capture crossection and N_{nri} is the density of the radiation induced defect sites [Ref.24]. N_{nri} is related to the number of irradiation electrons per unit area (referred to as fluence (Φ)) that is incident on a semiconductor material by

$$N_{nri} = C_1 \Phi \qquad (15)$$

where C_1 is a proportionality constant. Combining equations 15 and 14 and substituting into equation 13, the total post irradiation minority carrier lifetime (t) is expressed as

$$1/t = 1/t_o + \sigma_{nri} v_{th} C_1 \Phi. \qquad (16)$$

If a damage constant (K) is defined as

$$K = \sigma_{nri} v_{th} C_1 \qquad (17)$$

then equation 16 becomes

$$1/t = 1/t_o + K\Phi \qquad (18)$$

or

$$t_o/t = 1 + t_o K \Phi \qquad (19)$$

which is a phenomenological expression for the decrease in total carrier lifetimes for a given fluence.

For more than two decades, the lifetime-damage constant product ($t_o K$) has been used as an expression for the sensitivity of LEDs to radiation damage. A small lifetime-damage constant product of a material indicates a good immunity to radiation damage. However, it should be noted that besides the dependence on σ_{nri} and V_{th}, K is dependent on the type and intensity of the radiation, the irradiation temperature, the level of irradiation in the material during irradiation and other characteristics of the device [Ref.24].

2. Measurement of Lifetime-damage Constant Products

Since most carrier lifetimes are too small (frequently nanoseconds or less) to measure using typical laboratory equipment, procedures for measuring lifetime-damage constant products indirectly have been developed. The current controlling mechanism and the dopant profile of the LED must be known to utilize these methods. For most LEDs manufactured using heterojunctions, the dopant profile across the p-n junction can be assumed to be linerarly graded [Ref.21]. Additionally, LEDs are typically operated at large forward biases where diffusion current controlling mechanisms dominate. Barnes and Rose show that if these assumptions are made, the before irradiation light output (L_o) of a LED operated at a constant voltage can be expressed as

$$L_o = C_2 t_o \exp(qv/kT) \quad (20)$$

where C_2 is a constant of proportionality depending on parameters other than the before irradiation carrier lifetime (t_o), the after irradiation carrier lifetime (t) or the temperature (T) [Ref.16]. Likewise, the after irradiation light output can be expressed as

$$L = C_2 t \exp(qv/KT) \quad (21)$$

By dividing equation 20 by equation 21 and using equation 19, the relationship between light output degradation and fluence is shown to be

$$L_{o/L} = t_o/t = 1 + t_o K\Phi \quad (22)$$

Therefore, by measuring the decrease in light output of an LED exposed to a known fluence, the lifetime-damage constant product for that LED can be calculated.

Alternatively, the lifetime-damage constant product of an LED can also be determined by measuring the change in current output after an irradiation of a given fluence. Since the total current is due to the carrier recombination at all types of recombination centers, the increase in nonradiative recombination centers results in an increase in the total current during irradiation. Barnes shows that the expression for the total current of LEDs, biased (with a constant, lower voltage than in the case discussed above) where recombination in the depletion region is the dominant current controlling mechanism, is

$$I = (C_3/t)\exp(qv/2kT) \quad (23)$$

where C_3 is a proportionality constant [Ref.16]. Dividing the expression for the before irradiation total current by the expression for the after irradiation total current results in

$$I/I_o = 1 + t_o K\Phi \qquad (24)$$

where I_o is the before irradiation current and I is the after irradiation current. Therefore, the lifetime-damage constant for an LED can be determined by analyzing current degradation during irradiation in an analogous manner to the light output degradation analysis.

3. The Validity of Damage Constants

Despite the extensive past use of damage constants in determining the sensitivity of LEDs to radiation damage, caution is advised when using these constants to select an LED for a specific application. The validity of the use of damage constants is dependent on the accuracy of the assumptions made in their derivation. The derivation of the damage constant assumes that an exact knowledge of the allowed energy levels and the capture cross-sections exists. However, the radiation-induced nonradiative recombination centers create a wide variety of allowed energy levels in the band gap. Therefore, an analytical analysis of K is limited by an inexact knowledge of those energy levels and the capture cross-sections [Ref.29].

The use of damage constants also assumes that changes in the nonradiative lifetimes is the most significant effect of radiation on an LED. However, many other factors also help determine the total effect of radiation on a device. Some of these factors are listed in Table three. The importance of each factor varies for each LED and its intended application. If a factor other than carrier lifetime is of considerable importance, then the assumption that these factors are phenomenologically combined to form the constant K may be inappropriate.

TABLE 3: FACTORS AFFECTING RADIATION DAMAGE IN LEDS [Ref. 29]

1. Temperature of sample during radiation
2. Energy spectrum of radiation
3. Inactive impurity concentrations
4. Majority carrier type and density of impurities
5. Rate of minority carrier injection during irradiation
6. Orientation of semiconductor crystal with respect to direction of radiation
7. Rate of irradiation
8. History of time, temperature and injection ratio after irradiation

The preirradiation light output of an LED must also be considered with the radiation damage constant when determining the

quality of an LED. An inefficient LED, with an initial large number of nonradiative recombination centers, will have a ratio between radiative and nonradiative lifetimes that is insensitive to an increase in the nonradiative lifetimes. Thus radiation will cause little change in the light output of an inefficient LED [Ref. 26]. Hence, such inefficient LEDs would possess small radiation damage constants. In contrast, an ideal LED would have a small radiation damage constant and an initial small number of nonradiative recombination centers.

4. The Radiation Hardness of III-V Compounds

A radiation hardened device retains useful properties despite radiation damage such as large decreases in nonradiative lifetimes. III-V compounds, such as InGaAsP, have several properties which make them good candidates for radiation hardness. These direct bandgap materials have short diffusion lengths and short carrier lifetimes [Ref.4]. Therefore, only carriers in or near the p-n junction contribute to radiative recombination. Thus an increase in the number of radiation induced nonradiative recombination centers in the bulk regions of the semiconductor will have little effect on light produced in the depletion region. Additionally, the heterostructure configura-tions, typical of III-V compound LED designs, have energy bandgap mismatches between adjacent semiconductor layers [Ref. 13]. This causes the presence of an internal electric field which prevents

the radiation induced extraneous carriers from recombining in or near the depletion region.

H. PRINCIPLES OF PHOTODIODE OPERATION

1. Photocurrent Generation

In this section, the basic mechanism by which photodiodes convert light into current (referred to as the photocurrent) is presented. Photodiode operation is based on the creation of hole-electron pairs when photons are absorbed by a semiconductor material. If an electric field is present when the hole-electron pairs are created, the Coulomb force accelerates the holes and electrons in opposite directions. Thus, current is conducted [Ref.26]. If an electric field is not present, the hole-electron pairs recombine and no current is conducted. As discussed previously, when a bias is applied to a semiconductor most of the voltage occurs across the p-n junction. This causes a significant electric field to exist in the depletion region and a negligible field to exist in the bulk regions. Typically, the photocurrent is generated in the depletion region and approximately one minority carrier diffusion length into a lightly doped n region [Ref.18]. Figure nine illustrates the electric field intensity distribution and the photocurrent generation process in a photodiode.

The distance that a photon travels before it is absorbed depends upon the wavelength of the photon and the light absorption properties of the material it is travelling through. The absorption coefficient of a material (α) is wavelength dependent. The shorter the photon's wavelength, the shorter the distance it penetrates. Figure nine illustrates the wavelength dependence on the penetration depth of a photon before it is absorbed. It is usually assumed that little photocurrent is generated in the p region on top of the p-n junction. Therefore, in order to maximize the spectrum of absorbed wavelengths, most photodiodes have a very thin semiconductor layer above the p-n junction. Additionally, the penetration distance of a

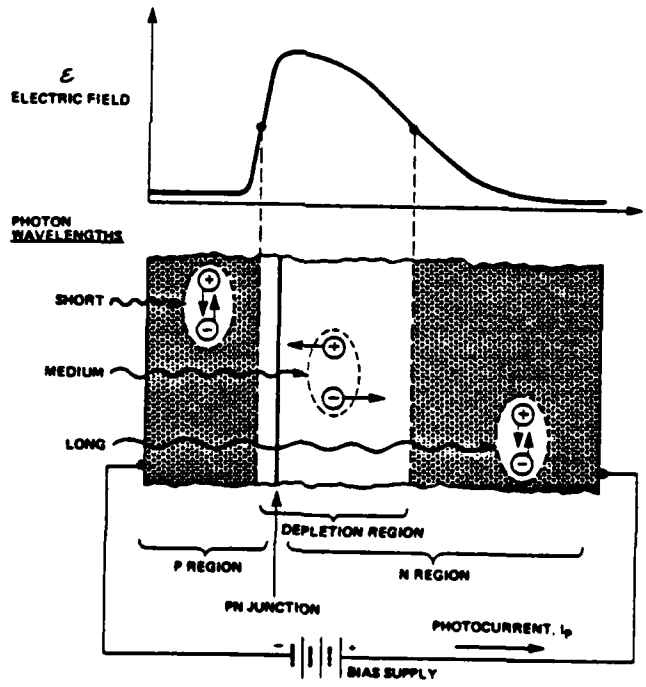

Figure 9. p-n Photodiode Junction Under Forward Bias [Ref.26]

photon is related to the properties of a specific semiconductor by the expression

$$\Phi(x) = \Phi_0 \exp(-\alpha x) \qquad (25)$$

where x is the penetration distance, Φ_0 is the incident photon flux, $\alpha(\lambda)$ is the material's absorption coefficient and $\Phi(x)$ is the photon flux at x [Ref.2].

2. PIN Photodiodes

Since most of the photocurrent is generated in the depletion region, an increase in the width of the depletion region allows deeper penetrating photons to be absorbed and thus increases the amount of photocurrent generated. Additionally, an increase in the width of the depletion region increases the spectrum of asorbed wavelengths; thus the sensitivity of the photodiode is also increased. One method of increasing the width of the depletion region is to place a layer of semiconductor material containing few charge carriers and having a large resistivity between the n and the p bulk regions. This layer is called the intrinsic region. The photodetector shown in Figure 10 utilizes an intrinsic region.

The large resistivity of the intrinsic region causes a large ohmic drop of the applied bias across the intrinsic region (thus increasing the efficiency of photocurrent generation). If the resistivity of the intrinsic region is large enough, a depletion region can exist between the n region and halfway across the intrinsic

region without any applied bias (referred to as photovoltaic operation) [Ref. 24]. Thus, for these photodiodes, photocurrent can be generated without an applied bias.

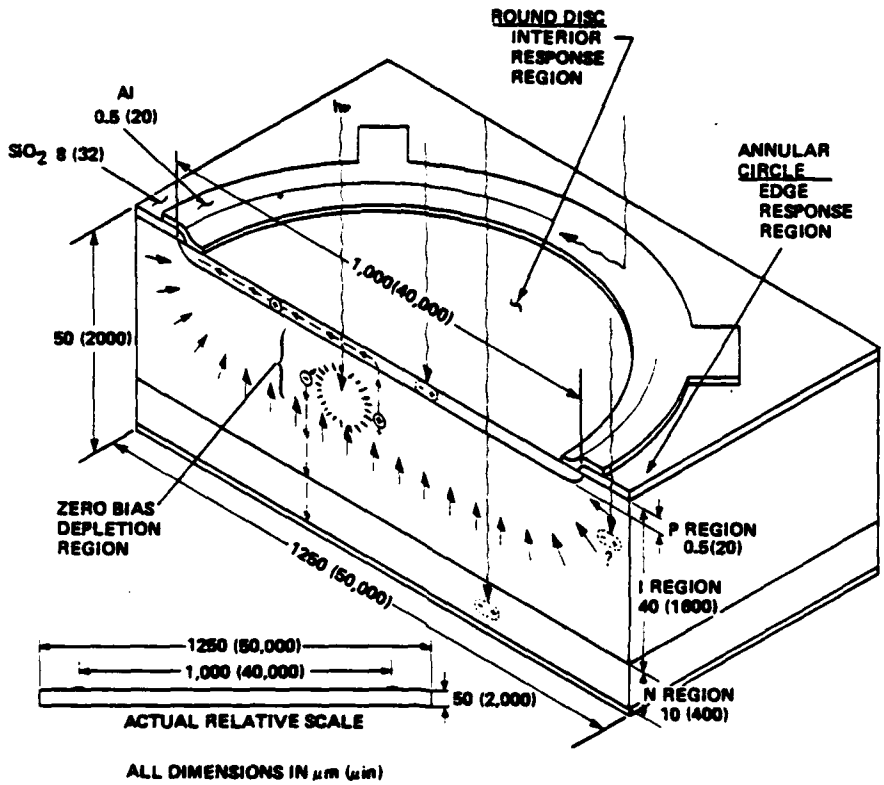

Figure 10. PIN Photodiode

3. Responsivity of Photodiodes

The quantum efficiency for both LEDs and photodiodes is a figure of merit of the efficiency of device operation. The photodiode quantum efficiency is defined as the number of electrons created for each incident photon absorbed. An extensively used, and related, figure of merit for photodiodes is the responsivity (R) which is the

ratio of the photocurrent generated to the incident photon flux. Responsivity (R) is related to photodiode quantum efficiency (n) by

$$R = \eta\lambda/1240 = I_p/\Phi_e \text{ Amperes/watt} \qquad (26)$$

where λ is the wavelength of incident photons in nanometers, I is the photocurrent and Φ_e is the incident photon flux in watts [Ref.26].

The responsivity of a photodiode is also a function of the photocurrent gain. Photocurrent gain is the efficiency of photocurrent production after an electron-hole pair has been created by a photon. The gain (G) is expressed as

$$G = t/t_t \qquad (27)$$

where t is the carrier lifetime and t_t is the time it takes the carrier to cross the intrinsic region (referred to as the carrier transit time). If t is sufficiently greater than t_t, then the carrier can travel across the depletion region several times before recombining thus causing a gain in the amount of current being conducted. The responsivity can thus be expressed as

$$R = GI_{ph}/\Phi_e \qquad (28)$$

where I_{ph} is the current ceated from the absorption of photons at the site of absorption (before the current has been conducted in the photoconductor material).

4. <u>The Dark Current</u>

In addition to the photocurrent, another current is produced by photodiodes even when no light is incident on them. This currrent

is referred to as the dark current. Its primary source is the thermal excitation of electrons in photodiodes at room temperature.

The dark current acts as a source of background noise. Noise is any unwanted current which masks the photocurrent of faint optical signals. The root mean square (rms) equivalent noise current is the sum of several types of noise which limits the ability of a photodiode to resolve faint optical signals.

5. III-V Compound Photodiodes

Infrared photodiodes are often manufactured from III-V compounds such as InGaAs. The typical quantum efficiency of InGaAs photodiodes without antireflective coatings is almost 70%. This is greater than for most other materials. The quantum efficiency of InGaAs photodiodes is *approximately uniform* over the range of wavelengths from 0.95 to 1.65 micrometers [Ref.2].

Because InGaAs is a direct bandgap material, it also has a large absorption coefficient. As equation 25 indicated, this large absorption coefficient contributes to a short photon penetration distance. Therefore, the InGaAs PIN photodiodes can be manufactured with small depletion regions and still absorb large fractions of incident photons [Ref.2]. A thinner depletion region causes a high signal response speed since the charge carriers do not travel very far when exiting the photodiode. These desirable properties indicate why

InGaAs is an attractive selection for near infrared photodiode applications.

I. RADIATION DAMAGE TO PHOTODIODES

1. Radiation Damage Mechanisms In Photodiodes

The two fundamental radiation damage mechanisms in photodiodes are the increase of the dark current and the degradation of the responsivity. The increase in the dark current is primarily due to the creation of radiation induced defect sites in the bulk region. The defect sites contribute to the number of thermally excited electrons. (As discussed previously, the dark current is a primary factor which limits the minimum signal that a photodiode can detect.) Photovoltaic photodiodes, when operated in the photovoltaic mode, have no electric field existing in the bulk regions to accelerate the thermally excited electrons. Thus, no dark current is generated in the bulk regions. The dark current in the depletion region is still generated. However, since the volume of the depletion region is much less than the volume of bulk regions, the total radiation induced dark current of photovoltaic photodiodes is significantly less than for other photodiodes.

The radiation induced reduction in the responsivity of photodiodes is due to the reduction in the photocurrent gain. By increasing the number of defect sites where carriers can recombine,

radiation reduces the carrier lifetimes. As shown in equation 28, if the transient time is much less than the carrier lifetime, only a small reduction in the gain results from the radiation induced decrease in the carrier lifetime. However, if the lifetime of a carrier is originally comparable to the magnitude of the carrier transient time, the radiation induced reduction in the photodiode's gain is significant. Photodiodes that do not depend on diffusion of carriers into bulk regions have quantum efficiencies that show little sensitivity to the increase in the number of defect sites in the depletion region.

Photodiodes are very susceptible to ionizing radiation damage. Intense transient radiation pulses (such as that which accompany nuclear weapons detonations) cause severe ionizating radiation. A large ionization induced current is produced by the same mechanisms that cause photon induced currents to be generated under normal photodiode operating conditions. The large pulse of ionization induced current is usually more threatening to the more sensitive external detector circuits than to the photodiode. The sensitvity of photodiodes to this type of radiation is due to their requirement for relatively large surface areas that are exposed to the environment.

2. Radiation Hardness Of III-V Compound Photodiodes

There are several reasons why photodiodes manufactured from III-V compounds exhibit characteristics of good radiation hardness.

The relatively large absorption coefficients of III-V compounds allow very efficient photodiodes to be manufactured with thin active regions [Ref.18]. For a given fluence, a small active region has fewer radiation induced defects than a large active region. Therefore, a thin action region causes III-V compound photodiodes to have less radiation induced dark current than other photodiodes. Additionally, these direct bandgap materials have been shown to have short carrier lifetimes [Ref.4] and corresponding carrier diffusion lengths of a few micrometers have been measured [Ref.14]. Therefore, only charge carriers generated in or near the depletion region contribute to the photodiode's current.

III-V compound photodiodes also exhibit less susceptibility to ionizing radiation than other photodiodes. The internal electric fields associated with the heterostructure configurations used in the fabrication of photodiodes from III-V compounds inhibit the movement of the excess carriers generated by ionizing radiation [Ref.16]. Researchers at Sandia National Laboratory have incorporated these heterostructure configurations in the manufacture of photodiodes that have exhibited superior immunity to ionizing radiation damage [Ref.4].

3. The Theoretical Radiation Hardness Of The InGaAs Photodiode

The previously discussed characteristics of radiation damage to photodiodes indicates that a PIN heterostructure photodiode manufactured using III-V compounds and operated in a photovoltaic mode

should exhibit considerable hardness to radiation. The InGaAs photodiode studied in this investigation possesses these characteristics. The primary radiation effects should be a reduction in the photodiode's responsivity and an increase in the dark current. The procedures used in conducting this investigation are discussed in the next chapter.

III. EXPERIMENTAL PROCEDURE

In this chapter, the experiemental procedures used to characterize and to irradiate the LEDs and photodiodes studied in this investigation are presented. The experiments involving the InGaAsP LEDs will be described first. After a description of the LED, the methods used to measure the before and after performance parameters are discussed. Next, a brief discussion of the characteristics and the operation of the Naval Postgraduate School Acceleration Laboratory's Linear Accelerator (NPSAL LINAC) is provided. The procedure used to measure LED performance parameters during irradiation is then presented. The second part of this chapter describes the experiments involving the InGaAs photodiode. First, the characteristics of the InGaAs photodiode are presented. Second, the procedures used to measure the before and after performance characteristics are described. Finally, the procedure used in measuring photodiode performance during irradiation is discussed.

An HP86A computer was used extensively in my investigation. It controlled the peripheral meters, the plotters and the power supply and stored their data on discs. Its use allowed accurate data collection and precise repetition of experiments. The data collected was easily analyzed using the HP 7090A measurement plotting system. All the programs used to execute the experiments were written using the HPL basic computer language (see Appendixes C, D, E and F).

A. InGaAsP LED MEASUREMENTS

1. Characteristics of the InGaAsP LED

The InGaAsP LEDs used in this investigation were manufactured by M/A-COM Laser Diode, Inc. (catalog number IRE-387-003). Table five lists the advertised operating characteristics. Figure 11 is a diagram of the LED's radiative surface area. Figure 12 is a schematic diagram of the InGaAsP LED studied in this investigation. It is probable that the heterojunction configuration of this LED was manufactured using the liquid phase crystal growth process. This process is often used in the growth of III-V compound materials [Ref.27]. The glass cap covering the LED is made of corning 7502 glass which is extensively used in the manufacture of most optoelectronic devices.

TABLE 5: ADVERTISED LED CHARACTERISTICS (AT 25°C) [Ref.30]

Parameters		Min.	Typ.	Max.	Units
Peak Wavelength of Emission		1280	1300	1320	nm
Spectral Width			100		nm
Temperature vs. Wavelength Coefficient			0.4		nm/°C
Operating Temperature Range		-10		+60	°C
Storage Temperature Range		-10		+60	°C
Rise Time, Fall Time			5		nsec
DC Drive Current			100	150	mA
Forward Voltage			1.3	1.5	V
Output Power at 100mA	Coupled into 50/125 0.2 N.A. fiber -				
	IRE-387-002	3			µW
	IRE-387-003	6			µW
	IRE-491	12	15		µW
	Coupled into 100/140 0.3 N.A. fiber -				
	IRE-387-002		20		µW
	IRE-387-003		40		µW
	IRE-491	70			µW
Temperature vs. Power Coefficient			-0.6		%/°C

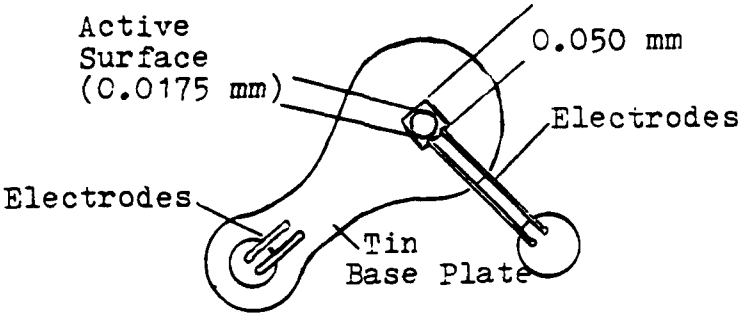

Figure 11. Top View Of LED

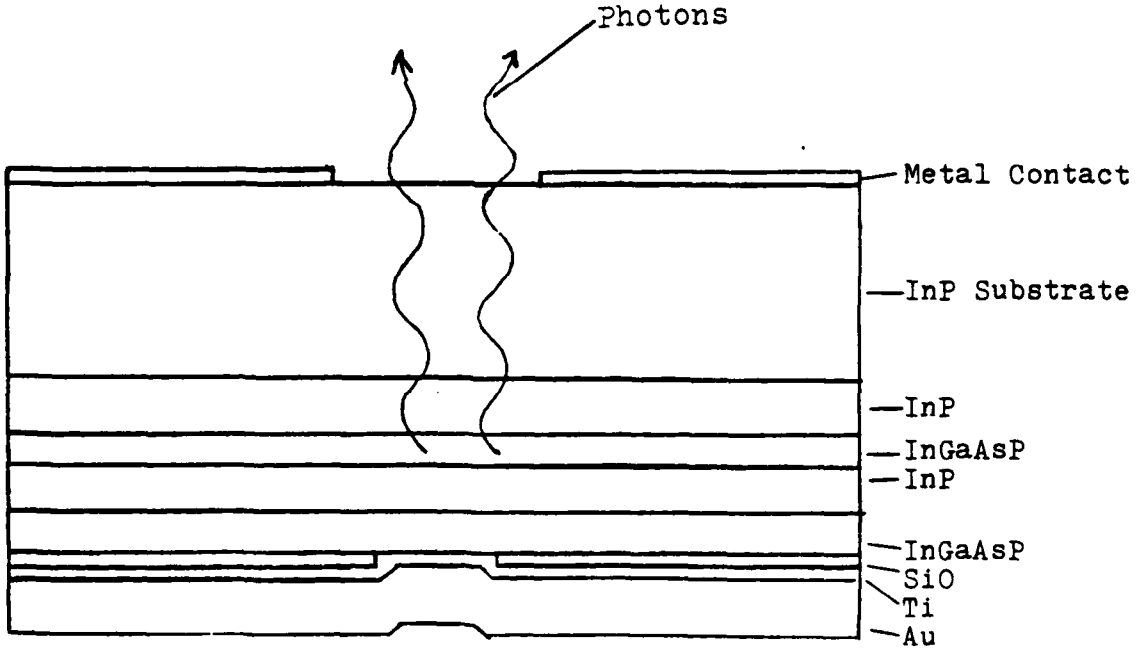

Figure 12. Heterojuction Configuration Of The InGaAsP LED

2. Measurement of Radiation Effects on the Glass Cap

As described in the previous chapter, radiation affects optical materials such as glass by creating defects called "color centers" which affect the transmission of light. Ness [Ref.19] and Foley [Ref.20] showed that the effect of radiation on the transmission of light through the glass cap covering the LED is wavelength dependent. Furthermore, their researth indicated that the effect of radiation on the transmission properties of the glass caps was negligible in the near infrared wavelength region. To confirm these results, three high intensity red (peak wavelength 637 nanometers) LEDs were irradiated with the glass caps attached and three LEDs were irradiated with the glass caps removed. Other than the removal of the glass caps, these LEDs showed only a slight nonuniformity in their performance (which is typical of mass produced electronic components) both before and after irradiation. Additionally, I measured the effect of 30 Mev electron irradiation on the transmission properties of glass caps that cover the InGaAsP LEDs.

The results of irradiating the glass caps and the red LEDs showed that the radiation induced transmission loss of glass caps was not significant when compared to the other errors discussed in Appendix B. The irradiation of the red LEDs showed that removal of the glass caps introduced less than a three percent change in the degradation of the performance of the LEDs. The irradiation of the glass caps showed that for fluences up to 10^{15} electrons per square

centimeter (e/cm^2), the radiation induced change in the glass cap's transmission of near infrared light was also negligible. A more detailed discussion of both experiments and the resulting data is provided in Appendix A. Similar results were attained by Barnes [Ref.5] and Stanley [Ref.13]. Therefore, all the 30 Mev electron irradiations of the InGaAsP LEDs and the InGaAs photodiodes were performed with the glass caps attached.

3. Before and After Irradiation LED Performance Measurements

Before and after the irradiation of each LED, the peak wavelength of the emitted light, the optical power output versus voltage and the current output versus voltage were measured.

a. Light Output Versus Wavelength Measurements

The wavelength of the peak light output was measured using a Beckman DK-1A spectrophotometer. The LEDs were powered by a HP 6286B twelve watt power supply in series with a 26 ohm resistor (used to limit the current). The light emitted from the LEDs passed through the monochrometer of the Beckman DK-1A (which has a wavelength resolution of 5.0 nanometers). The monochrometer scanned the transmitted wavelengths from 2.0 to 0.8 nanometers. A variable resistor was attached to the wavelength selection dial on the monochrometer (which turned as the wavelength was decreased). This variable resistor was connected in series with a HP 6286A 60 watt power supply and the abscissa input of the X-Y recorder resulting in

the X axis reading wavelength. The X-Y recorder's abscissa sensitivity was adjusted to correspond to the region of measured wavelengths.

Since the original photomultiplier in the spectrophotometer did not have enough sensitivity in the infrared wavelength region, the spectrophotometer was modified. The visible wavelength photomultiplier was replaced by an infrared photodiode (Judson model J16-18A). The photodiode's signal was amplified by a United Detector model 101A amplifier and recorded by the ordinate input of the same Hewlett Packard Moseley 7035B X-Y recorder. Thus, a light output versus wavelength plot was obtained. Figure 13 is a diagram of the equipment configuration used in this measurement.

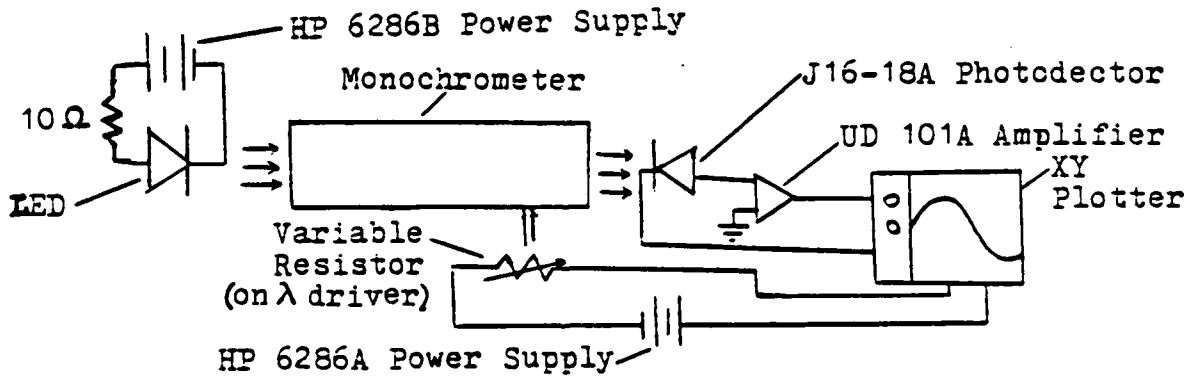

Figure 13. LED Peak Wavelength Measurement

b. Light and Current Output Versus Voltage Measurements

Figure 14 is a diagram of the equipment configuration used for these measurements. The LED forward bias was supplied by a HP

6002A programmable power supply. The LED optical power output was recorded using a Fiberoptic 550 powermeter (connected to an infrared photodetector head). The bias was increased in 0.02 volt increments between 0.5 and 1.3 volts. (The manufacturer's maximum allowable current of 150 milliamps was attained near 1.3 volts.) To avoid any possible hysteresis effects the forward bias was always changed with increments of increasing voltage.

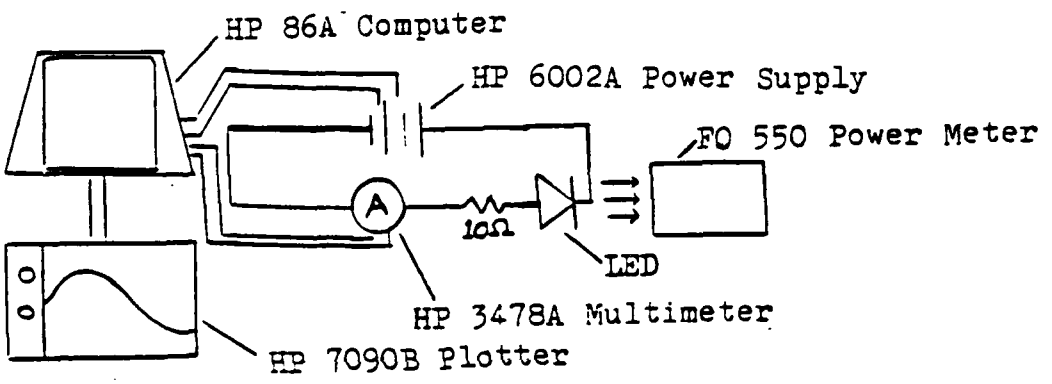

Figure 14. LED Current And Light Measurement

The LED light and current output versus voltage measurements were made before and immediately after irradiations. This ensured that only changes that occurred during irradiations were recorded. Additonally, in order to detect long term annealing at room temperature, additional measurements were made several days after each irradiation.

By programing the computer to perform most of the required collecting, storage and plotting of data, the measurements were made quickly. However, the optical power measurement data was manually entered into the computer. Appendix C lists the computer program that was used to perform the experiments.

4. Measurement of Temperature Effects on Device Performance

During irradiation, the incident electrons collide with the lattice atoms, thereby transferring some of their kinetic energy to the lattice atoms. Some of the kinetic energy of the lattice atoms is then dissipated through vibrations which causes an increase in the temperature of the lattice. As previously discussed, temperature affects many aspects of a semiconductor's performance. Therefore, in order to determine the effect of radiation on the performance of LEDs, the effect of the temperature on the performance of LEDs during irradiation has to be known.

The effect of temperature on the LED's performance was determined by controlling the temperature of the LEDs while repeating the light output and current output measurements described in the previous section. The temperature of the LEDs was monitored by attaching an Omega chromel-constantan thermocouple to the back surface of the LEDs using Omegatherm 201 thermally conductive paste. The thermocouple leads were connected to a Fluke 2190A digital thermometer adjusted to read thermocouples made from chromel-constantan.

Two different methods were used to control the temperature of the LEDs during these measurements. While recording the current versus temperature data, the LEDs were placed in a heating device which allowed no incident light to illuminate the LEDs. The heating device was a ceramic cylinder wrapped with thin nicrome wire that was connected to a HP 6286B power supply. By adjusting the current of the power supply, the temperature of the ceramic cylinder was controlled (see Figure 15.a). This method would not work during the light output versus temperature measurements since it would cause the entire head of the power meter to be heated. The effect of increased temperature on the power meter head was unknown. Therefore, to minimize the temperature change of the power meter head, the LED was heated by focusing the light from a DYNA-LUME high intensity radiant heat projector (model 3151-2, produced by the Cole-Parmer Company) on the back surface of the LED (see Figure 15.b). A Variac variable resistor was used to adjust the intensity of the projected heat. The temperature was increased in approximate increments of five degrees Kelvin (°K) between LED performance measurements. LED temperatures ranged from 297°K to 343°K.

During irradiation, the temperature of the LEDs was monitored by the digital thermometer and the thermocouple used in the measurements mentioned above. The twelve inch thermocouple leads were extended to reach the control room (one hundred feet away from the target chamber) with two identical 115 foot copper and nickel wires.

By extending the leads, the accuracy of the temperature shown on the digital thermometer was decreased. However, the relative change in the temperature of a target device recorded during irradiations appeared accurate. Thus, the relative change in the temperature of a device during irradiation was measured and the corresponding effect of the temperature increase on the device performance was determined.

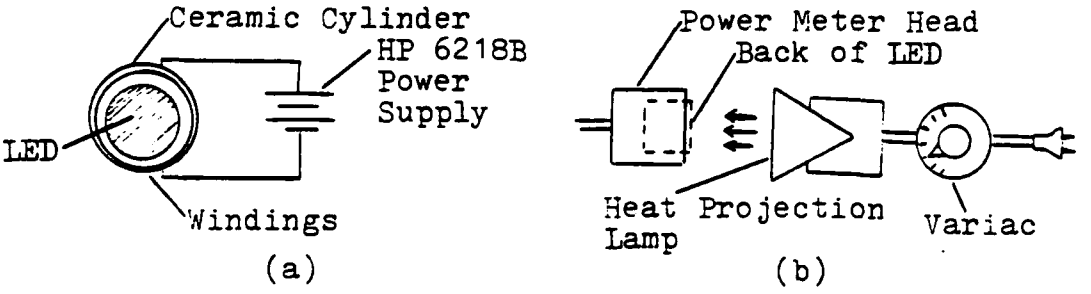

Figure 15. (a) Current Output Versus Temperature Measurement, (b) Light Output Versus Temperature Measurement

5. The Irradiation Procedure

The LEDs and photodiodes studied in this investigation were irradiated using the U.S. Naval Postgraduate School's 110 Mev linear electron accelerator. This travelling wave type accelerator is comprised of three ten foot long accelerator sections that are each powered by a twenty-two megawatt Kylstron amplifier. Figure 16 is a diagram of the linear accelerator. The Kylstrons produce radio frequency waves in 60 Hertz pulses. Each pulse lasts 2.5

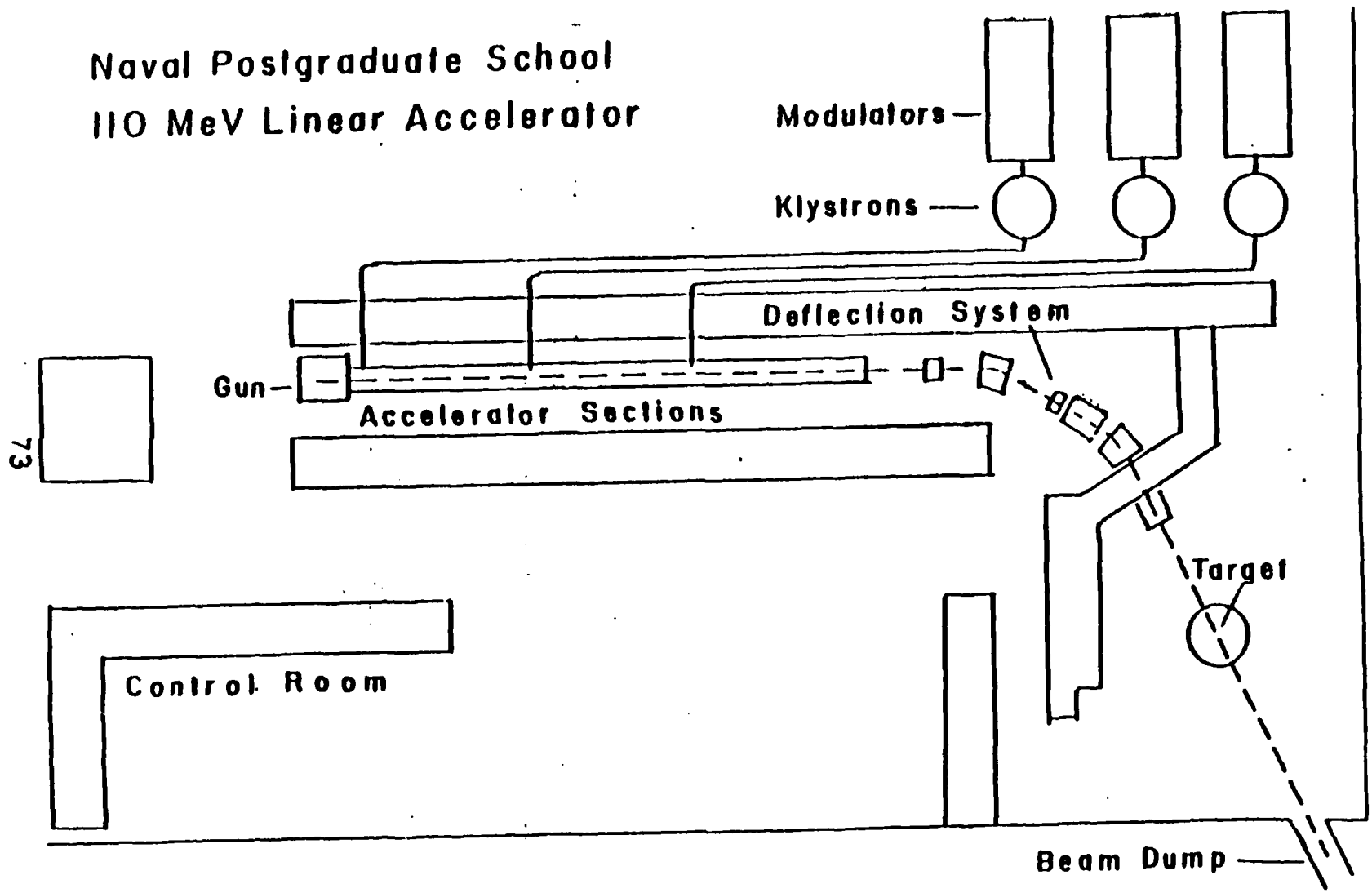

Figure 16. The NPSAI Linear Accelerator [Ref. 31]

microseconds. Electrons having an energy of 80 kilovolts are injected from the electron gun into the first accelerator section. As the electrons exit the final accelerator section, they are focused onto the target device using two quadrapole magnets. The electron beam is observed in the control room via a closed circuit television system. All irradiations were performed in a vacuum of approximately 10^{-6} Torr. Reference 31 provides a detailed description of the design and performance characteristics of the NPSAL LINAC.

In this investigation, the LEDs and photodiodes were irradiated with 30 Mev electrons. The fluence of each irradiation was calculated using a Secondary Emissions Monitor (SEM) located inside the target chamber. Wher the electron beam passes through the SEM, a charge is stored in the capacitor of the SEM. A digital voltage integrator in the control room is connected to this capacitor. The charge which accumulates in the capacitor is measured using the voltage integrator and the relationship

$$Q = Nq = cv \tag{29}$$

where Q is the total charge, N is the total number of electrons, q is the charge per electron, c is the capacitance of the capacitor and v is the accumulated voltage in the capacitor. Therefore, the total number of electrons that have passed through the SEM is

$$N = cv/q \ . \tag{30}$$

Previous research [Ref.31 and 20] has revealed that only 2.6% of the total number of electrons that pass through the SEM are counted

using this procedure. Therefore, the correct number of electrons that pass through the SEM for an accumulated SEM voltage v is

$$N = cv/(.026)q \ . \qquad (31)$$

Previously, fluence (Φ) was defined as the number of particles (electrons) per unit area. Using equation 31, the relationship between the accumulated fluence on a target and the accumulated SEM voltage is

$$\Phi = N/A = cv/(.026)qA \qquad (32)$$

where A is the cross-sectional area of the electron beam.

The calculation of the electron fluence using the above procedure is the major source of error in this investigation. The accuracy of the capacitor (±10%), the voltage of the SEM and the 0.026 efficiency factor all contribute to this error. However, the innacurate cross-sectional beam area measurements was the most significant factor.

Originally, the beam's cross-sectional area was recorded by visually observing the image of the electron beam on a phoshor screen placed inside the target chamber. In order to improve the accuracy of this procedure, Foley [Ref.20] attempted to measure the cross-sectional area by passing a horizontal wire through the beam. The wire was connected to a current integrator which produced a signal voltage when electrons were incident on it. Displacing of the wire while observing if the current integrator showed a current indicated the vertical dimensions of the beam. In order to measure the beam's

horizontal dimensions, the beam was steered through a vertical wire utilizing the quadrapole magnets used to focus the electron beam. Foley's procedure revealed that the previously used phosphor screen method was up to 30% inaccurate for one cross-sectional dimension [Ref.20]. In this investigation, further refinement of Foley's procedure resulted in an even greater accuracy of the flunce calculations.

In order to improve Foley's method of measuring the area of the beam, a motorized arm was used to move a vertical wire through the beam in the horizontal direction allowing the horizontal dimensions of the beam's cross-section to be measured. The use of the arm avoided the problems associated with steering the beam across a vertical wire as done previously. The motorized arm was attached to a stand on which the LED was mounted on during irradiations (referred to as a ladder) inside the target chamber. Figure 17 is a sketch of the ladder assembly used in the irradiation of LEDs and photodiodes during this investigation.

The vertical dimensions of the electron beam's cross-section was measured using a horizontal wire. An EASYMOVER remote control moving stage (attached to the ladder) moved the horizontal wire through the electron beam at a very slow pace, thus allowing the beam's vertical dimensions to be measured to an accuracy of one micrometer.

The results of the vertical and horizontal measurements support Foley's suggestion that the cross-sectional area of the beam is much smaller than it appears on a phosphor screen. Equation 31 reveals that an error in the measurement of the cross-sectional area of the beam is inversely proportional to an error in the calculation of electron fluence. This effect is included in the detailed error analysis of the fluence calculations provided in Appendix B.

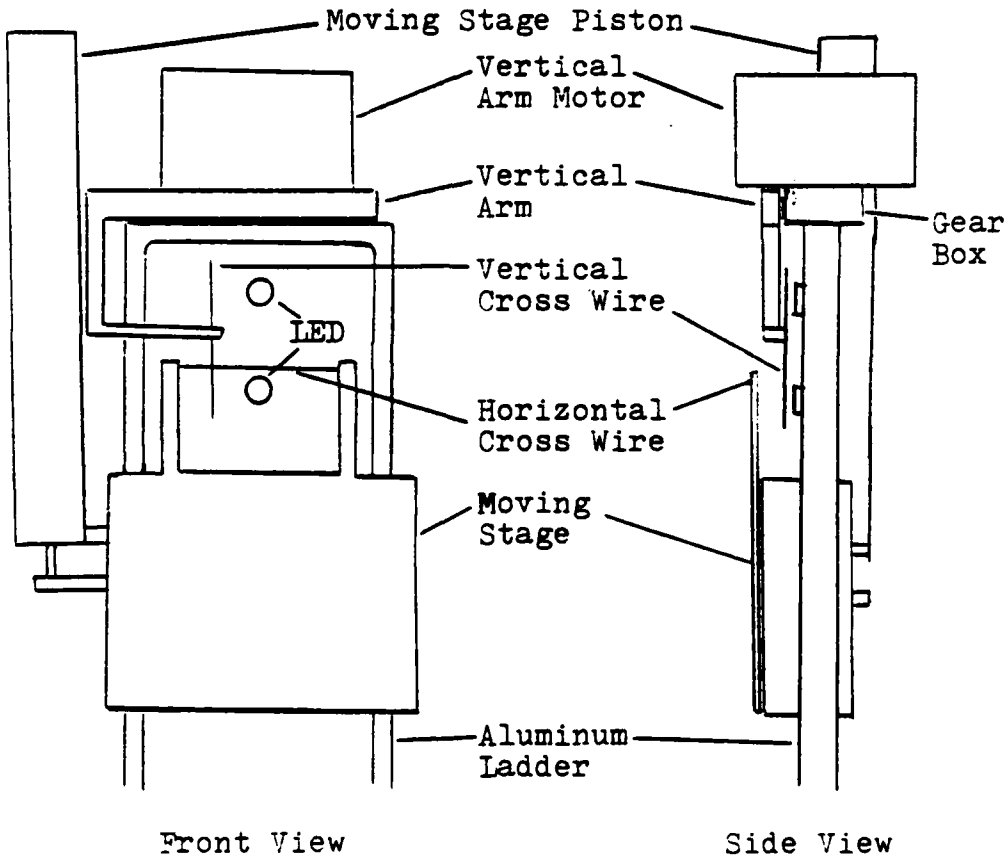

Figure 17. The Ladder Assembly

The accuracy of the electron beam's cross-sectional profile was also improved by the measurement of the beam's cross-sectional fluence intensity distribution. A Keithly 610BR Electrometer integrated the current from the cross wires in the beam and sent a voltage signal to a HP 7090A plotter which plotted the electron beam's cross-sectional fluence intensity distribution. Figure 18 is a typical plot of the intensity of the electron beam fluence versus the vertical dimension of the beam's cross-section. It is apparent that the electron beam's intensity is not uniform over it's cross-section. Therefore, the electron fluence that a device is exposed to depends on the size of the irradiated surface and the location of that surface in the beam's cross-section. Futher discussion of this is provided in Appendix B.

Measurements of the beam's cross-sectional intensity profile also revealed that the intensity of the electron beam fluctuates frequently during irradiations due to the circuit breakers connected to the vacuum pumps switching on and off. The switching of the circuit breakers interferes with the circuits of the electron gun and the focusing magnets. The pumps are essential to the operation of the LINAC and therefore must be operated during the irradiation of the devices. Appendix B provides a more detailed description of the results attained in the measurement of the profile of the electron beam.

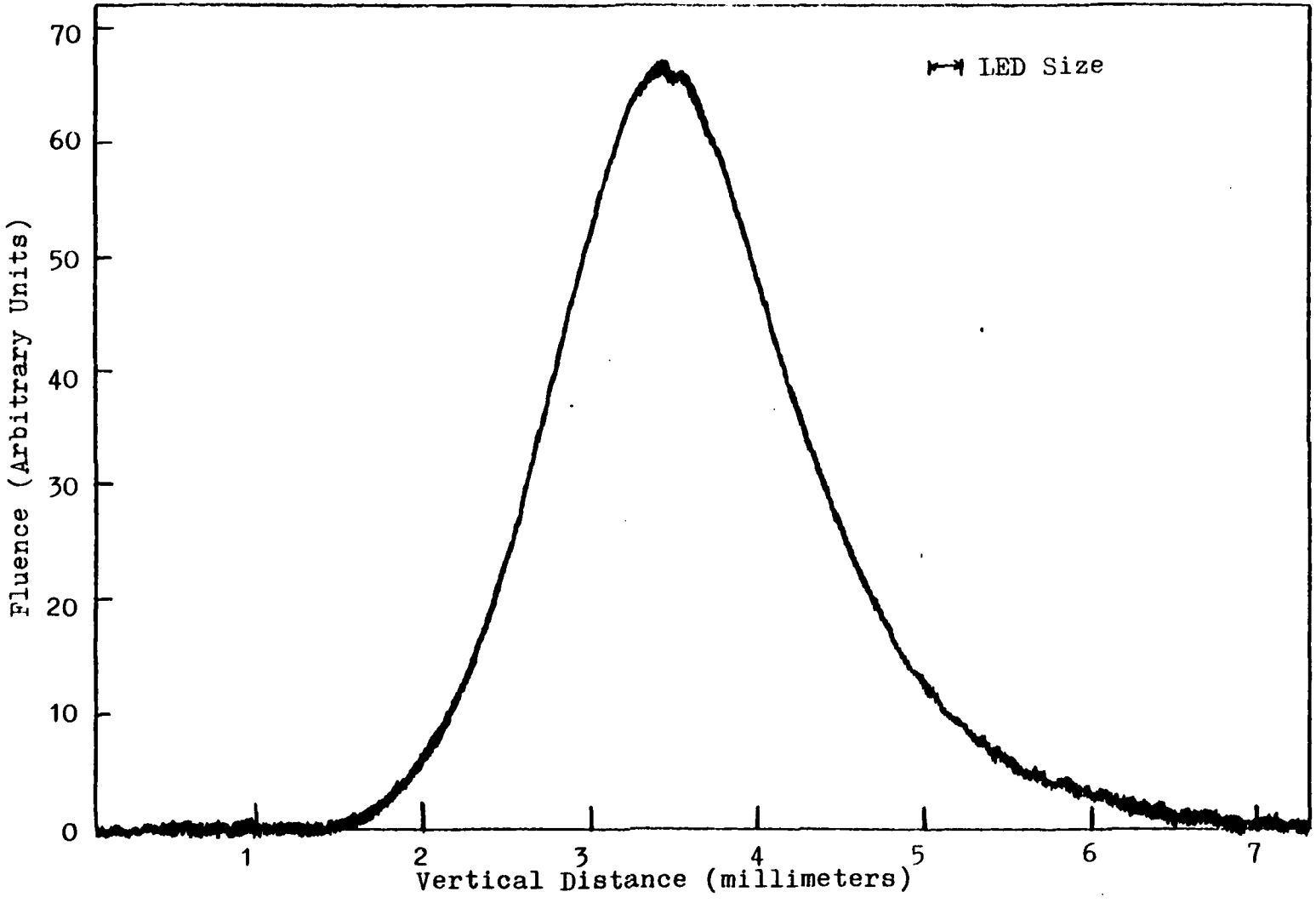

Figure 18. Electron Fluence Distribution Of LED # 4 Irradiation

6. During Irradiation LED Performance Measurements

In order to measure the rate of an LED's performance degradation during irradiation, the LED was operated and monitored while it was being irradiated. Figure 19 is a diagram of the equipment configuration used during this experiment. A constant forward bias of 1.2 volts was supplied to the LED by the HP 6002A power supply. This bias was selected in order to power the LED at a typical operating bias without approaching the manufacturer's maximum suggested operating current. This limited the effect that factors other than irradiation fluence had on the performance of the LED.

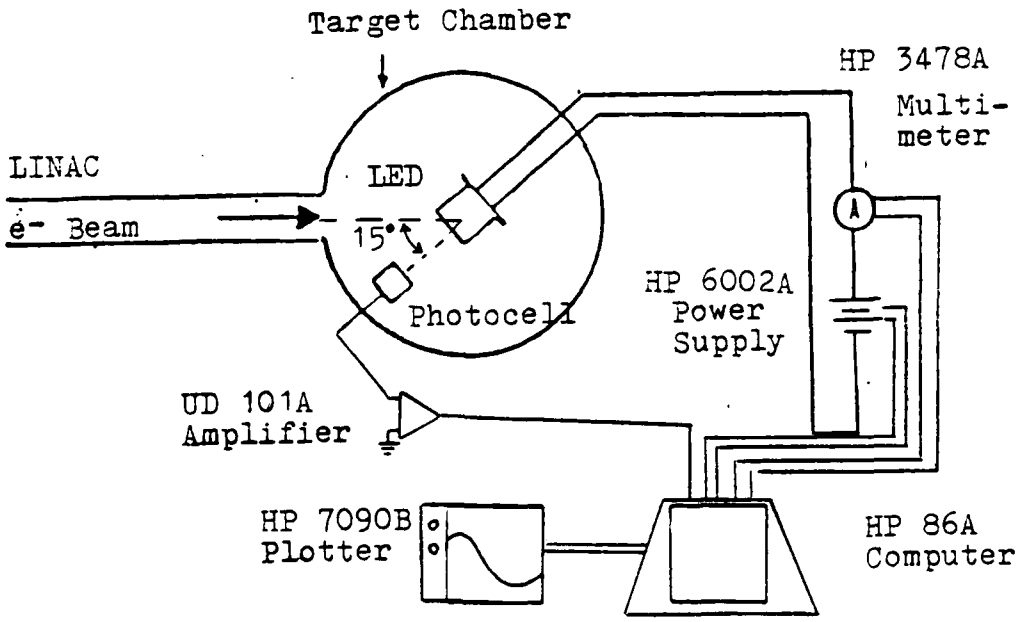

Figure 19. The During Irradiation LED Performance Measurement

While the LED was being irradiated, the output current of the LED was measured with an HP 3478A multimeter. The LED light output was measured with a Judson J16-18 infrared photodetector that was placed eight centimeters in front of the LED's emitting surface. To insure that the photodetector was not affected by the electrons that were scattered off the surface of the LED during irradiations, the responsivity of the photodetector was measured after each irradiation experiment. The signal from the infrared light detector was amplified using a United Detector model 101A amplifier (operated in the low sensitivity mode). The light detector's amplified output voltage was measured and recorded by the HP 7090 plotter connected to the HP 86A computer. Appendix C lists the computer program used to execute and record the measurements during this experiment. One thousand light output data points and five hundred current data points were recorded during each experiment.

Before irradiation, two LEDs were placed inside the target chamber in a position which maximized the light detected by the photodetector and maximized the exposure of the LED to the electron beam. Figure 20 shows that 85% of the LED's emitted light is projected within a cone seven degrees off the axis perpendicular to the center of the emitting surface. Figure 19 showed the relationship between the position of the LED, the photodetector and the electron beam. The light detector was centered on the perpendicular axis of the LED's emitting surface and the LED was positioned 15 degrees off

the central axis of the incident electron beam. Foley determined that the difference between the effects of the radiation at normal incidence and the effects of the radiation at a 15 degree angle of incidence from the normal of the LED surface could not be detected with the equipment currently used at NPSAL [Ref.20]. Thus, all irradiations were performed with the radiation at a 15 degree angle of incidence.

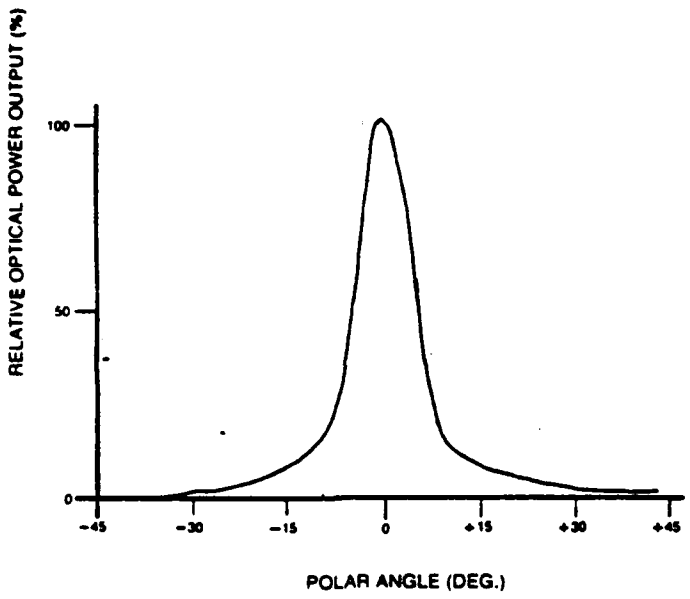

Figure 20. Radiant Intensity of the LED Versus Polar Angle [Ref.30]

As discussed previously, some of the energy that the irradiating electrons deposit in a semiconductor material is in the form of heat. Due to the limited amount of atmosphere in the target chamber to conduct this heat away from the LED during irradiation, an aluminum heat sink was attached to the LED. The heat sink had a three

square inch surface area. When compared to the temperature increase when the LEDs were operated without the heat sink, measurements showed that the use of the heat sink reduced the temperature increase of the LED during operation by an average of 40°K.

B. THE InGaAs PHOTODIODE MEASUREMENTS

1. Characteristics of the InGaAsP Photodiode

The InGaAs photodiodes that were studied in this investigation were manufactured by Epitax, Inc. (model ETX100). These photovoltaic PIN photodiodes had an advertised responsivity of 0.7 Amperes/watts at 1550 nanometer wavelengths and 0.6 Amperes/watts at 1300 nanometer wavelengths [Ref. 32]. Figure 21 is a sketch of the radiative surface area of this photodiode. The manufacturer advertises that the photodiode's performance parameters will not change for temperatures below 400°K. The glass cap of the photodiode was made from Corning 7052 glass (the same glass used in the LED cap).

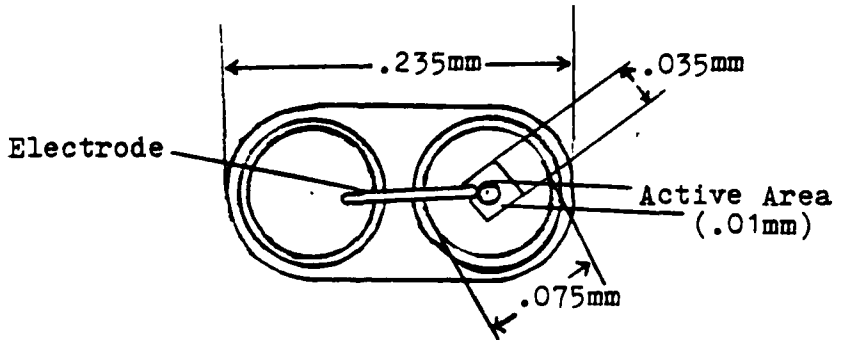

Figure 21. Top View Of Photodiode

2. Before and After Irradiation Photodiode Performance Measurements

The before and after irradiation photodiode performance measurements were similar to the LED performance measurements. The photodiodes' relative responsivity versus wavelength was measured using the same procedure that was used to measure the peak wavelength of light emitted from the LEDs. However, for these measurements the light source was the original white light source of the Beckman DK-1A spectrophotometer and the Judson J16-18A photodiode was replace by the InGaAs photodiode being measured.

Although the InGaAs photodiode is usually operated in the photovoltaic mode, current versus forward bias measurements were made in order to gain more information on the effects of radiation on these photodiodes. The procedure used to measure the current versus forward bias of the photodiodes was the same procedure used for the LED current versus forward bias measurements. Figure 22 shows the equipment configuration used for the photodiode current versus voltage measurement. The photodiodes were placed in the ceramic heater in order to prevent ambient light from effecting the measurements. The temperature of the photodiodes was 302°K for all measurements. Appendix E lists the computer program used in these measurements.

The photodiode's dark current was measured with a Kiethly 485 picoammeter while no bias voltage was applied. Ambient light was again blocked out by placing the photodiode in the heater. Due to the

very low range of current encountered in these measurements (nanoamperes to picoamperes) random noise was a significant problem. Therefore, only the order of magnitude of these measurements was considered accurate. Figure 23 shows the equipment configuration used for the photodiode dark current measurements.

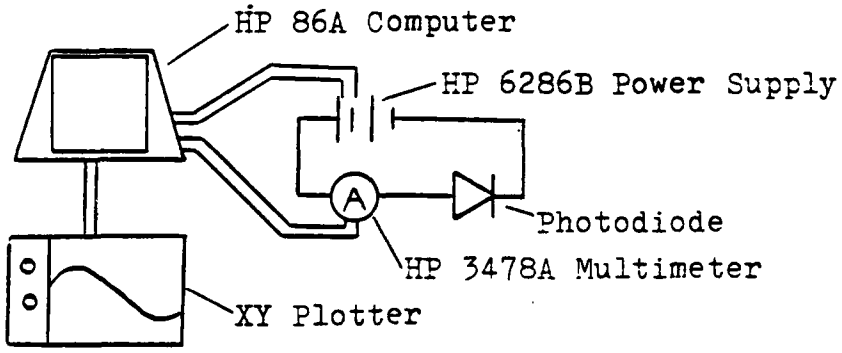

Figure 22. The Photodiode Current Measurement

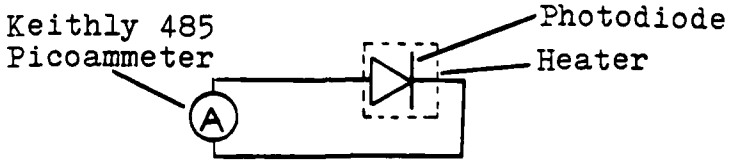

Figure 23. The Photodiode Dark Current Measurement

3. During Irradiation Photodiode Performance Measurements

The same procedure used to irradiate the LEDs was used to irradiate the photodiodes. Figure 24 shows the equipment configuration used during the measurements. The photodiodes were mounted on the ladder assembly in the same manner that the LEDs were mounted. Since the photodiodes were operated in the photovoltaic mode, no power supply was necessary. The only performance parameter measured was the photocurrent. A United Detector model 101A amplifier was used to amplify and convert the photocurrent into a signal voltage. This voltage was linearly related to the photocurrent by Ohm's Law:

$$V = IR \tag{33}$$

where V is the amplifier's voltage output, I is the photocurrent and R is the amplifier's feedback resistance (9.25 megaohms). The line resistance (1.5 ohms) in the wires between the target chamber and the control room was neglected. The amplifier's output voltage was measured with the HP 3478A multimeter and recorded with the HP 86A computer located in the control room. Appendix F lists the computer program used to execute and record the measurements. The temperature of the photodiodes during irradiation was monitored using the same method that was used during the LED irradiations.

The infrared light source used to illuminate the photodiode during irradiation was the same DYNA-LUME high intensity heat projector used to measure the temperature effect on the LEDs.

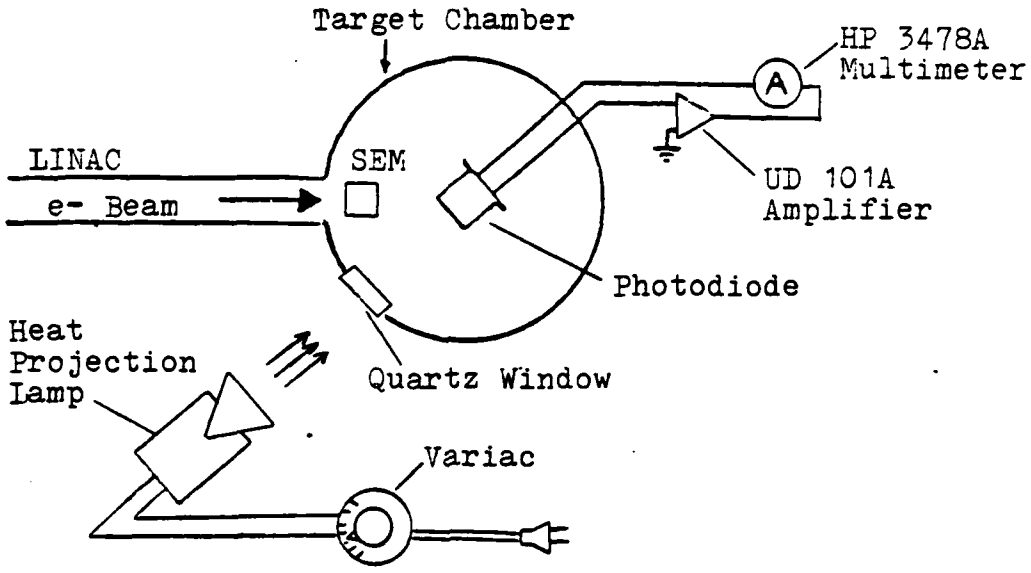

Figure 24. The During Irradiation Photodiode Performance Measurement

This infrared light source was located outside the target chamber and centered directly in front of and 90 centimeters from the photodiode. The infrared light was transmitted into the target chamber through a quartz crystal port hole. Measurements using the Fiberoptics 550 powermeter indicated that the transmission loss of the infrared light passing through the quartz crystal was less than ten percent. At this distance the infrared light source provided a uniform illumination of the surface of the photodiode's active region without increasing the temperature of the photodiode. By maintaining a constant illumination light flux (Φ_e) during the photodiode irradiations, it can be seen from equation 26 (repeated here)

$$R = I/\Phi_e \qquad (26)$$

that a decrease in the photocurrent is proportional to a decrease in the responsivity of the photodiode.

IV. RESULTS

This chapter begins with the presentation of the results on the LED. First, the measurements on the InGaAsP LEDs during irradiation are shown. The effects of temperature on LED performance (before irradiation) is included in this section. Next, the before and after irradiation LED performance measurements results are presented.

The second part of this chapter presents the photodiode performance measurements. First, the data from the during irradiation photocurrent measurements are shown. This is followed by a comparison of the before and after irradiation photodiode performance measurements. The results of the dark current measurements are included in this section.

A. THE RESULTS OF THE InGaAsP LED MEASUREMENTS

1. LED Performance During Irradiation

Seven InGaAsP LEDs powered at a constant forward bias of 1.2 volts were irradiated with 30 MeV electrons as described in the previous chapter. Plots with fluence as the independent variable were derived using the assumption that the radiation flux is constant. (Flux is defined as the flow of electrons (or any other particle) per unit area per unit time.) The validity of this assumption is discussed in Appendix B.

a. During Irradiation LED Measurement Results

LEDs number four, five, six, eight and ten had a bias of 1.2 volts applied during irradiation in order to observe the rate at which the total current increased and the light output decreased. LEDs number seven and eight were turned off during irradiation to observe the effect that the manner in which the LEDs were operated had on the radiation damage of the LEDs. Severe arcing occurred during the irradiation of LEDs number five, six, eight and ten. Therefore, only the during irradiation data for LED number four was available. First this data for LED number four will be presented, then the data from the other LEDs will be compared to it.

A plot of current output versus fluence for LED number four is shown in Figure 25. The effect of electron radiation at fluences below 10^{12} e/cm^2 was found to be negligible. A fluence of 10^{14} e/cm^2 caused an 8% increase in the output current. The rate of current increase was not constant. The greatest rate of current increase was during the first 10^{13} e/cm^2 (where the current increased nonlinearly by 3.2%). However, the curve becomes approximately linear at fluences greater than 3×10^{13} e/cm^2 where the current is given by

$$I = 63 + 2.9\times10^{-14}\,\Phi \quad \text{(milliamperes)} \qquad (32)$$

The sharp dips and peaks on the curve are fluctuations in the current over the short, tenth of a second, integration periods required by the multimeter. Allowing more time for the multimeter to integrate

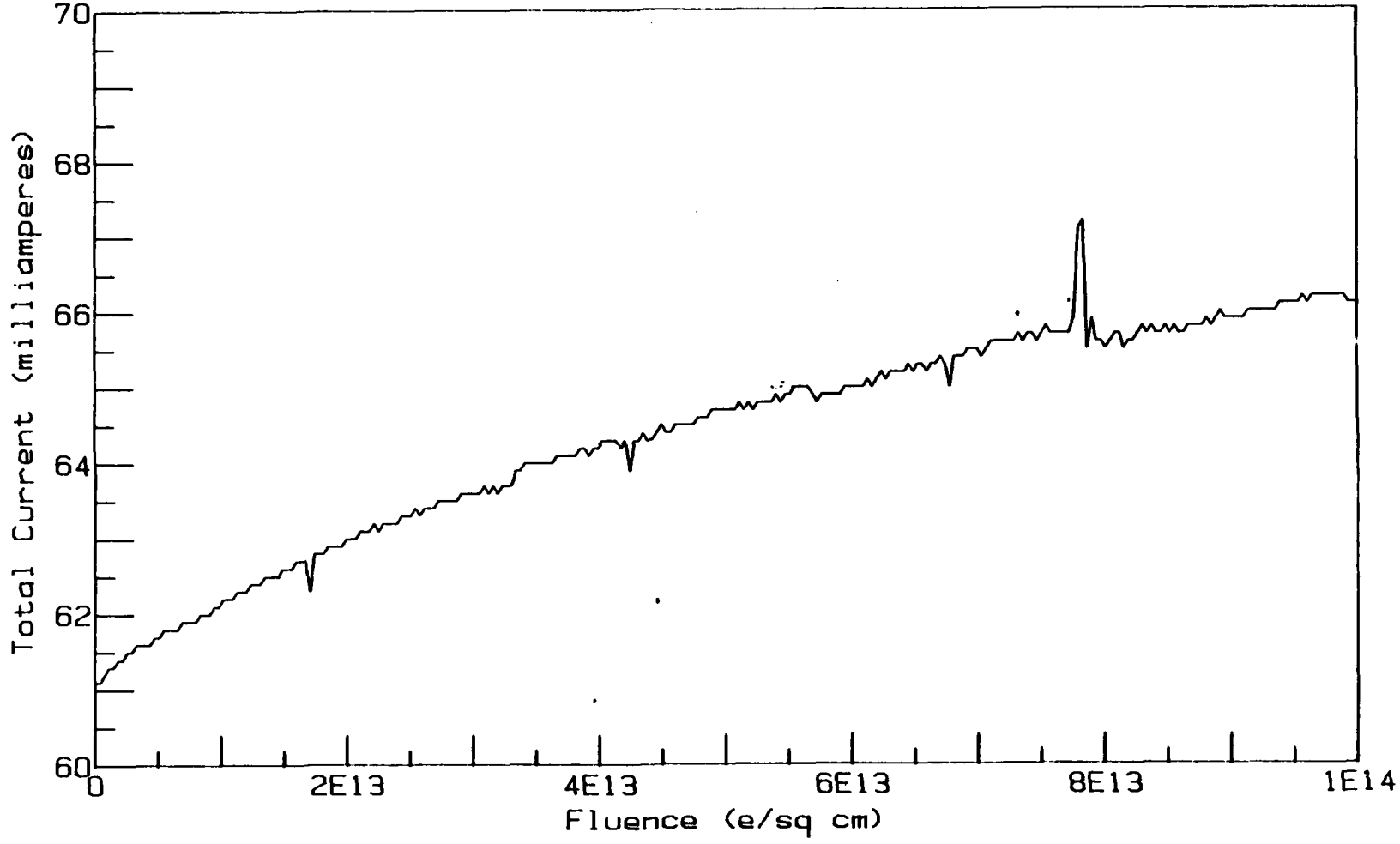

Figure 25. Total Current vs. Fluence of LED # 4

between data points would have caused fewer data points to have been taken during irradiation.

A plot of the relative intensity of the light output of LED number four versus fluence is shown in Figure 26. A fluence of 10^{14} e/cm^2 caused a 77% reduction in the light output. The rate of light output degradation decreased nonlinearly as the fluence increased. The light output decreased 33% during the first 10^{13} e/cm^2. Then the rate of light output degradation decreased significantly until the light output degraded only one percent between $9x10^{13}$ e/cm^2 and 10^{14} e/cm^2.

Table six is the results of the during irradiation measurements of LEDs number four through ten. All of the LEDs showed performance degradation rates that were similar to number four's. LEDs number six and seven and LEDs number eight and nine were irradiated with the same electron beam. Note that when compared to the other LED irradiated in the same beam, the rates of light output decrease or current increase were the largest for the LEDs that had no bias applied during irradiation.

Most annealing occurred within the first 30 seconds after irradiation. No annealing was observed after the first four minutes. This indicates that most annealing occurred before the LED has cooled down after irradiation. Table seven shows the annealing that was measured for LEDs number eight and nine.

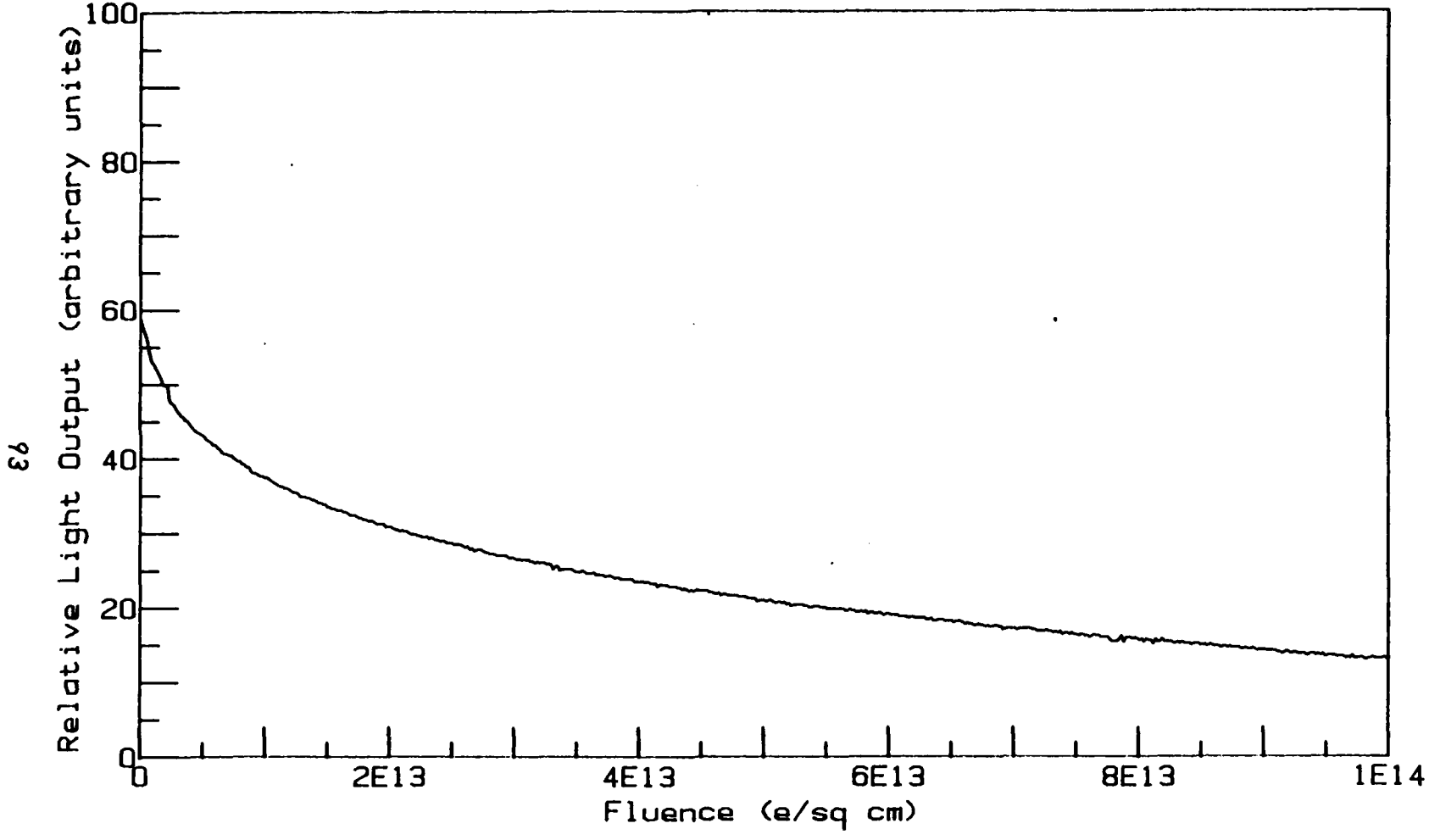

Figure 26. Relative Light Output vs. Fluence of LED#4

TABLE 6. RATE OF LED PERFORMANCE DEGRADATION (% per fluence increment)

	(cumulative fluence - e/cm^2)							
	% Light Degradation				% Current Degradation			
LED #	10^{13}	$5x10^{13}$	10^{14}	$2x10^{14}$	10^{13}	$5x10^{13}$	10^{14}	$2x10^{14}$
4	34%	43%	52%		2%	5%	6%	
5*			63%				7%	
6*			51%				3%	
7**			53%				26%	
8	23%	46%	67%	90%	3%	9%	15%	28%
9**	47%	76%	87%	94%	5%	15%	23%	38%
10	44%	61%	69%	77%	4%	9%	13%	19%

* indicates that irradiation was done in one increment

** indicates that no bias was applied during irradiation

TABLE 7. ANNEALING OF LEDS #8 AND #9 *

	LED #8 (% annealed)**		LED #9 (% annealed)**	
Fluence (e/cm^2)	Light	Current	Light	Current
10^{13}	4%	1.5%	2%	1%
$5x10^{13}$	6%	2%	4%	4%
10^{14}	5%	4%	3%	4%
$2x10^{14}$	2%	3%	1%	6%

* four minutes after irradiation

** % of initial values

b. The Results Of The Measurement Of The Effect Of Temperature On LED Performance

In order to know how the temperature increase during irradiation affects the current measurements, the effect of the temperature on the total LED current was measured using four InGaAsP LEDs. The effects on the current versus bias curves of LEDs number three and seven as the temperature was increased are shown in Figures 27 and 28. The dependence of the temperature effects on current is apparent. Figure 27 shows that at 1.2 and 1.3 volt bias the current of LED number three increased 4% and 2% respectively when the temperature increased 29°K. However, at a 0.5 volt bias, this temperature increase caused a 184% current increase. Similarly, Figure 28 shows that at 1.2 and 1.3 volt bias the current of LED number seven increased 4% and 2% respectively when the temperature increased 34°K. At 0.5 volt bias, this temperature increase caused a 156% current increase.

After a temperature increase (and subsequent cooling) of 31°K and 46°K respectively, Figures 29 and 30 show that LEDs number four and eight had no permanent change in their current output. Likewise, after LEDs number three and seven cooled down to their original temperatures, they also exhibited current versus voltage curves identical to their original current versus voltage curves. Therefore, no permanent effects on current due to temperature were measured.

AD-A173 617 EFFECTS OF 30 MEV ELECTRON IRRADIATION ON INGAASP LEDS 2/2
(LIGHT EMITTING DIODES) AND INGAAS PHOTODIODES(U) NAVAL
POSTGRADUATE SCHOOL MONTEREY CA P J O'REILLY JUN 86
UNCLASSIFIED F/G 20/12 NL

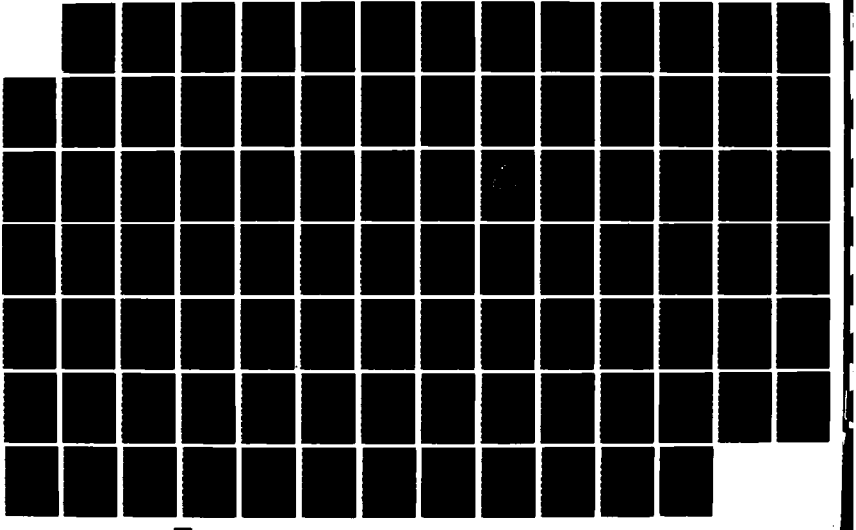

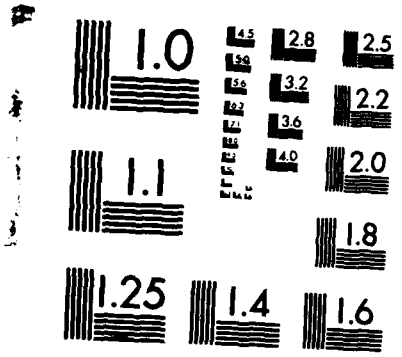

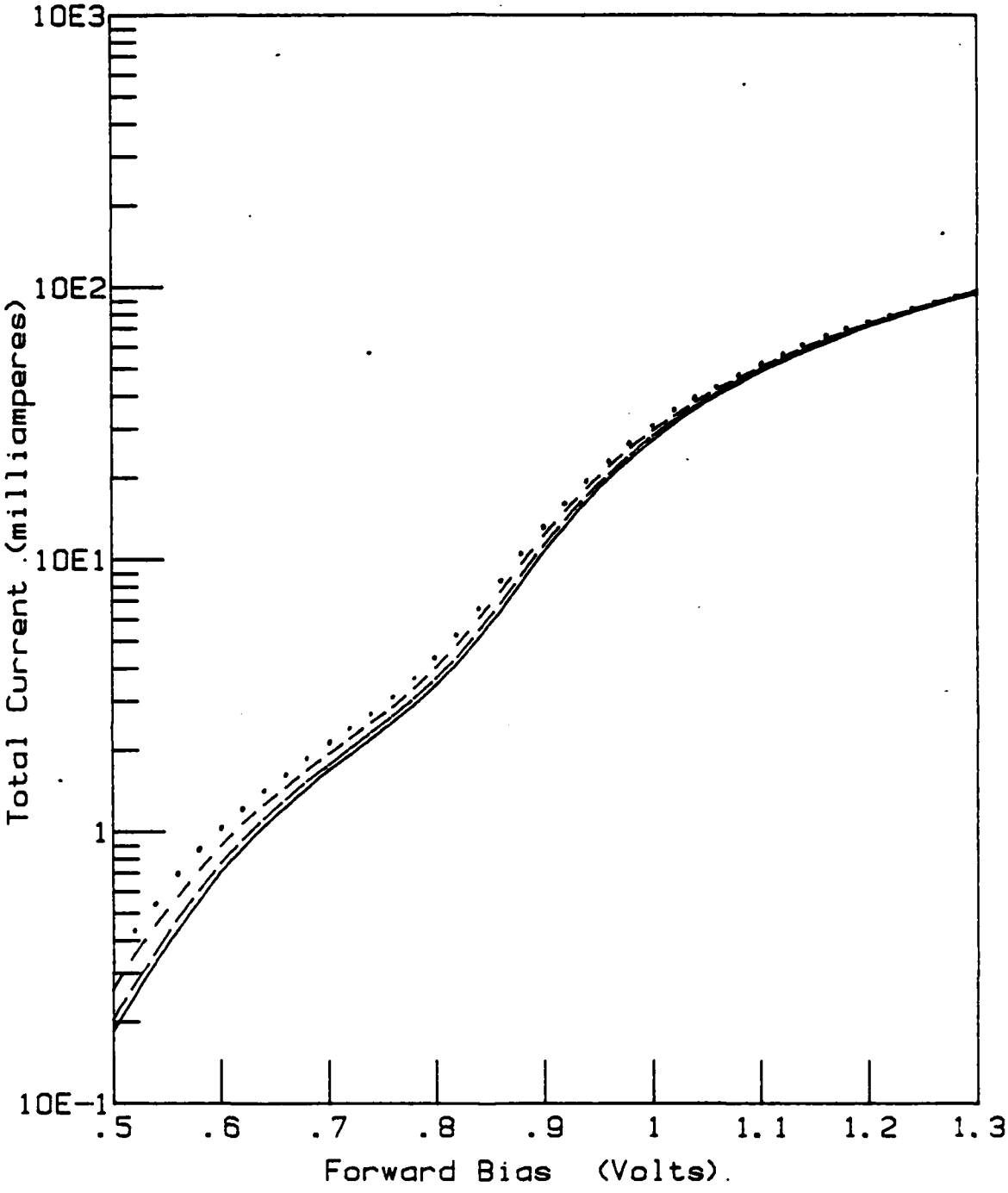

Figure 27. Temperature Effect on LED # 3 Current.

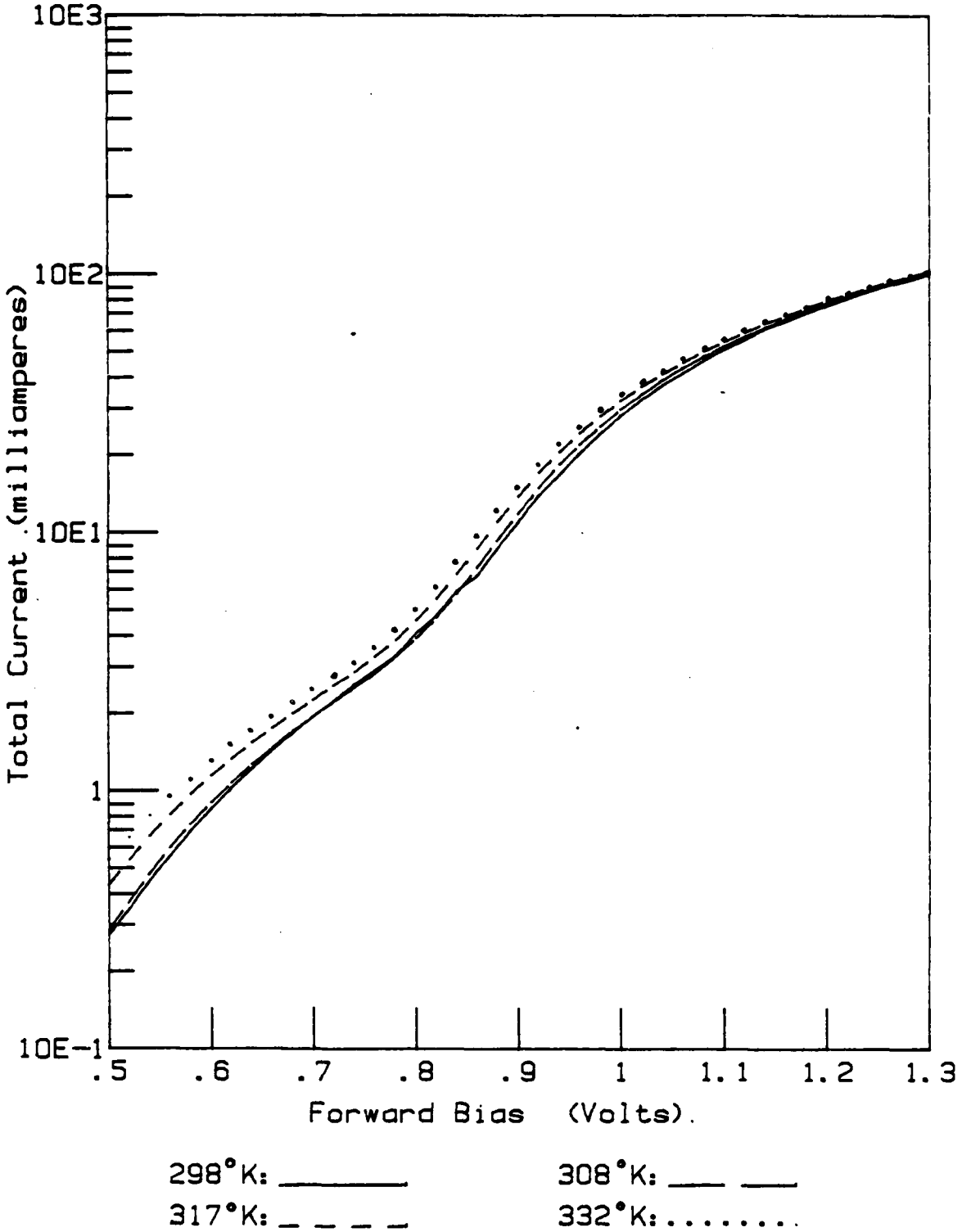

Figure 28. Temperature Effect on LED # 7 Current.

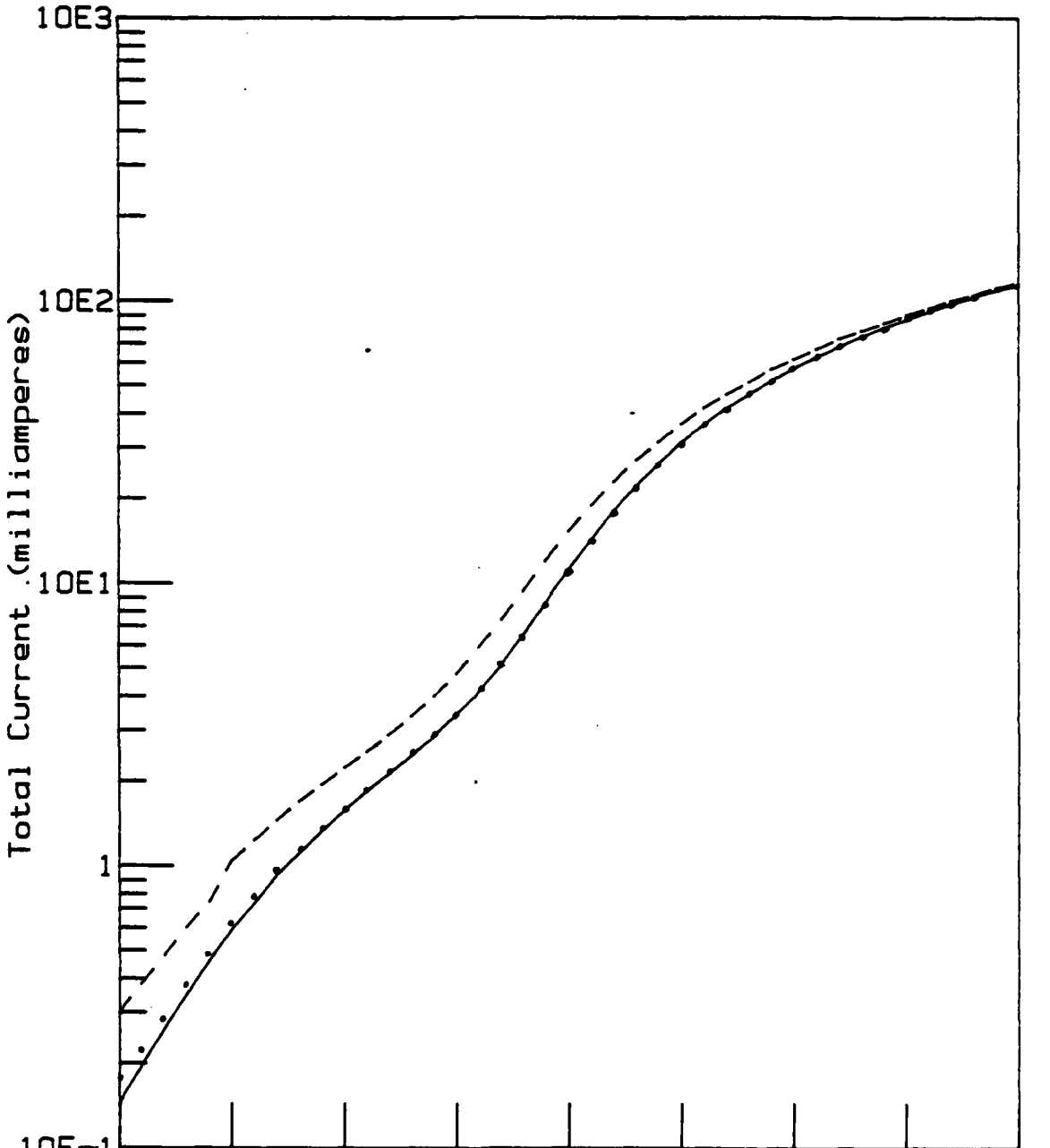

297°K : ____ 328°K : _ _ _

295°K : ..... (after cooling).

Figure 29. Temperature Effect on LED # 4 Current.

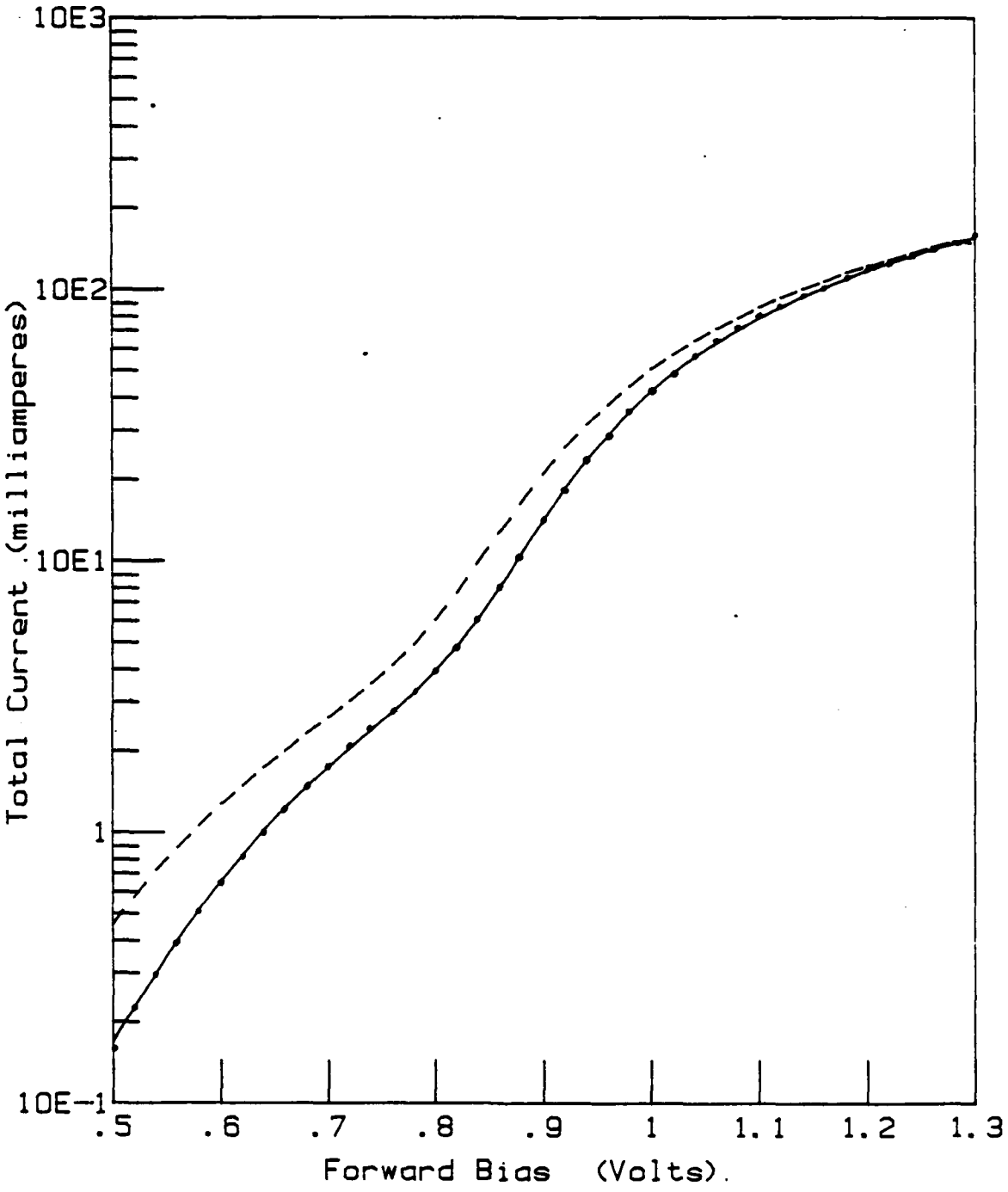

299°K : ____ 345°K : _ _ _

299°K : ..... (after cooling).

Figure 30. Temperature Effect on LED # 8 Current.

The increase in temperature was the largest during the first $2x10^{13} e/cm^2$ of each irradiation. The temperature increase of LED number four is shown in Figure 31. The initial large increase in temperature indicated that the temperature might have caused the initial large increase in the effect of radiation on LED number four's

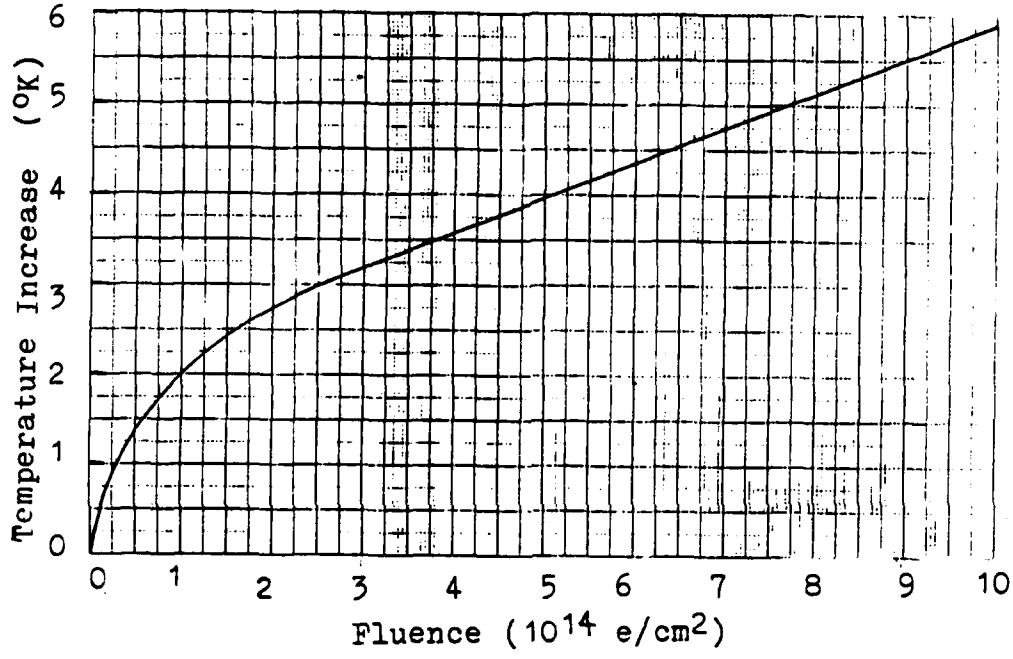

Figure 31. Temperature of LED # 4 During Irradiation

total current. However, the results of the temperature effect measurements presented previously show that the effect of a 6° K temperature increase on the LED current at 1.2 volts forward bias is less than 0.3% (which is less than the accuracy of the current measurements). Since the maximum LED temperature increase recorded during any irradiation of $10^{14} e/cm^2$ was 6°K, the effect of temperature on the LED current measurements was neglected.

The effect of temperature on the light output versus bias curves for LEDs number three, four and five were measured using the procedures described in Chapter three. The effect on the light output versus bias curve of LED number three as the temperature increased is shown in Figure 32. (Below 0.7 volts bias, the 321°K and the 331°K light output curves are inaccurate due to the effect of the bright infrared lamp used to heat the LEDs during this measurement and thus are not shown.) Again, the effect of temperature is bias dependent. For biases below 0.94 volts, the light output increases with temperature. However, for biases greater than 0.94 volts the light output decreases with temperature.

After increasing the temperature of LEDs number four and five by 31°K and 33°K and then letting them cool, there was no permanent change in the light output versus bias curves. Figure 33 shows that an increase of 31°K caused a 18% and 16% decrease in the light output of LED number four at 1.2 and 1.3 volts bias respectively. Figure 34 shows that an increase of 33°K caused a 24% and 25% decrease in the light output of LED number five at 1.2 and 1.3 volts respectively. After cooling, the light output returns to the initial values.

In conclusion, the effect of temperature on the LED current versus fluence curve was negligible (Figure 25). However, temperature effects should be considered when measuring the light output intensity versus fluence (Figure 26). The temperature increase

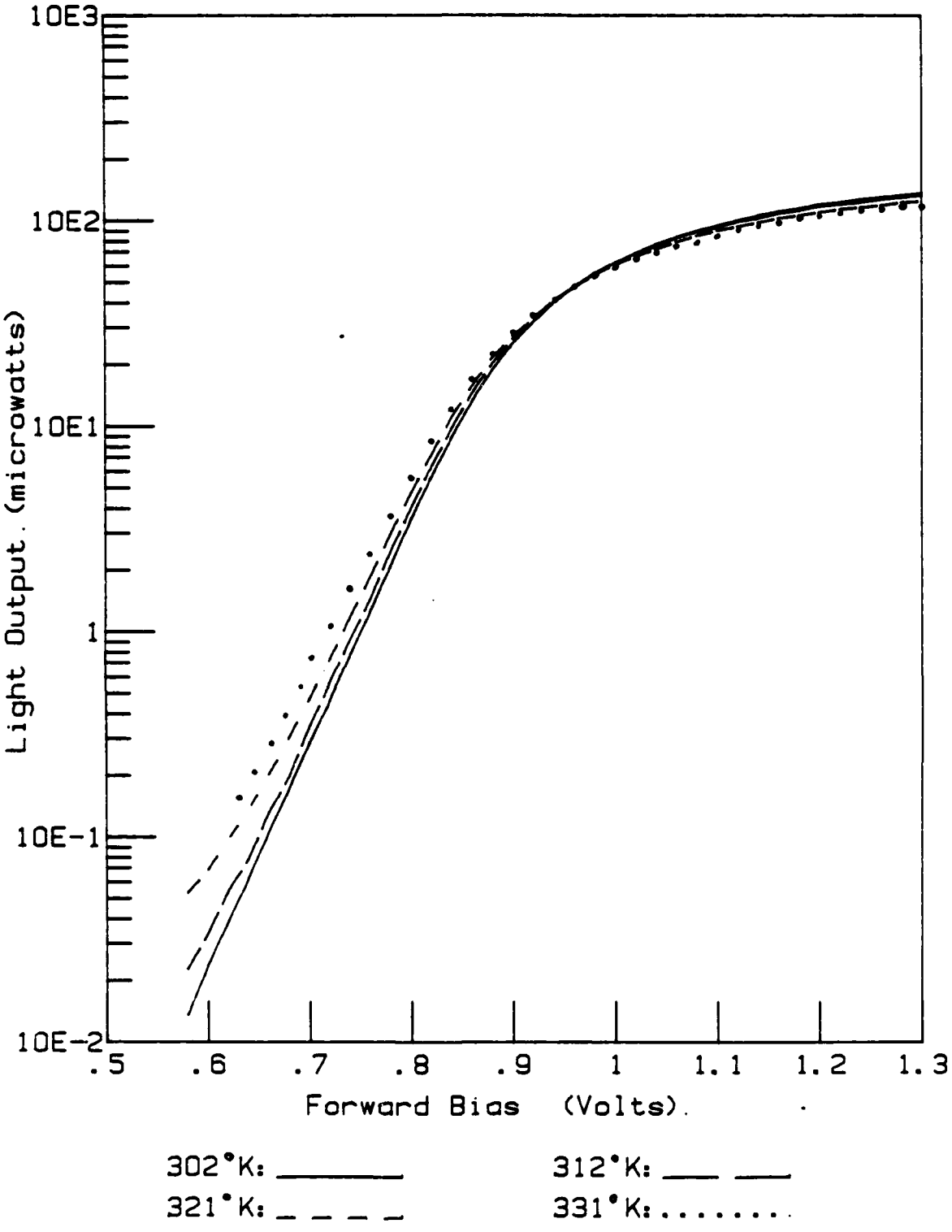

Figure 32. Temperature Effect on LED # 3 Radiance.

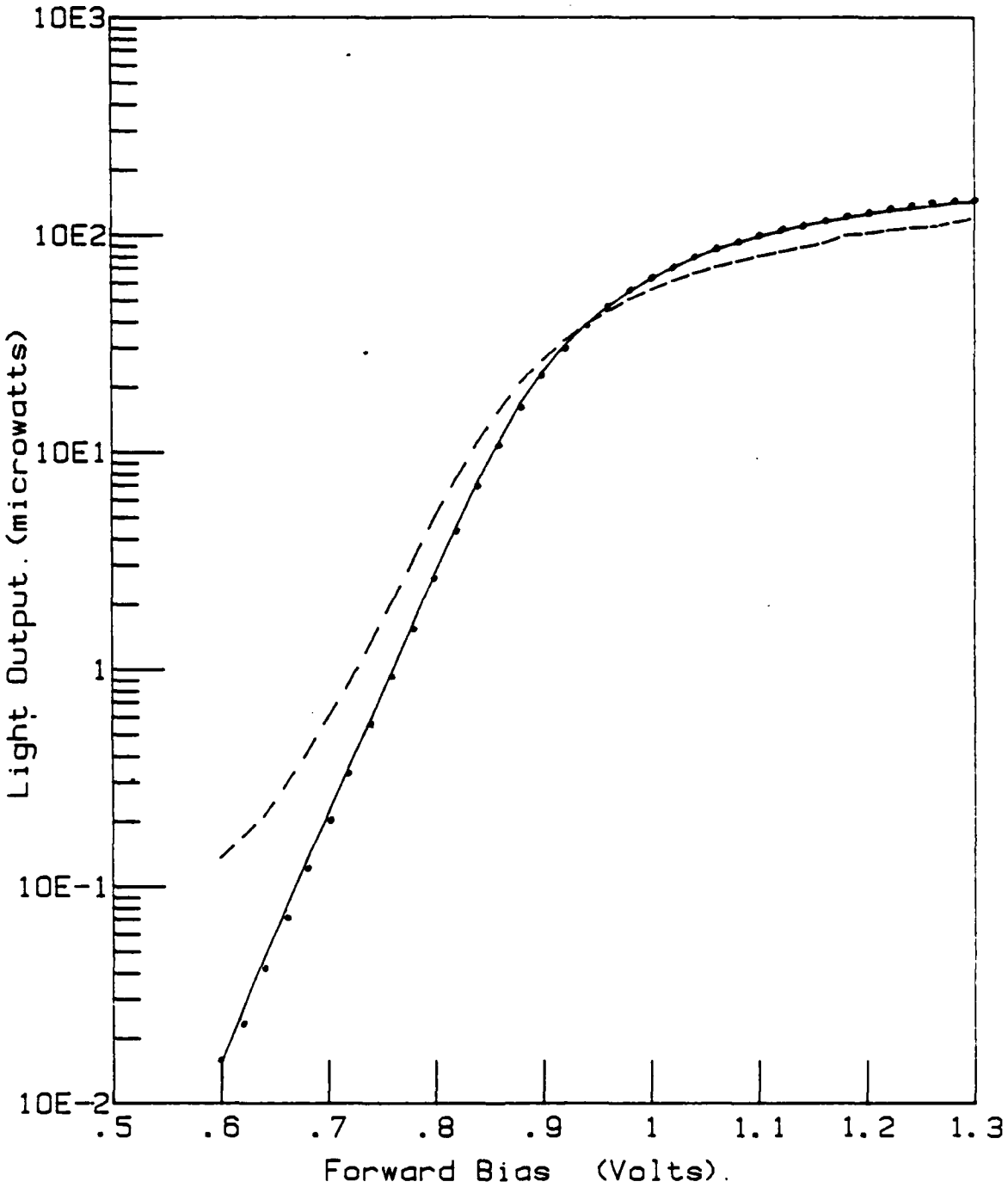

Figure 33. Temperature Effect on LED # 4 Radiance.

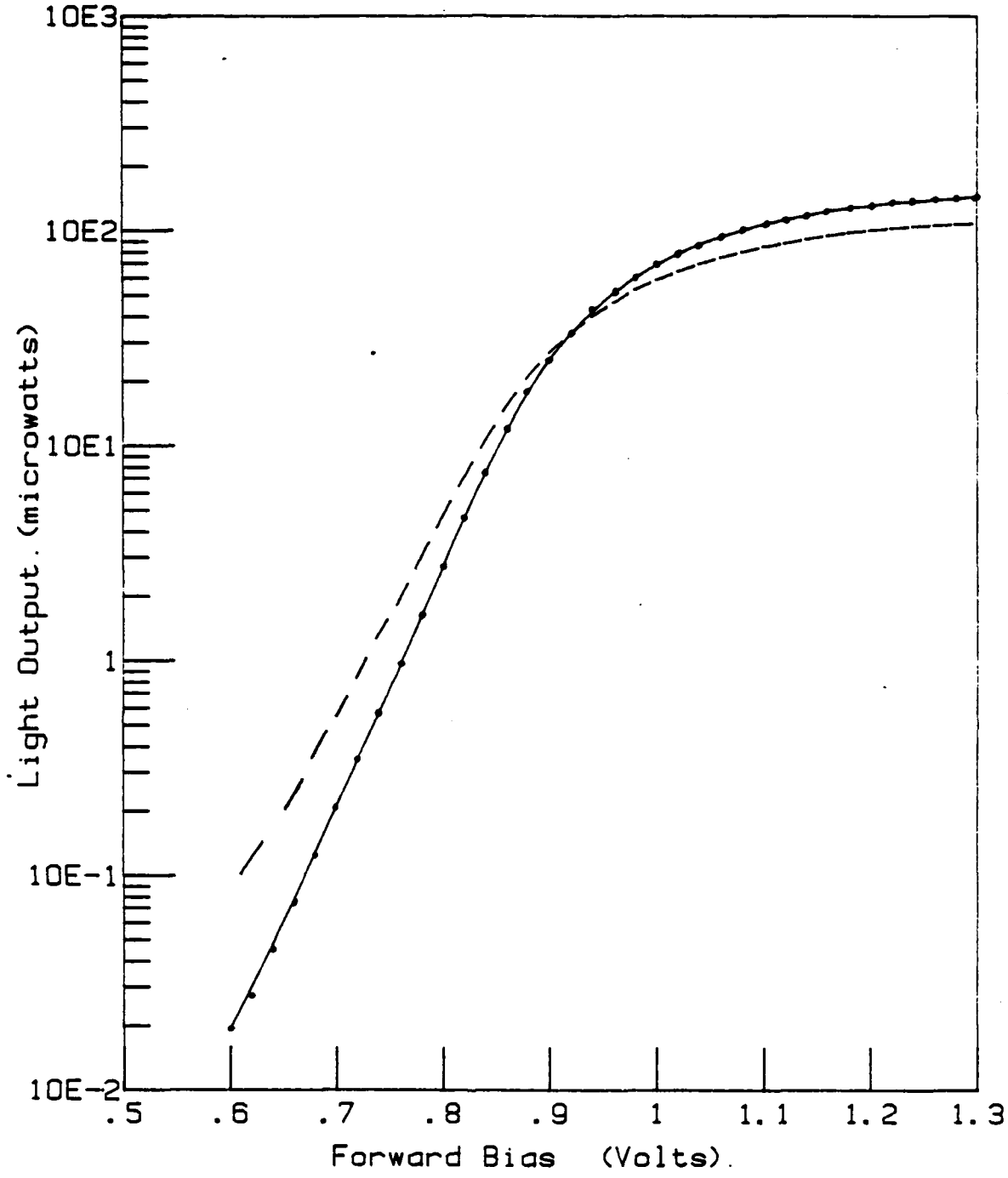

297°K: _____ 330°K: _ _ _ _

297°K: ..... (after cooling).

Figure 34. Temperature Effect on LED # 5 Radiance.

of LED number four accounted for 5% of the light decrease at $10^{14} e/cm^2$. Note, however, that the effect of the temperature increase was less than the fluence measurement uncertainties discussed in Appendix B.

2. LED Performance Before and After Irradiation

a. Radiation Effects on LED Current

The current measurement results on LED numbers four through ten before and after irradiation are shown in Figures 35 through 39. For comparison purposes, the current versus bias curves for all of the LEDs are shown in Figure 35. LEDs number eight, nine and ten were irradiated to $2x10^{14} e/cm^2$. The other LEDs were irradiated to $10^{14} e/cm^2$. LEDs number seven and nine had no bias applied during irradiations. Note that the after irradiation curves are much less uniform than the before irradiation curves.

The radiation effects on current were much greater at low biases than at high biases. At 0.5 volts forward bias, LED number four's and five's current increased 3000% and 440% respectively; however, at a forward bias of 1.3 volts, the LEDs' current increased only 10% and 8% respectively. Table eight shows that the radiation damage on the other LEDs had a similar dependence on bias. However, the dependence of the radiation damage on bias was less significant than the nonuniformity between devices.

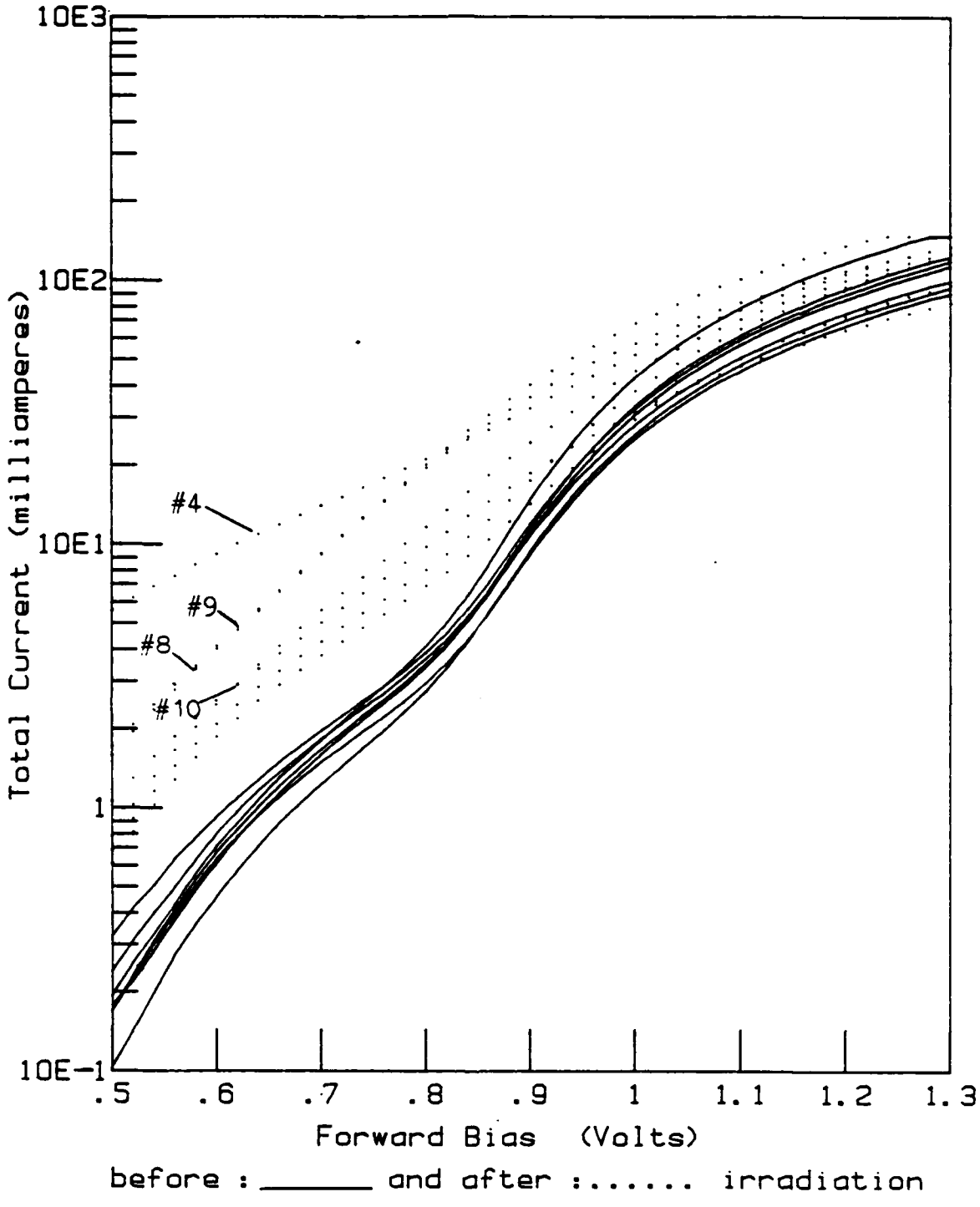

Figure 35. Summary of Radiation Effects on LED Current.

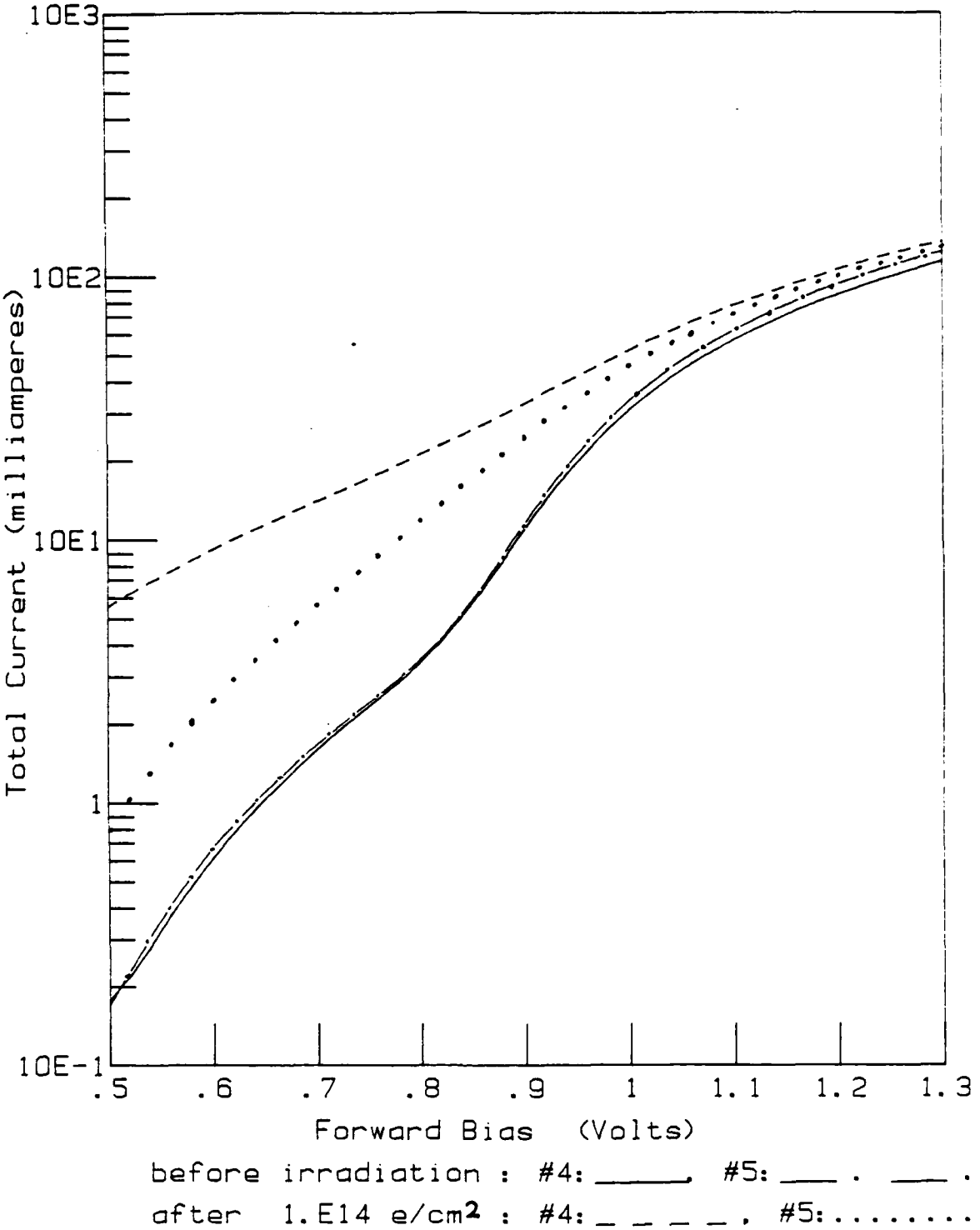

Figure 36. Radiation Effect on LEDs # 4 & 5 Current

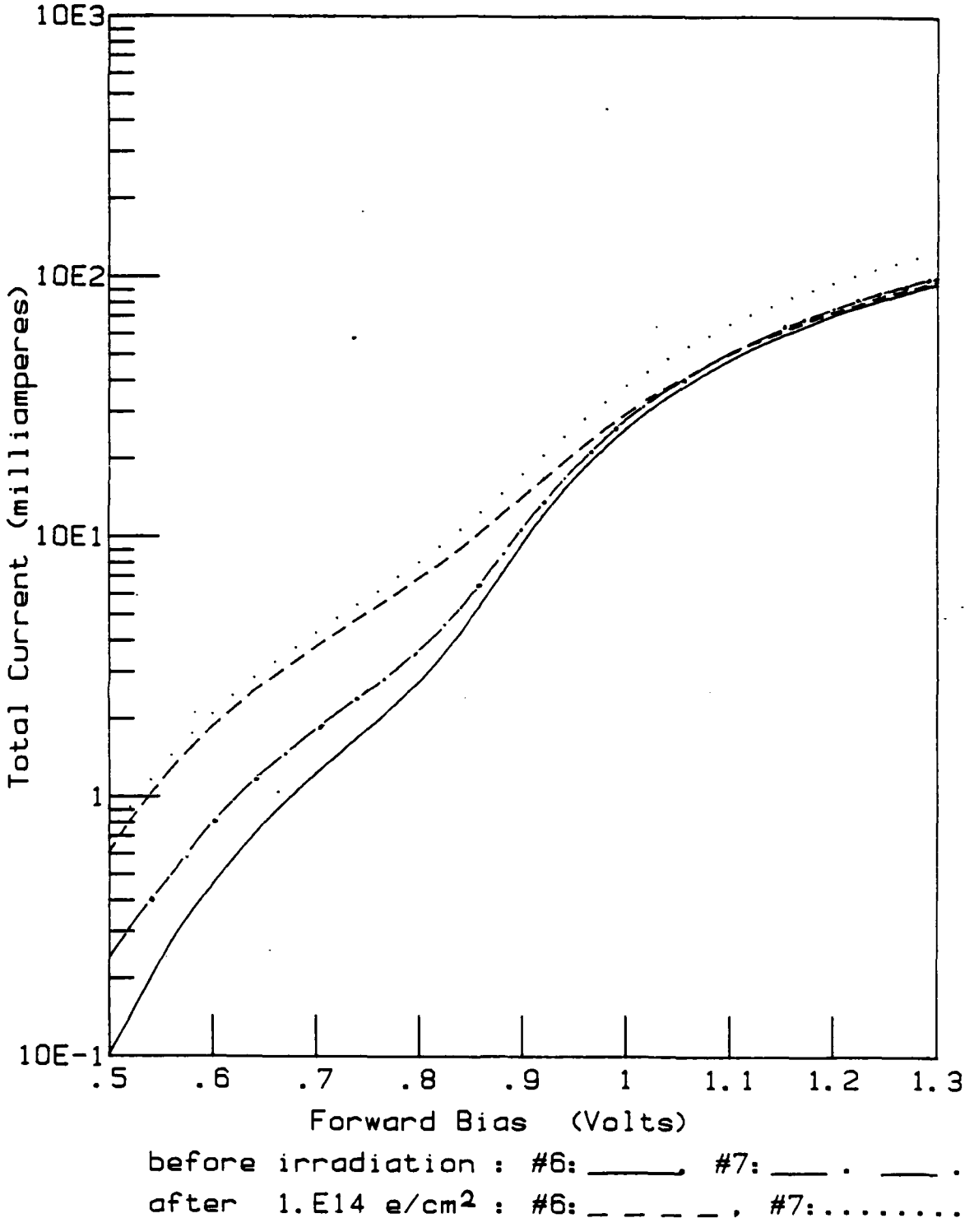

Figure 37. Radiation Effect on LEDs # 6 & 7 Current

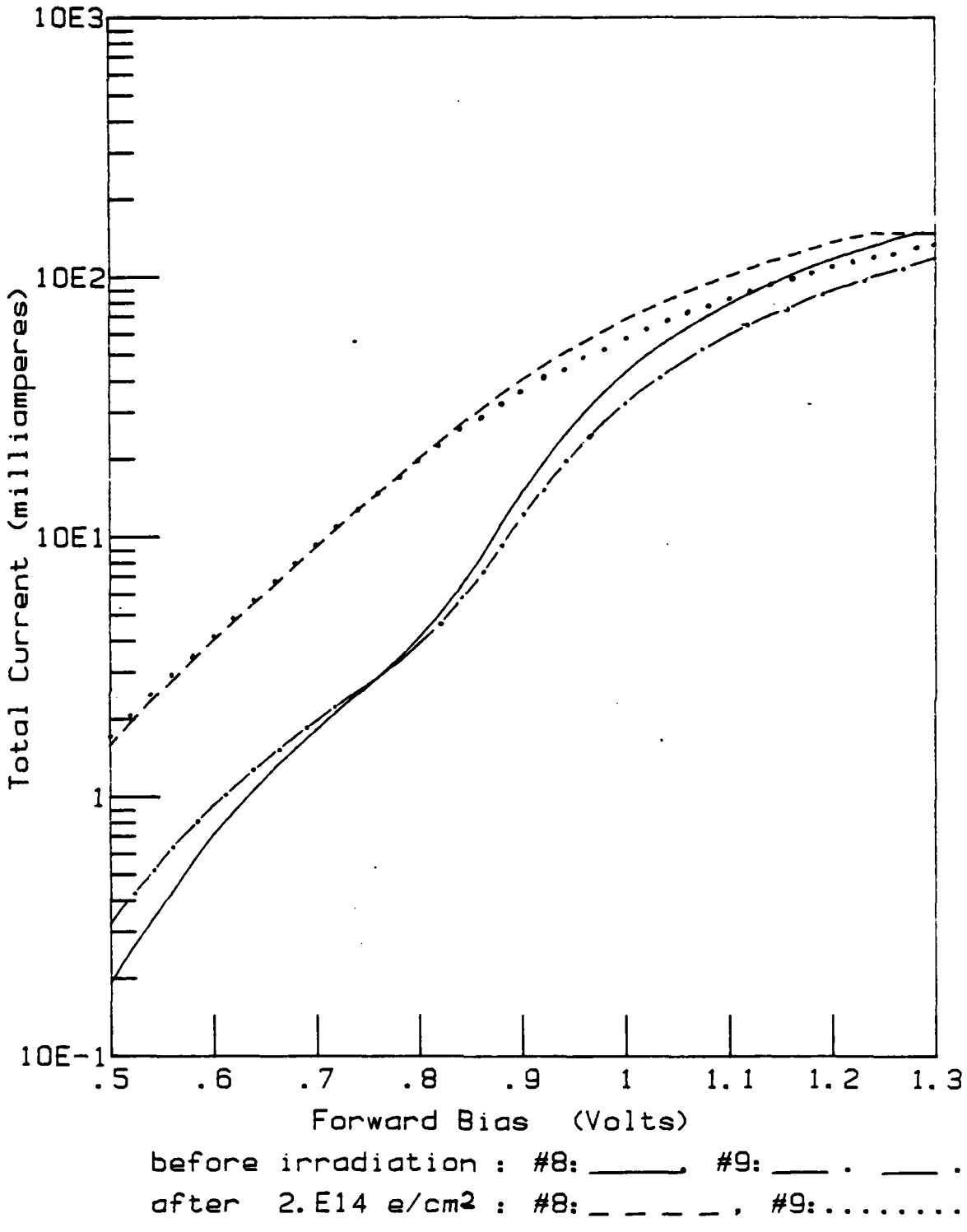

Figure 38. Radiation Effect on LEDs # 8 & 9 Current

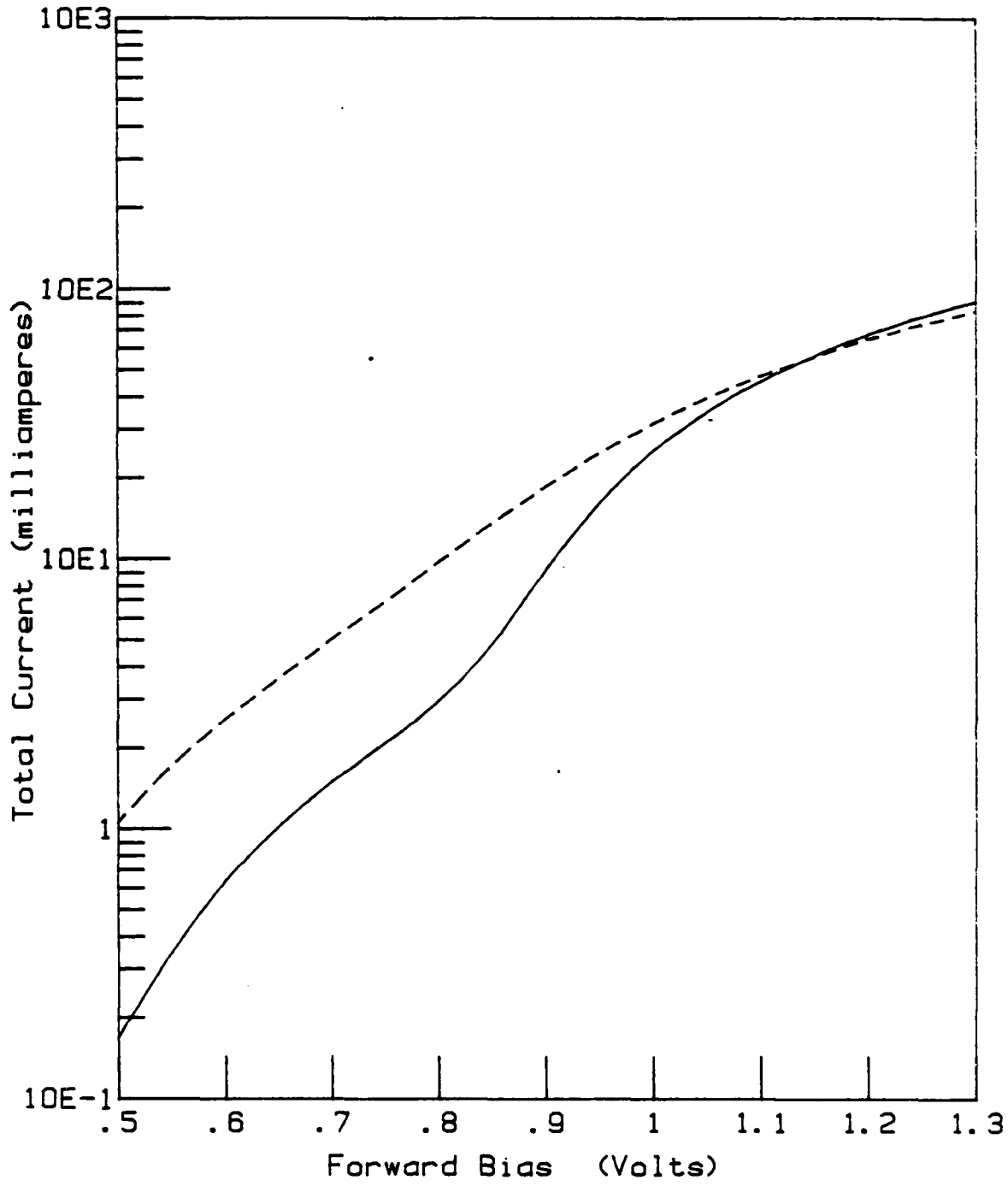

before: _____ and after: _ _ _ irradiation of 2.E14 e/cm^2

Figure 39. Radiation Effect on LED # 10 Current

TABLE 8. LED PERFORMANCE BEFORE AND AFTER IRRADIATION

LED #	Fluence (e/cm^2)	% Current Decrease Bias: 1.2 volts	1.3 volts	% Light Output Decrease 1.2 volts	1.3 volts
4	10^{14}	6%	10%	52%	57%
5	10^{14}	7%	8%	63%	61%
6	10^{14}	3%	2%	51%	48%
7*	10^{14}	26%	25%	53%	41%
8	$2x10^{14}$	23%	11%	90%	82%
9*	$2x10^{14}$	23%	13%	94%	91%
10	$2x10^{14}$	13%	8%	77%	73%

* indicates that no bias was applied during irradiation

b. Radiation Effects on LED Light Output

The light output versus bias measurements of LEDs number four through ten before and after irradiation are shown in Figures 40 through 44. The light out put versus bias curves for all the LEDs are shown in Figure 40. LEDs eight, nine and ten were irradiated to $2x10^{14}$ e/cm^2 and the other LEDs were irradiated to 10^{14} e/cm^2. Note that the before irradiation curves are more uniform than the after irradiation curves. Above 0.9 volts, the curves bend over indicating that a large part of the voltage was being dropped across the bulk regions instead of across the p-n junction.

c. Radiation Effects on the Wavelength of the Peak Emitted Light

A plot of the relative light output intensity versus wavelength of LED number four (before and after irradiation of 10^{14}

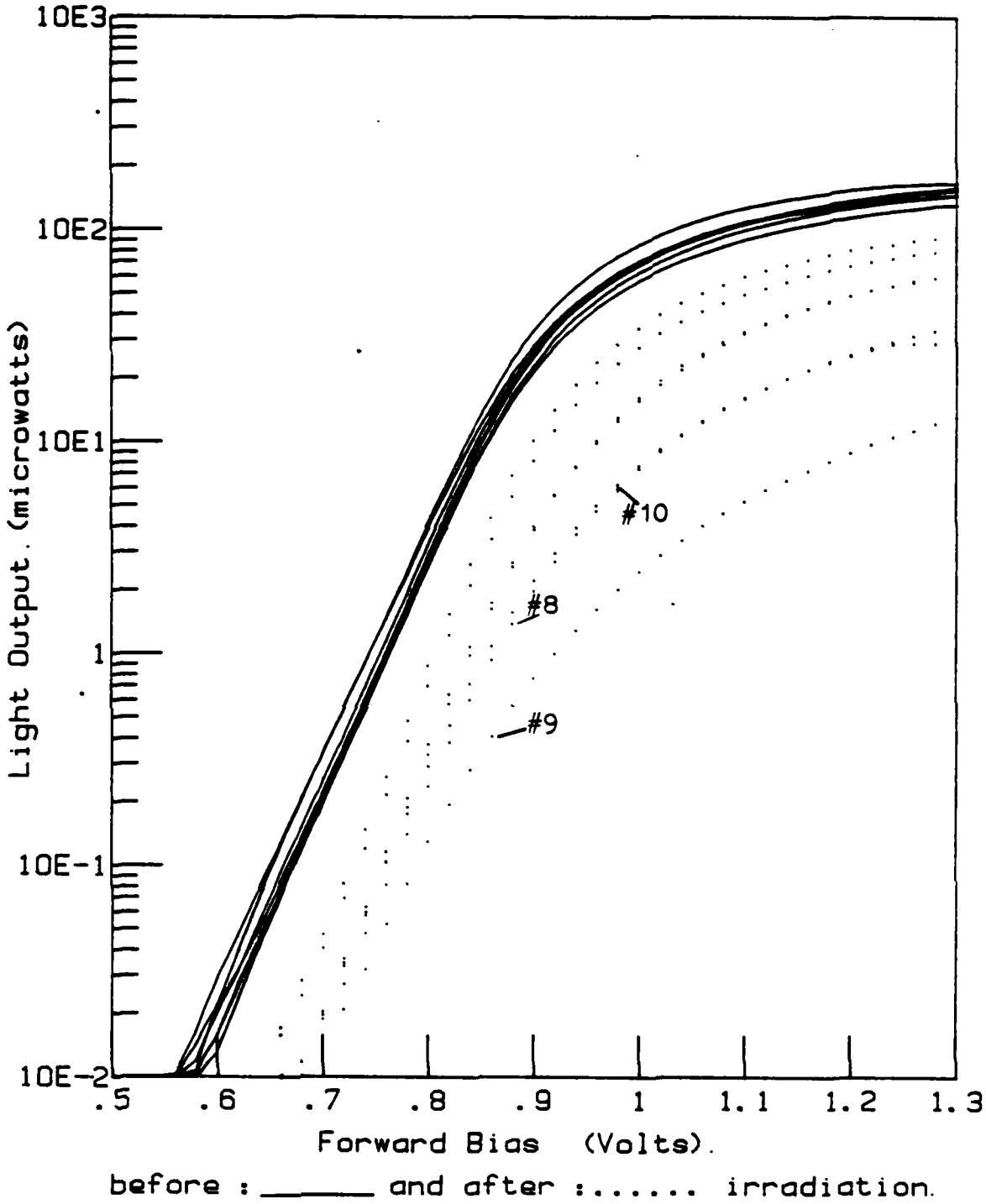

Figure 40. Summary of Radiation Effects on LED Radiance.

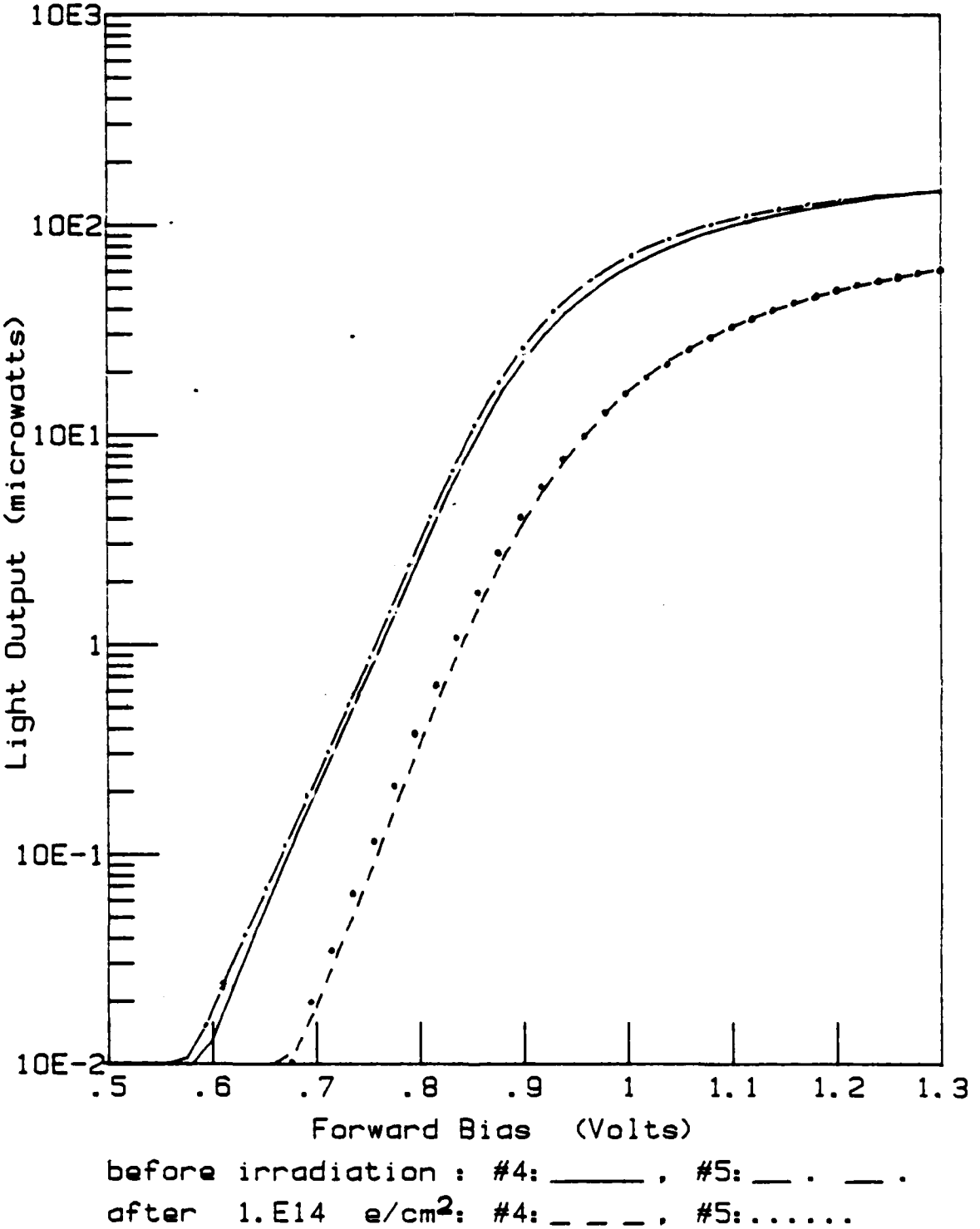

Figure 41. Radiation Effect on LEDS # 4 & 5 Radiance

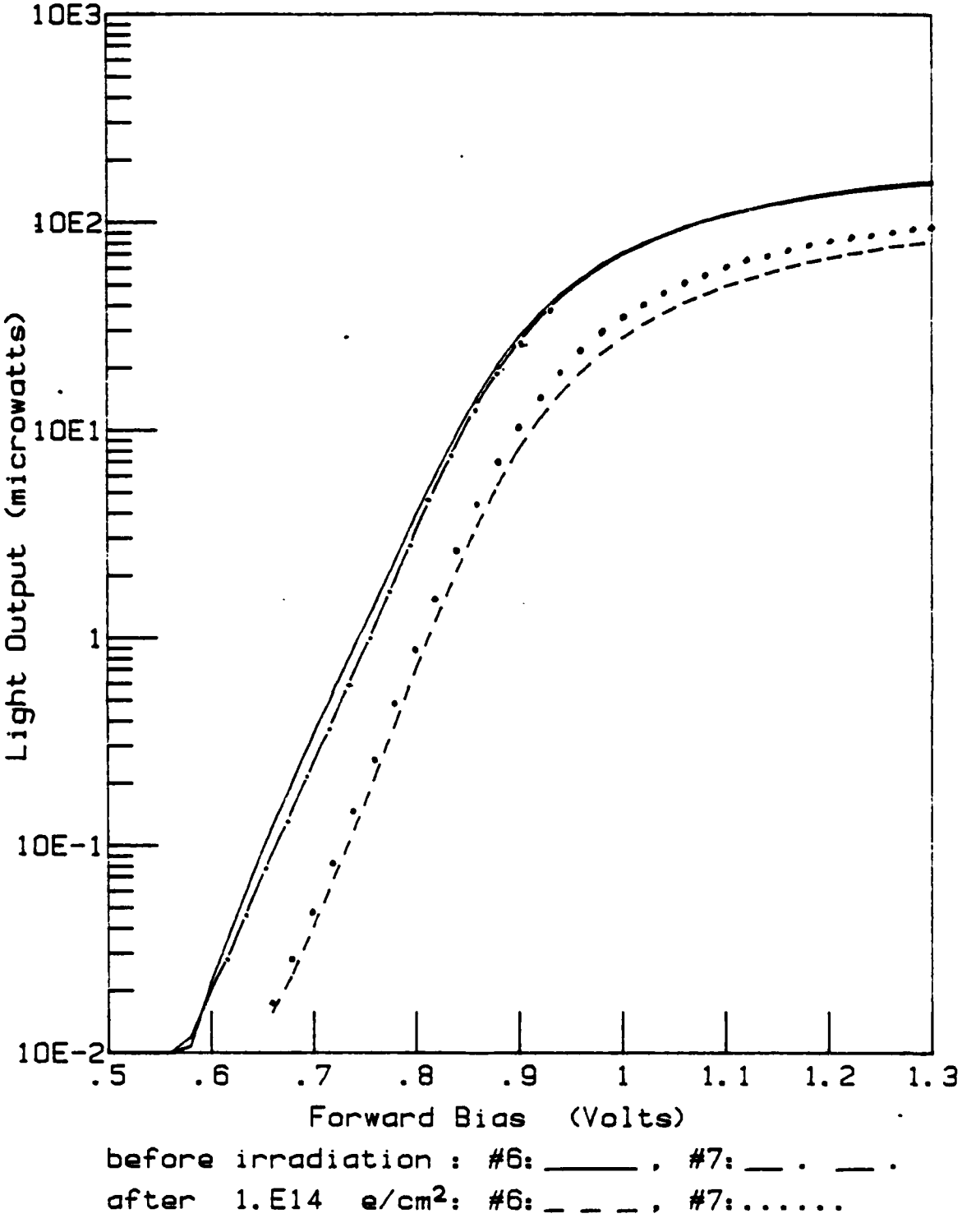

Figure 42. Radiation Effect on LEDS # 6 & 7 Radiance

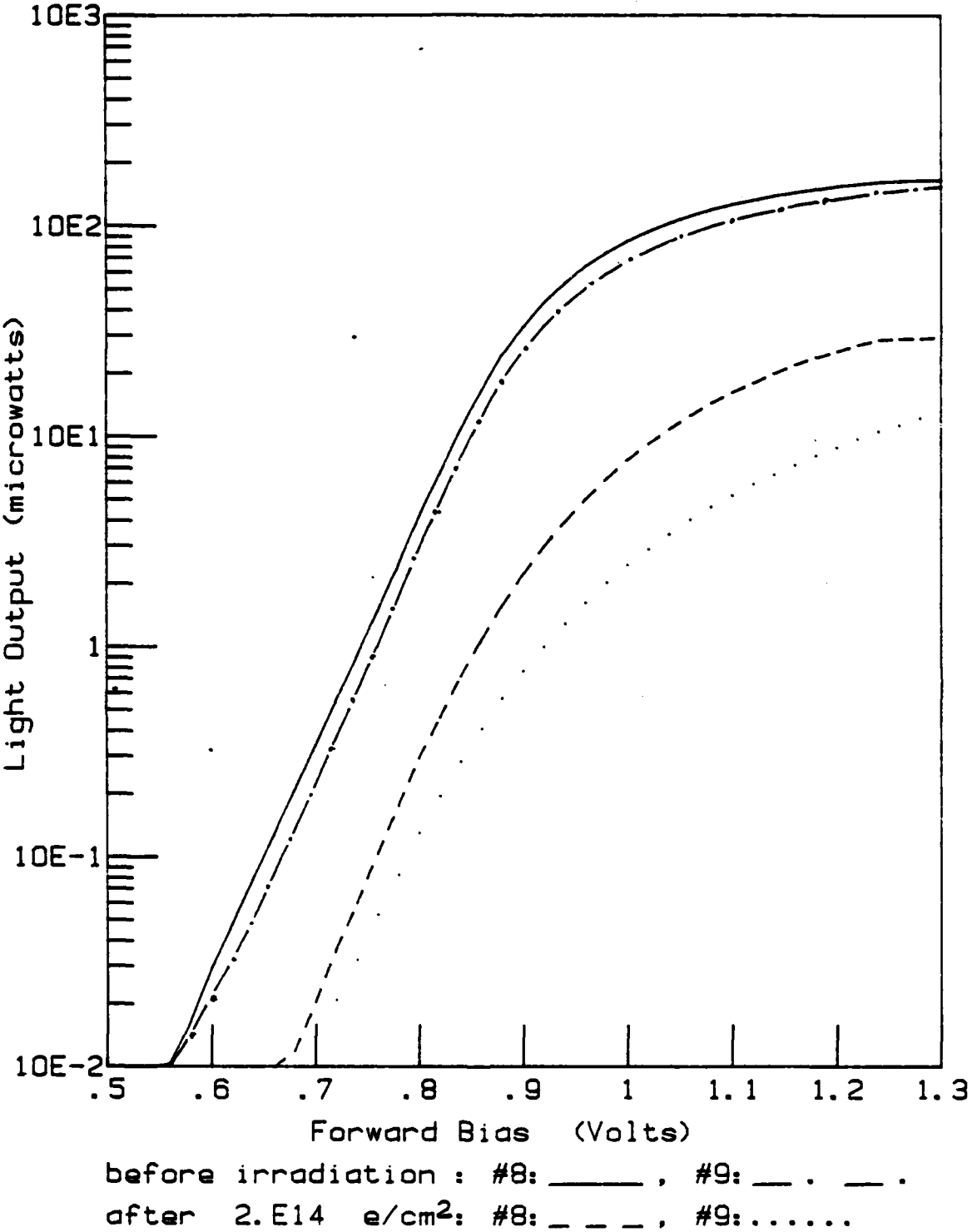

Figure 43. Radiation Effect on LEDS # 8 & 9 Radiance

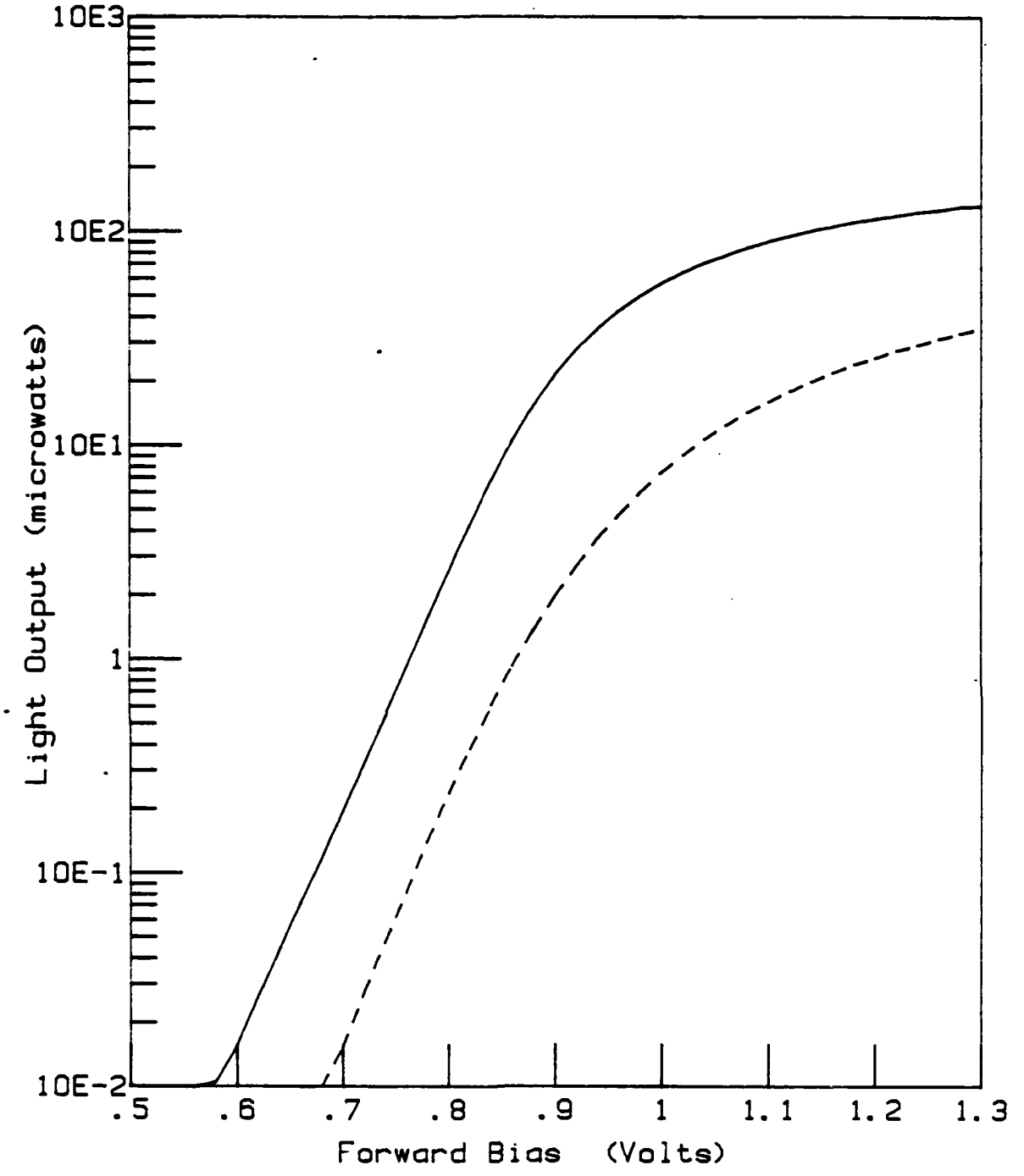

Before: —— and after: - - - irradiation of 2.E14 e/cm^2

Figure 44. Radiation Effect on LED # 10 Radiance

e/cm^2) is shown in Figure 45. (Because of the reduction in light output, the after irradiation curve was amplified to twice the original light intensity in order to determine the shape of the curve.) The region of wavelengths of emitted light did not change. The wavelength of the peak light output intensity of the LED changed from 1310 nanometers before irradiation to 1305 nanometers after irradiation. However, this difference in wavelengths was smaller than the resolution of the monochrometer; therefore, the change in peak wavelength after a fluence of 10^{14} e/cm^2 was not considered significant. Since no measurable change was found the other LEDs were not investigated.

B. RESULTS OF THE InGaAs PHOTODIODE MEASUREMENTS

1. Photodiode Performance During Irradiation

As explained in Chapter two, when a photodiode is operated in the photovoltaic mode with the illuminating flux (Φe) held constant, a reduction in photocurrent (Ip) indicates a reduction in the responsivity (R) of the photodiode. This relationship was expressed in equation 26 (repeated here):

$$R = Ip/\Phi e. \qquad (26)$$

Therefore, by measuring the radiation induced decrease in the photocurrent the radiation induced decrease in the responsivity can be determined.

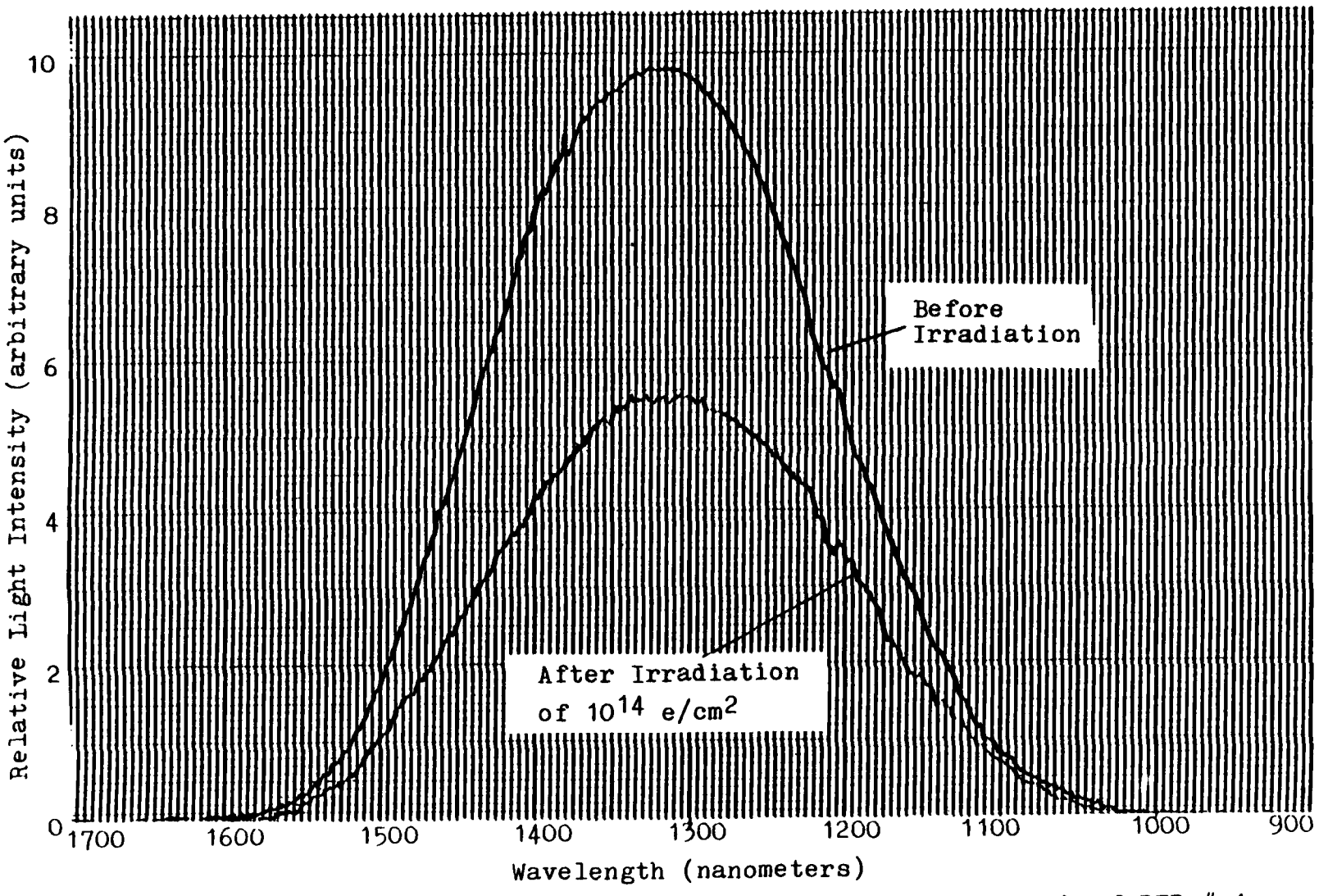

Figure 45. Relative Emitted Light Intensity vs. Wavelength of LED # 4

The plots of the relative decrease in the photocurrent of photodiodes number one, three, seven and nine during irradiation (with no bias applied) is shown in Figure 46. (The dicontinuities in Figure 46 were due to incremental irradiations which are discussed in the next paragraph.) As was found during the LED irradiations, the rate of radiation induced decrease in the device performance depended on the total accumulated fluence. The relative rates of responsivity degradation for each radiation increment of the photodiodes is presented in Table nine. The responsivitity degrades at a substantial rate (up to 44% per 10^{14} e/cm^2) for fluences below $2x10^{14}$ e/cm^2. However, at higher fluences the rate of degradation decreased significantly. Figure 47 indicates that an additional fluence of $4.5x10^{14}$ e/cm^2 was required to reduce the responsivity of photodiode number four by 80%. No photocurrent output was measured after a fluence of $1.5x10^{15}$ e/cm^2.

The irradiations were performed in increments in order to observe any occurance of annealing. The annealing caused the discontinuities in the photocurrent versus fluence curves. Figures 46 and 47 reveal that annealing occurred at fluences of 10^{14} e/cm^2 and greater. Table 10 shows the annealing that was observed. Four minutes elapsed between irradiations. The increase in the amount of annealing at higher fluences might be explained by an increase in the temperature of the photodiode at higher accumulated fluences. The temperature increase of the InGaAs photodiode during iradiations of

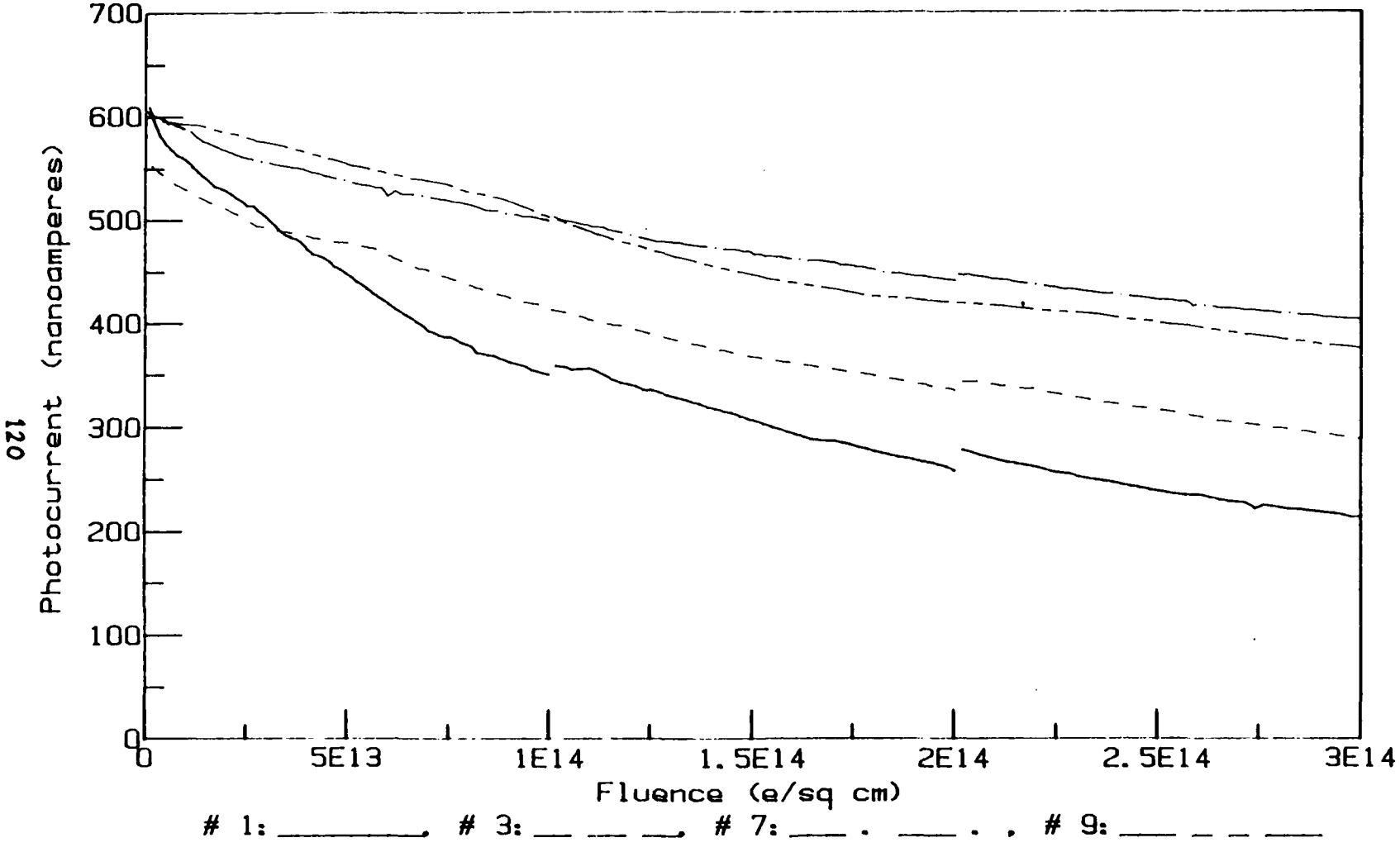

Figure 46. Photocurrent vs. Fluence of Photodiodes # 1, 3, 7 & 9

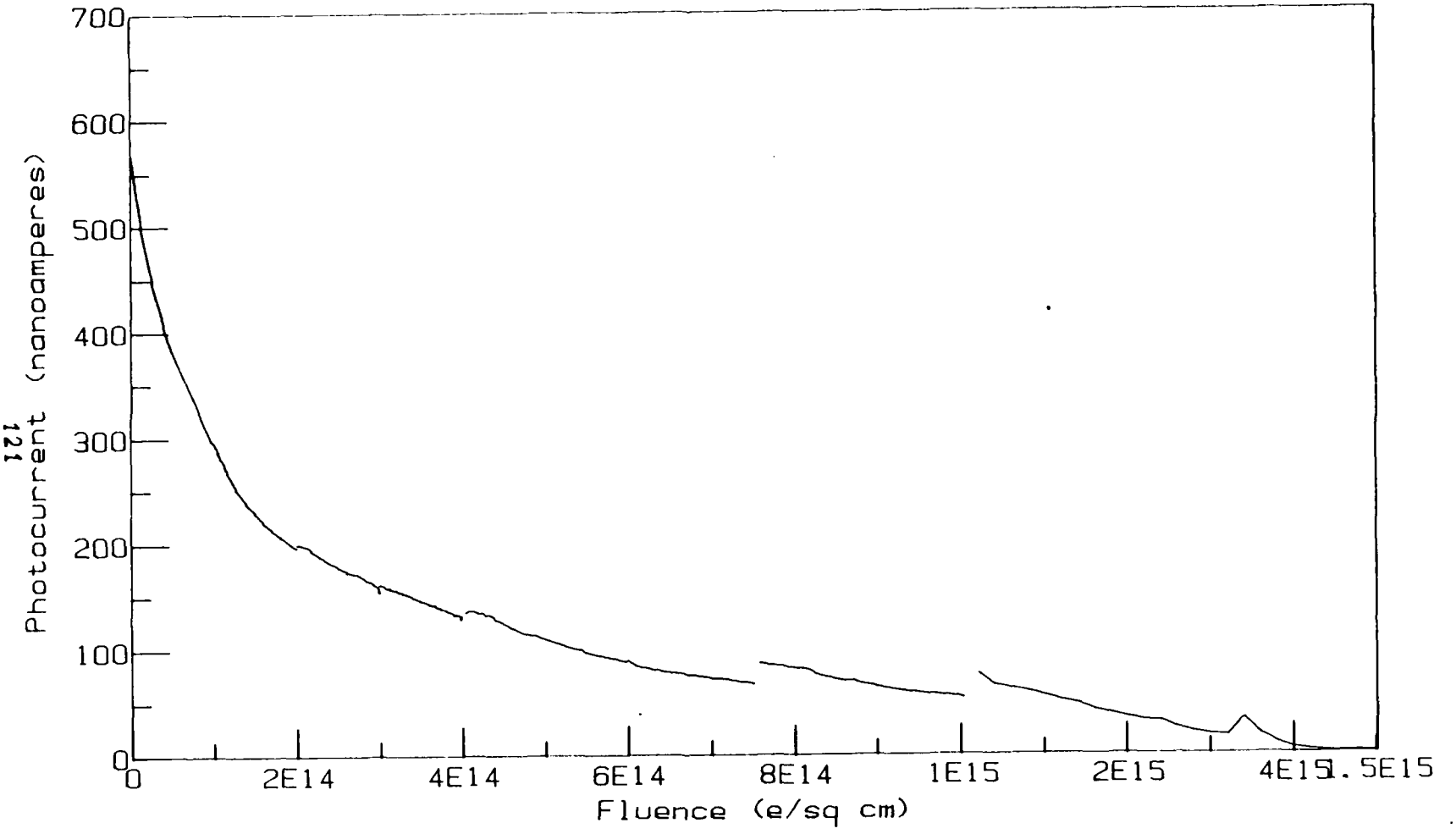

Figure 47. Photocurrent vs. Fluence of Photodiode # 4

TABLE 9. RATE OF RESPONSIVITY DEGRADATION (% per e/cm increment)*

Fluence Increment (10^{14} e/cm^2)	0-1	1-2	2-3	3-4	4-7.5	7.5-10	10-15
Photodiode #							
1	42%	16%	7%				
3	30%	10%	9%				
4	48%	8%	11%	6%	7%	8%	12%
7	16%	12%	7%				
9	15%	14%	10%				

* % of initial value of photocurrent

10^{15} e/cm^2 is shown in Figure 48. The rate of temperature increase of the InGaAs photodiode was much less than the rate of temperature increase of the InGaAsP LED during irradiation. The manufacturer claimed that a 40°K increase in the temperatrure of the photodiode would not significantly affect it's performance. Although the affect of temperature on the photodiode under an applied bias is discussed in the next section, the effect of temperature on the photodiode under no applied bias was not investigated.

TABLE 10. ANNEALING OF PHOTODIODE RESPONSIVITY AFTER IRRADIATION *

Photodiode #	Fluence. (e/cm^2): 10^{14}	$2x10^{14}$	$3x10^{14}$
1	3.3%	6.5%	8.0%
3	0.9%	3.4%	5.2%
7	0.8%	1.6%	3.2%
8**	1.4%	1.4%	3.0%
9			2.9%
10**			3.0%

* four minutes after radiation increment (% of initial responsivity)

** indicates irradiation in darkened target chamber

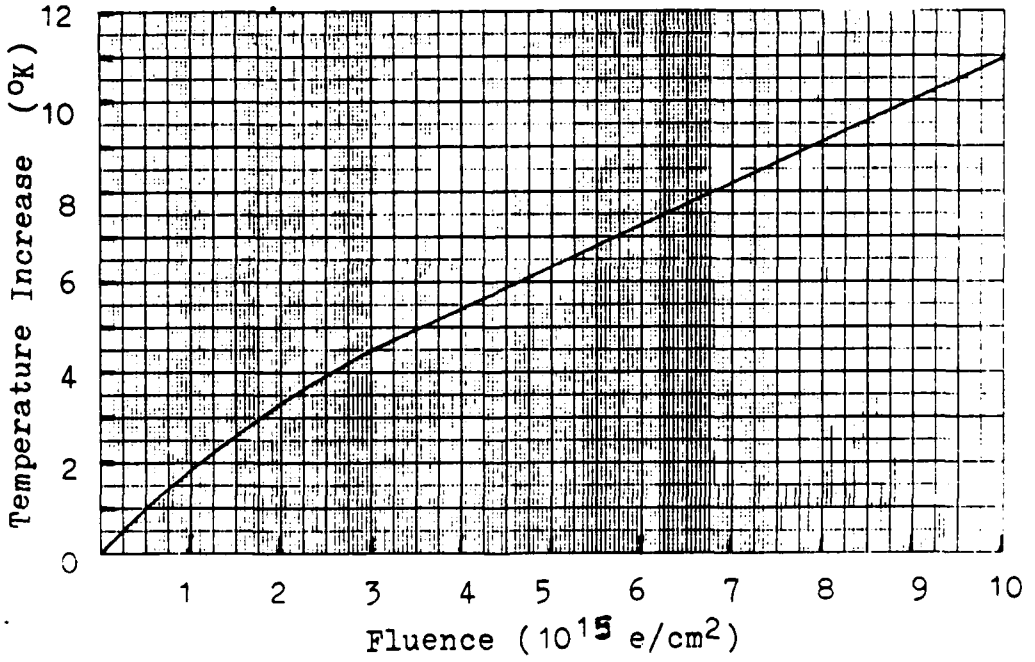

Figure 48. Temperature of Photodiode # 3 During Irradiation

2. Photodiode Performance Before and After Irradiation

a. Radiation Effects on the Total Photodiode Current

The current versus bias curves of photodiodes number seven through ten, before and after irradiation of $3x10^{14} e/cm^2$, are shown in Figures 49 through 51. Photodiodes number seven and nine were irradiated while being illuminated with an infrared light source as described in Chapter three. Photodiodes number eight and ten were irradiated in a completely darkened target chamber. The affect of illumination on the total current versus bias curves is shown in Figure 49. Table 11 presents the decreases in photocurrent at 1.3 volts bias.

TABLE 11. BEFORE AND AFTER IRRADIATION PHOTODIODE PERFORMANCE RESULTS

Photodiode :	1	4	7	8**	9	10**
% Decrease in Photocurrent*	64%	62%	34%	58%	37%	67%

* after $3x10^{14} e/cm^2$ at 1.3 volts bias

** indicates that irradiation was done in a darkened target chamber

As mentioned in the previous section, the temperature of the photodiodes increased during irradiations (see Figure 48). The effect of temperature on the total preirradiation current of photodiodes number seven and eight is shown in Figures 52 and 53. After cooling to their original temperatures, no significant change in the current versus bias curves of the photodiodes was measured.

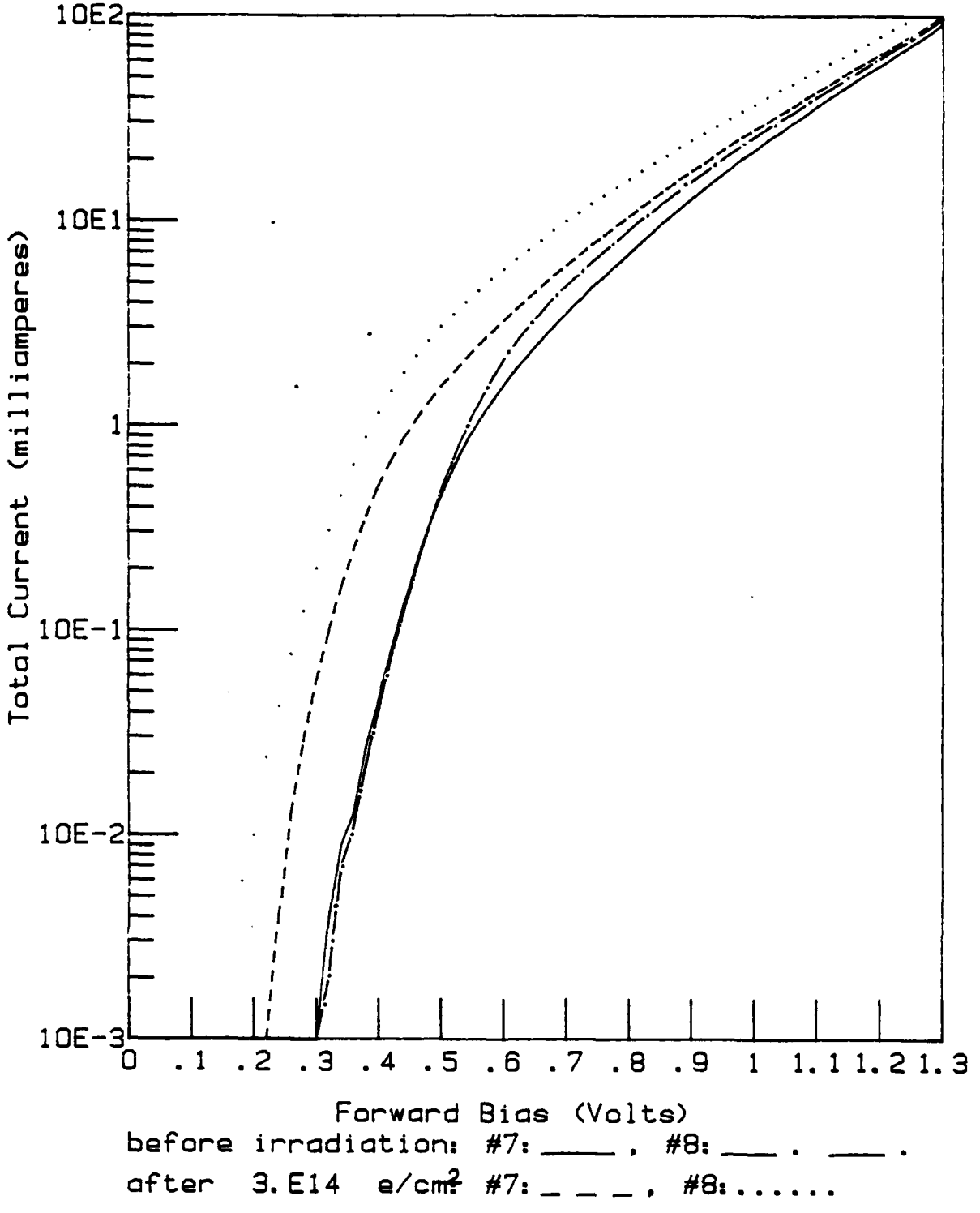

Figure 50. Radiation Effect on Photodectors #7 & #8

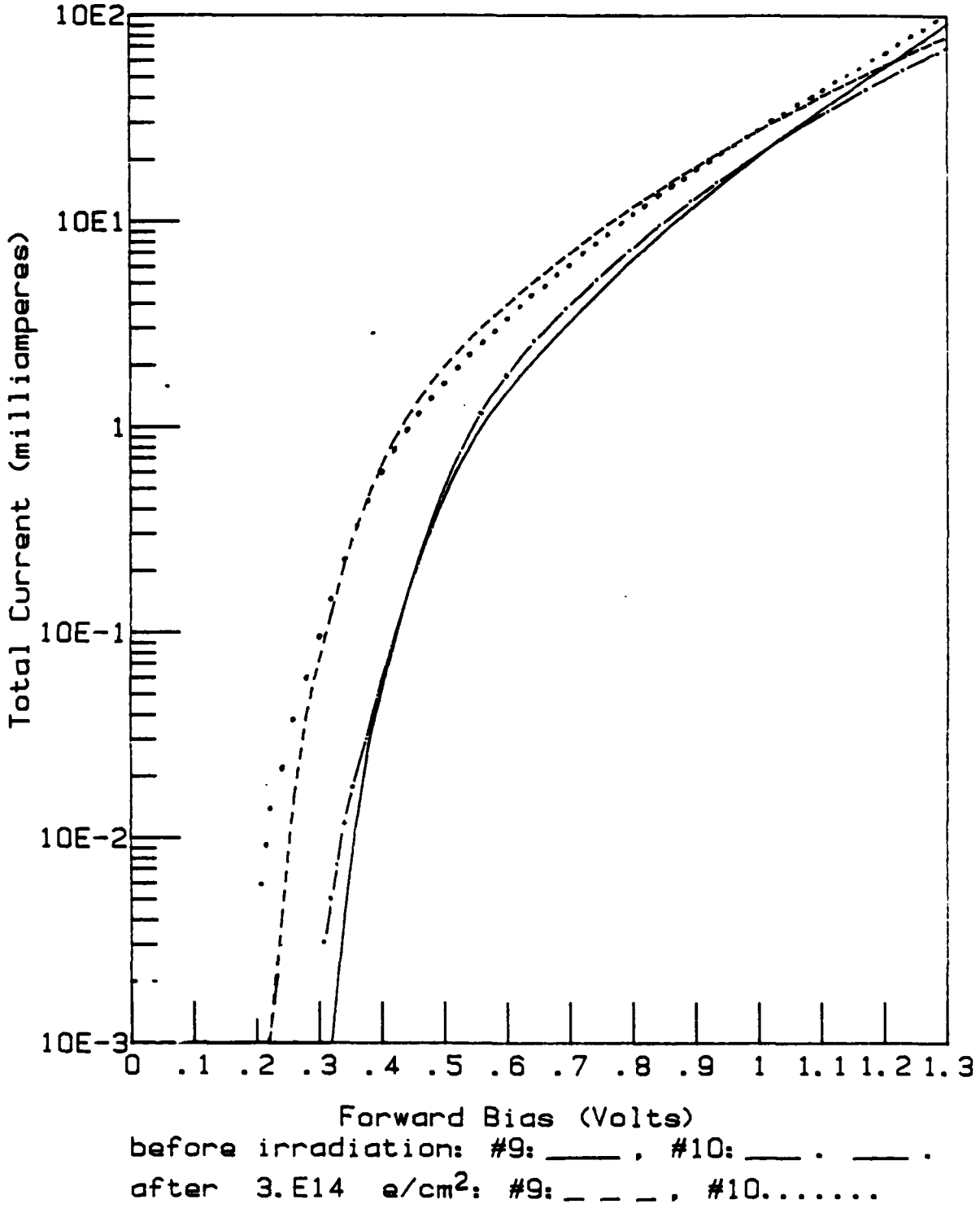

Figure 51. Radiation Effect on Photodectors #9 & #10

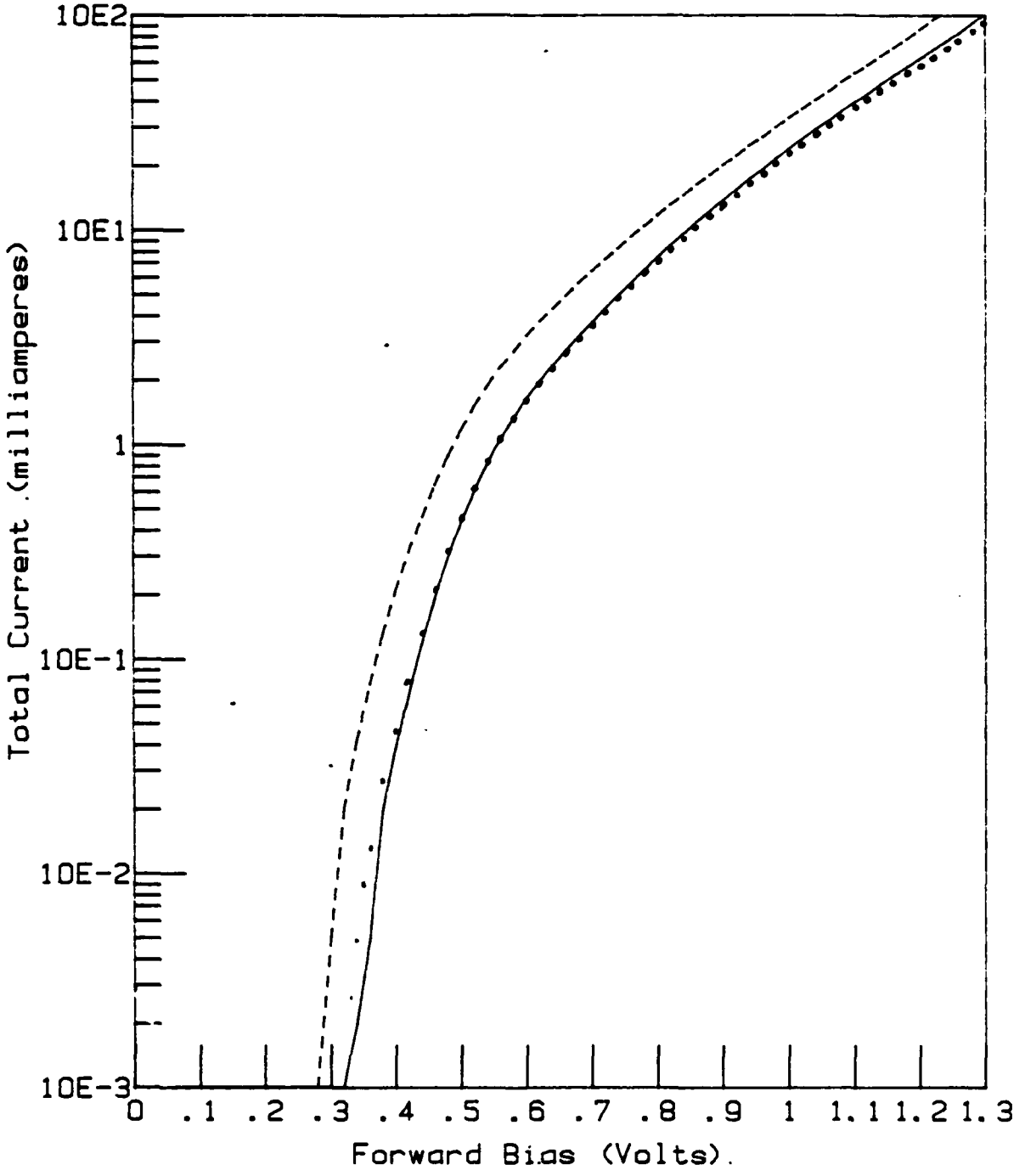

Figure 52. Temperature Effect on Photodiode # 7.

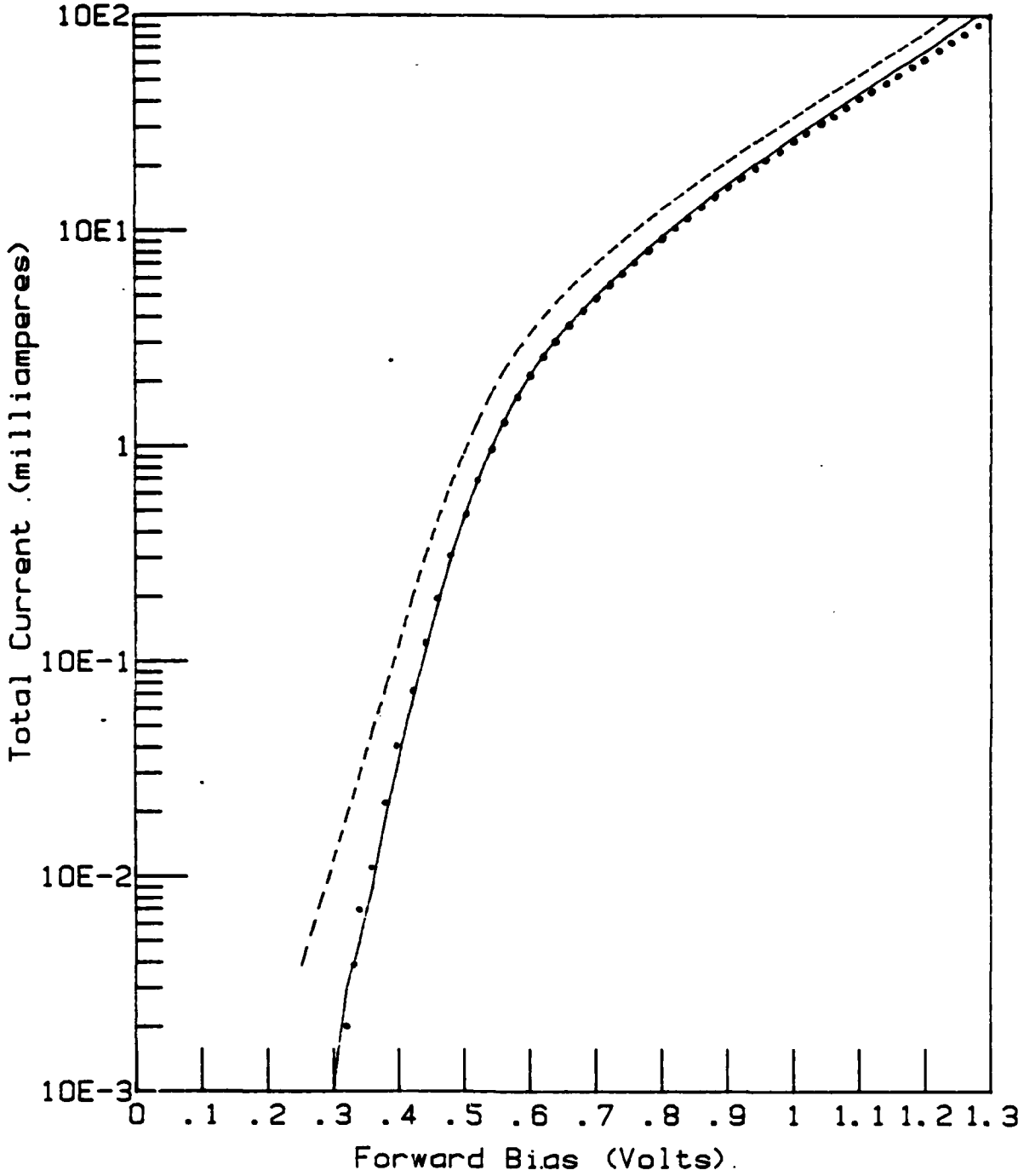

298°K: ____ 326°K: _ _ _

298°K :..... (after cooling)

Figure 53. Temperature Effect on Photodiode # 8.

b. Radiation Effects on Dark Current

The results of the dark current measurements before and after irradiation are presented in Table 12. The total fluence and the illumination condition of each irradiation are noted. Due to the nonuniformity of the original values of the dark current, the percent increase of the dark current varied greatly.

TABLE 12. INCREASE IN PHOTODIODE DARK CURRENT AFTER IRRADIATION

Photodiode Number	Original Dark Current	After Irradiation	Total Fluence	Percent Increase
7	4.9 pa	420 pa	$3x10^{14}$ e/cm2	8,400%
8*	10.2 pa	1.73 na	$3x10^{14}$ e/cm^2	17,000%
9	6.6 pa	610 pa	$3x10^{14}$ e/cm^2	9,200%
10*	5.5 pa	660 pa	$3x10^{14}$ e/cm^2	12,000%

* indicates irradiation in darkened target chamber

c. Radiation Effects on the Wavelength of the Peak Responsivity

The before and after irradiation photocurrent versus wavelength curves of photodiodes number one and two are shown in Figures 54 and 55. Both photodiodes were irradiated to 10^{14} e/cm^2. The periodic discontinuities in all of the curves was caused by a worn drive gear in the monochronometer used in these measurements (see Chapter three). In order to properly interpret these curves the lower side of each of these discontinuities must be ignored. These

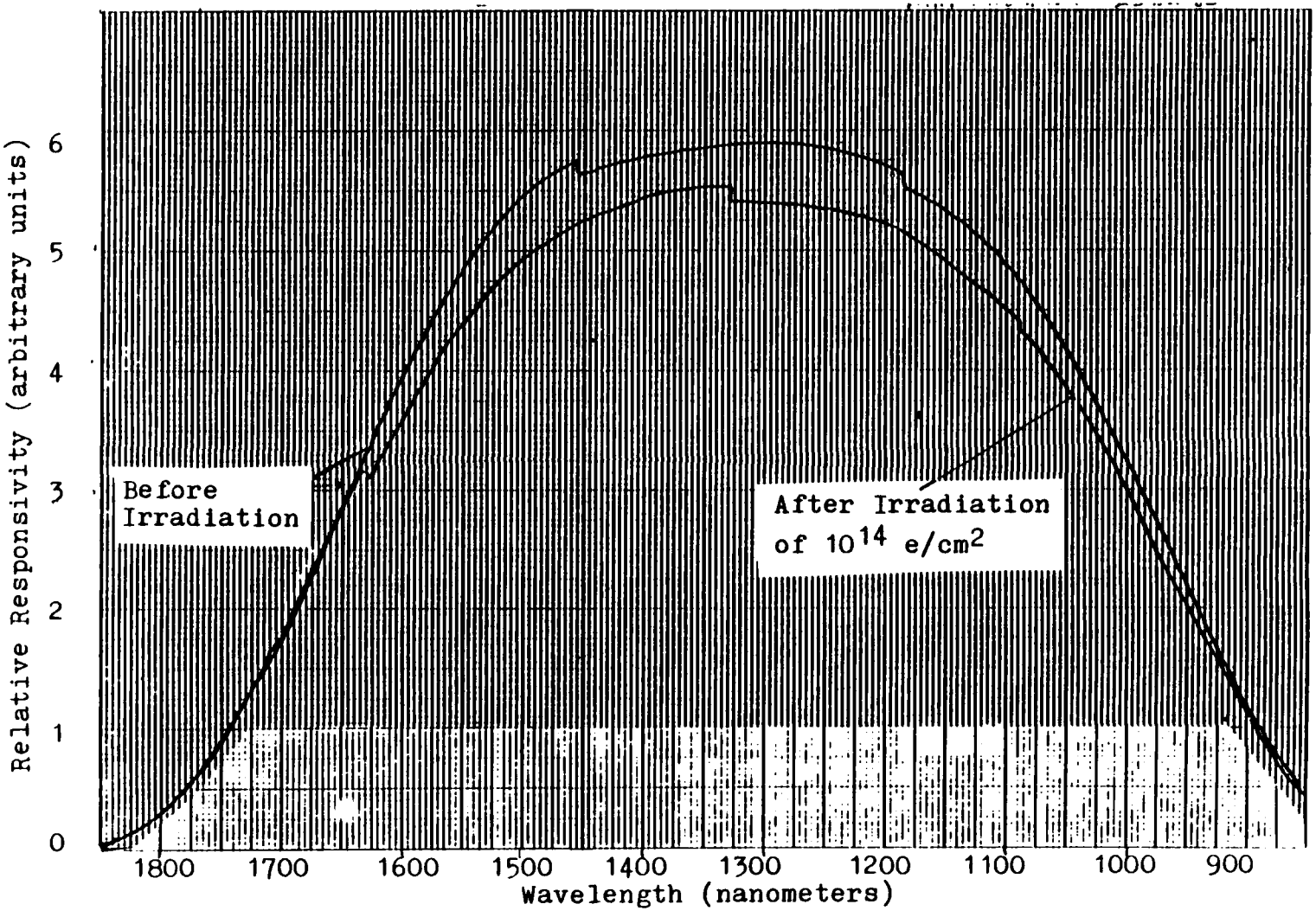

Figure 55. Relative Responsivity vs. Wavelength of Photodiode #2

discontinuities distort portions of the curves, but the overall shape and the peak responsivity wavelength is identifiable. Due to the reduction in the responsivity at all wavelengths after irradiation, the peak of the responsivity curves were less pronounced. Therefore, the after irradiation curves were amplified to twice their initial photocurrent in order to identify the peak responsivity wavelengths.

As indicated in Figures 54 and 55, the photodiodes responded to light of wavelengths between 800 and 1850 nanometers before and after radiation. The maximum responsivity of photodiodes number one and two was 1340 and 1330 nanometers respectively (both before and after irradiation). It is also apparent that the shapes of the responsivity versus wavelength curves did not change after irradiation of $10^{14} e/cm^2$.

V. DISCUSSION

In this chapter, the results of the InGaAsP LED and the InGaAs photodiode performance measurements before, during and after irradiation are compared to theory and previous research. First, the radiation hardness of the InGaAsP LED is discussed. The InGaAsP LED lifetime-damage constant product calculations and a discussion of their validity are included. Next, the radiation hardness of the InGaAs photodiode is discussed. Finally, the relative radiation hardness of the LEDs and photodiodes is compared. A discussion of the radiation hardness of an optoelectronic system comprised of these devices is included in this final section.

A. *THE RADIATION HARDNESS OF THE InGaAsP LED*

1. Comparison of Experimental Results with Theory and Previous Research

Comparison of the experimental results of this thesis with previous research is difficult since no results of electron irradiation of InGaAsP LEDs have been previously reported. Therefore, the results will be compared with, and the theory drawn from, the closest related experiments (electron irradiations of other materials or other types of irradiations of InGaAsP LEDs). As mentioned in Chapter one, Stanley [Ref.13] performed 2 Mev electron irradiations on LEDs and Barnes [Ref.2 and 17] performed neutron and 16 Mev proton

irradiations on two different InGaAsP LEDs (which emitted light of 1.27 um and 1.3 um). Ness [Ref.19] irradiated GaAs, GaP and GaAsP LEDs with 30 Mev electrons and Foley [Ref.20] irradiated GaAsP LEDs with 30 Mev electrons.

a. During Irradiation Performance Measurements

Figures 25 and 26 and Table six revealed that effects of 30 Mev electron radiation are greatest during the initial fluence of $2x10^{13}e/cm^2$. Glasstone [ref.11] states that the rate of annealing increases as the fluence increases (due to the greater temperature at the higher fluences). Therefore, the increased annealing reduces the rate of performance degradation at higher fluences. Stanley [Ref.13] and Barnes [Ref.17] also found that the temperature increased and the light output decreased during irradiation. However, after a fluence of $10^{13}p/cm^2$, Barnes found the InGsAsP LEDs emitted less than 90% of their original light while this study showed that after $10^{13}e/cm^2$ the InGaAsP LEDs emitted greater than 55% of their original light. This is consistent with theory since the more massive protons cause more damage (especially displacemant damage) than electrons.

Figure 25 shows that the LEDs' total current increased during irradiation (while under a bias of 1.2 volts). As explained in Chapter two, this is due to the ionization of the lattice atoms and the increase in recombination centers in the bulk regions caused by the displacement of lattice atoms. Since most of the increase in the

total current was a permanent effect, the displacement of lattice atoms was the dominant radiation damage mechanism. The increase in nonradiative recombination centers caused a decrease in the radiative current (thus a decrease in the light output) as shown in Figure 26.

b. Temperature Effects on the InGaAsP LEDs

As predicted in chapter two, Figures 27 through 30 show that increased temperatures increased the total current of the LEDs. At higher biases, where the total current was proportional to exp(qv/kT), the effect of the temperature increase was less than at lower biases, where the total current was proportional to exp(qv/2kT). The nonpermanent effects of temperature are consistent with previous research on InGaAsP LEDs. RCA has operated InGaAsP LEDs at 363°K for greater than 4,000 hours without any light output degradation [Ref.27].

As seen in Figures 32 through 34, for biases less than 0.94 volts the the light output increased with increased temperature. However, for biases greater than 0.94 volts the light output decreased with increased temperature. This indicates that the InGaAsP LEDs are exceedingly resistent to the effects of temperature at a bias of 0.94 volts. A possible explanation is that the increased temperature enhances the radiative recombination in the depletion region and enhances nonradiative recombination in the bulk regions of the LED (since the factors which affect the current controlling mechanisms are

different in the two regions). At biases less than 0.94 volts, the excess radiative current in the depletion region dominates the excess nonradiative current in generated in the bulk regions. At biases greater than 0.94 the nonradiative excess current dominates. Thus, the increased temperature increased the light output at biases below 0.94 volts and decreased the light output at biases greater than 0.94 volts.

c. Annealing

The observance of annealing, as indicated in Table seven, indicates that the displacement damage consisted primarily of Frenkel defects as predicted in Chapter two [Ref.17]. The relatively small mass of the irradiating electrons prohibited the transfer of enough energy to cause cluster defects during collisions with the lattice atoms. The annealing occurred when some of the interstitial atoms were relocated into the vacant lattice sites left by other interstitial atoms. The annealing was small since most of the damage caused by the 30 Mev electrons was ionization damage as indicated in Table three. (The ionization damage anneals too fast to be observed by the equipment used in this investigation.)

d. The Determination of Current Controlling Mechanisms

As mentioned in Chapter two, for forward biases greater than a few kT (where k is Boltzmann's constant and T is the

temperature), the slope of the current versus bias curve is determined by n in equation five (repeated here)

$$I = I_o[\exp(qv/nkT) - 1] \tag{5}$$

or

$$I = C\exp(qv/nkT) \tag{32}$$

where C is a constant. Current controlled by diffusion in the bulk regions is indicated by n=1 and curent controlled by recombination in depletion region is indicated by n=2. Solving equation 32 for n results in :

$$\ln I = \ln C + qv/nkT \tag{33}$$

and

$$\Delta(\ln I) = (q/nkT)\Delta v \tag{34}$$

thus,

$$n = (q/kT)\,\Delta v/\Delta(\ln I) \tag{35}$$

where $\Delta v/\Delta(\ln I)$ is the reciprocal of the slope of Figures 35 through 39. Thus slope (or the n) indicates the dominant current controlling mechanism in an LED.

The linear portion of the curves in Figures 40 through 44 were used in the calculation of n. Since the radiative current versus bias curves are linear over a large region of bias, the radiative current controlling mechanism was considered to be accurately determined. The values of n calculated for the InGaAsP LEDs are shown in Table 13. The average value for n for the LED

radiative current was n=1.54 before irradiation and n=1.41 after irradiation.

TABLE 13. CALCULATION OF n FOR InGaAsP LEDS

LED #	Fluence (e/cm^2)	Total Current n before	Total Current n after	Radiative Current n before	Radiative Current n after
4	10^{14}	3.1	8.3	1.5	1.4
5	10^{14}	3.0	6.8	1.5	1.3
6	10^{14}	3.8	5.2	1.6	1.4
7*	10^{14}	3.5	4.7	1.5	1.3
8	$2x10^{14}$	2.9	6.1	1.6	1.5
9*	$2x10^{14}$	3.3	6.6	1.5	1.7
10	$2x10^{14}$	3.3	6.7	1.5	1.4

* indicates that no bias was applied during irradiation

The shapes of the light output versus bias curves shown in Figures 40 through 44 are similar to the light output versus voltage curves plotted by Barnes [Ref.5 and 17]. The small, radiation induced change of the slope of the curves in Figures 40 through 44 indicates that the irradiation had a small effect on the dominant radiative current controlling mechanism. The large region of constant slope of the after irradiation curves indicate that the radiation damage was uniform over all the biases measured. The bend in these curves at higher biases was due to the ohmic losses of the applied voltages across the bulk regions of the LEDs.

The total current controlling mechanism was determined by a method analogous to the method used to determine the radiative current controlling mechanism. Therefore, linear portions of the current versus voltage curves were required for the determination of the total current controlling mechanism. Figures 35 through 39 show that the total current versus bias curves are not linear over any portion of the plot. This is due to the total current being controlled by a combination of both diffusion and depletion region controlling mechanisms. The straightest portion of the total current versus bias curve of LED number four was between 0.88 and 0.94 volts. Between these data points the value of n changes from n=3.1 before irradiation to n=8.3 after irradiation (see Figure 36). Similarly, the values of n for LED number five changed from n=3.0 to n=5.8 between the 0.86 volt and 0.94 volt data points (see Figure 36). Despite these changes, the values of n indicate that the current controlling mechanism for the total LED current, both before and after irradiation, was dominated by depletion region recombination. (This is discussed futher below.)

Previous research has shown that the radiation induced nonradiative excess current is depletion region recombination controlled [Ref.17]. At large biases, where the depletion region is narrow, the total current is dominated by the diffusion current controlling mechanism in the bulk regions. Therefore, at biases

greater than 1.3 volts, the excess current becomes less significant when compared to the total LED current.

The results of the before and after irradiation total current measurements did not precisely agree with theory. Table 13 indicates that the values of n for the total current controlling mechanism are all much greater than 2.0 (which the theory states is the maximum value for n). Barnes [Ref.5 and 17] and Stanley [Ref.13] also found the values for n to be greater than 2.0. Although this does not agree with theory, they assumed that any value greater than n=1.5 indicates that the current is depletion region controlled. A possible explaination for this inconsistency is that ohmic losses of the applied bias voltage in the bulk regions over all biases reduces the amount of voltage actually applied across the p-n junction below the total amount applied to the LED. Stanley proposed that the nonlinear shape of the curves was also due to the surface effects caused by the oxide layer usually used in the manufacture of III-V compound LEDs [Ref.13]. Muller and Kamins [Ref.23] provide a description of how the surface effects modify the operation of a p-n junction.

In summary, the different shapes of the plots of Figures 25 and 26 indicate that the radiation damage effects on the total LED current and the radiative current (or light output) were independent of each other. This indicates that the curent controlling mchanisms for the total current and the radiative current were different. Table

14 shows that the total current was depletion region recombination controlled (the values of n closer to 2.0) and the radiative current was diffusion controlled (the values of n closer to 1.0). The results of the before and after irradiation current and light output measurements showed that the dominant total and radiative current controlling mechanisms did not change during irradiation. Stanley and Barnes [Ref.13 and 17] also found that the radiative current and the total current were dominated by different types of current controlling mechanisms which did not change during irradiation.

e. Radiation Effects on the Peak Emitted Light Wavelength

Figure 43 shows that the wavelength of the peak intensity of the emitted light did not change during irradiation. This result is consistent with previous research involving various types of radiation [Ref.2, 4, 5, 8, 13 and 17]. This is consistent with radiation damage theory which does not indicate any damage mechanisms that would change the bandgap of a semiconductor.

2. Lifetime-damage Constant Product Calculations

a. Calculated Lifetime-damage Constant Products

In Chapter two, equation 24 expressed the relationship between light output degradation and irradiation fluence (for radiative current that is diffusion controlled before and after irradiation) as

$$L_o/L = t_o/t = 1 + t_oK\Phi \quad . \qquad (24)$$

Solving equation 24 for the lifetime-damage constant product results in

$$t_oK = (L_o/L - 1)/\Phi \qquad (36)$$

[Ref.17]. Table 14 shows the lifetime-damage constant product calculations for the InGaAsP LEDs studied in this thesis. The average lifetime-damage constant product for the InGaAsP LED was $t_oK = 1.5x10^{-14}$ cm^2/e sec (with a standard diviation of $6.2x10^{-15}$ cm^2/e sec).

TABLE 14. InGaAsP LED LIFETIME-DAMAGE CONSTANT PRODUCTS

	t_oK (cm^2/e sec)	
LED#	bias: 7.6 volts	1.2 volts
4	$8.4x10^{-14}$	$1.6x10^{-14}$
5	$7.2x10^{-14}$	$1.7x10^{-14}$
6	$5.7x10^{-14}$	$1.0x10^{-14}$
7	$3.4x10^{-14}$	$7.2x10^{-15}$
8	$6.7x10^{-14}$	$2.5x10^{-14}$
10	$5.1x10^{-14}$	$1.7x10^{-14}$

b. Comparison of the Lifetime-damage Constant Products with Previous Research

As mentioned previously, research on the effects of electron irradiation on InGaAsP LEDs has not been reported in the literature. However, research has been conducted on InGaAsP LEDs that have been exposed to other types of radiation. Table 15 compares the

lifetime-damage constant products calculated by other authors to the average lifetime-damage product constants calculated in this investigation. The reader is reminded that the smaller the lifetime-damage constant product, the greater the immunity of the device to radiation damage.

TABLE 15. LED LIFETIME-DAMAGE PRODUCT CONSTANTS

Authors	Material	Type of Radiation	t_oK	Ref.
Rose, Barnes	InGaAsP (2 types)	16 Mev Protons	3.0×10^{-13} cm^2/p sec	17
			1.5×10^{-13} cm^2/p sec	
Barnes	InGaAsP	10 Kev Neutrons	6.7×10^{-13} cm^2/n sec	2
Stanley	GaAs (expitaxial)	2 Mev electrons	$1\text{-}2 \times 10^{-14}$ cm^2/e sec	13
	GaAs (diffused)		$1.2\text{-}1.5 \times 10^{-14}$ cm^2/e sec	
	GaP		4×10^{-15} cm^2/e sec	
Ness	GaAsP, GaP	30 Mev electrons	$0.6\text{-}9.7 \times 10^{-13}$ cm^2/e sec	19
Foley	GaAsP	30 Mev electrons	$1.4\text{-}2.9 \times 10^{-14}$ cm^2/e sec	20
This work	InGaAsP	30 Mev electrons	1.5×10^{-14} cm^2/e sec	

Although they can only be compared to devices exposed to the same type of radiation, Table 15 indicates that the InGaAsP LED was not significantly harder than other LEDs investigated previously. Stanley [Ref.13] irradiated many LEDs (not shown in Table 15) that had t_oK that were much larger than the t_oK of the InGaAsP LEDs used in

this study. The t_0K of the InGaAsP LED is of the same order of magnitude as the t_0K calculated for GaAsP LEDs [Ref.20]. The next section will explain why the InGaAsP LEDs was considered to have exhibited significant radiation hardness.

c. Discussion of the Validity of the Assumptions Used

The use of lifetime-damage constant products is based on a simplistic model of the effects of radiation on LEDs where the factors listed in Table three of Chapter two are phenomenologically included in the damage constant. Barnes [Ref.2] and Chaffin [Ref.29] present extensive discussions on the falacy of only using the t_0K when determining the radiation hardness of an LED. Therefore, the t_0K for the InGaAsP LEDs must be interpreted cautiously.

In Chapter two the relative ease of manufacturing an inefficient LED with a very low t_0K was discussed. Therefore, it should not be assumed that the other LEDs with which the InGaAsP LED was compared had the same radiant efficiency. The InGaAsP LED studied in this investigation is a strong emitter of infrared light (see the light output versus bias curves in chapter four) with a very small active region ($0.24mm^2$). As defined by Barnes [Ref.2] and by the manufacturer (M/A-COM Laser Diode, Inc.), this LED is a high radiance LED. By utilizing the advantages of III-V compounds, this InGaAsP LED was distinguished from most other LEDs by having both high radiance and good radiation hardness.

The derivation of the equation used to determine the t K of the InGaAsP LED was based on the assumption that the radiative current was diffusion controlled. As explained previously, the radiative current control mechanism for this LED is complex and thus it is very difficult to identify. Futhermore, the disproportionate degradation of total current and light output indicated that they were not controlled by the same mechanism. Therefore, the correct equation to use to identify the dominant current controlling mechanism was very difficult to determine. The equation used must be considered only an approximation.

Although the effect of temperature on the light output intensity was shown not to be significant, the synergistic effects of both temperature and irradiation during irradiations were not measured. If the use of a heat sink of a significant size is allowed in an application of the LEDs, then the assumption that the effect of increased temperature can be ignored may be justified. However, this approach would not be applicable in space where size and weight limitations are substantial.

It is assumed that the t_0Ks reported represent the radiation hardness of LEDs for all biases. However, since the radiation effects were shown to be dependent on bias, the value of t K can vary greatly depending on the bias at which the data was measured. The linear portion of Figures 40 through 44 (which was the criteria previously used to select the bias at which t_0K was calculated) is not

the region of bias at which this LED is typically operated. Therefore, the values of t_0K in Table 14 were given for 7.6 volt and 1.2 volt biases (the typical operating biases for this LED).

B. THE RADIATION HARDNESS OF THE InGaAs PHOTODIODE

Although the during irradiation photocurrent was measured during this investigation, the primary objective of the photodiode performance measurements was to record the permanent effects of electron radiation on the InGaAs photodiodes. As explained in Chapter two the two primary types of permanent radiation damage on photodiodes are a decrease in the responsivity and an increase in the dark current. Unfortunately, no previous research has been reported on the effects of electron radiation on any type of III-V compound photodiodes.

Much research has been previously performed on the ionization effects of gamma and X-rays on photodiodes. Table three showed that much of the effect of electron radiation on the InGaAs photodiodes should have been ionization damage. The ions and excess free electrons created in this process can cause significant disruption of the photocurrent. However, lattice mismatch of the heterojunctions used in the design of the InGaAs photodiodes should have caused internal electric fields which would limit the excess currents. The effects of ionizing radiation were not investigated in this study.

1. Responsivity Degradation

The results of the relative responsivity degradation measurements reveal that the InGaAs photodiode's responsivity degrades less than 1.0% for electron radiation fluences less than 10^{13} e/cm^2. Figures 46 and 47 and Table nine show that greater than 80% of the total loss in responsivity that occured at $3x10^{14}$ e/cm^2 occured before a fluence of $2x10^{14}$ e/cm^2 was accumulated. Although not closely related to electron radiation damage, research has shown that silicon photodiodes show little radiation induced degradation in responsivity for neutron fluences less than 10^{14} n/cm^2 [Ref.7].

The most probable mechanism by which responsivity degrades in a PIN photodiode is a reduction in the carrier lifetimes (due to the radiation induced increase in recombination sites). The optical absorption coefficient of InGaAs decreases as the photon energy of the incident light approaches the bandgap energy [Ref.3]. Therfore, long wavelength photons, such as infrared photons, will penetrate beyond the intrinsic region (into the bulk region). Since the carrier lifetimes have been reduced during irradiation, not as many carriers that were created in the bulk region will drift to the intrinsic region before recombining. Thus the responsivity is reduced.

The responsivity degradation of the InGaAs photodiodes (shown in Figures 46 and 47) was significantly less than the light output degradation of the InGaAsP LED at similar fluences. Although less

significant than for the InGaAsP LEDs, the observed annealing after irradiation of the InGaAs photodiodes (shown in Table 10) is consistent with the Frenkel defects observed in the InGaAsP LEDs.

Although the photovoltaic (no applied bias) photocurrent was the primary interest of this investigation, Table 11 indicates that a significant reduction in the photocurrent also occurred at 1.3 volts bias. The controlling mechanism for the total current of the InGaAs photodiode was calculated by the same method used to calculate the current controling mechanisms in the InGaAsP LEDs. Table 16 shows that the total current control mechanism did not change during irradiation (n=1.0 indicates that the current was controlled by diffusion in the bulk regions and n=2.0 indicates that the current was controlled by recombination in the depletion region).

TABLE 16. CALCULATION OF n FOR THE InGaAs PHOTODIODES

Photodiode #	n Before Irradiation	n After Irradiation
7	1.4	0.8
8	1.5	1.4
9	1.0	0.7
10	1.7	1.5

2. Increase in the Dark Current

Barnes [Ref.2] states that the increase in the dark current is the most important permanent radiation damage effect on PIN

photodiodes. As explained in Capter two, when the dark current increases, the minimum detectible signal of a photodiode also increases. Table 12 shows that the increase in the dark current of the InGaAs photodiodes after a fluence of $3x10^{14} e/cm^2$ was significant. Previous research using different types of radiation has also shown dark currents to increase by over a factor of 100 [Ref.2 and 15].

The results of this investigation show that an electron fluence of $3x10^{14} e/cm^2$ causes an average decrease in responsivity of 50% and an average increase in the dark current of 120 times. These results are consistent with the theory presented in Chapter two. Only the displacement damage in and near the thin depletion region contributes to the decrease in the responsivity. However, the increase in the number of defect sites throughout the volume of the photodiode material contributes to the increase in the dark current. Although the large increase in the dark current at $3x10^{14} e/cm^2$ makes this photodiode appear to be very susceptible to radiation effects, the lack of previous research with electron radiation makes a comparison of this photodiode with other photodiodes difficult. Additionally, the increase in the dark current of the InGaAs photodiode as a function of fluence was not measured.

C. THE RADIATION HARDNESS OF A SYSTEM COMPRISED OF THE InGaAsP LED AND THE InGaAs PHOTODIODE

Adequate radiation hardness can only be defined in terms of the system performance required for a specific application. Although the

lifetime-damage constant product of the InGaAsP LED is not exceptionally small and the dark current of the InGaAs photodiode increased by an average of 120 times at $3x10^{14} e/cm^2$, an optoelectronic system comprised on these LEDs and photodiodes would be very useful for certain applications in an electron radiation environment. Due to the large active regions required for sufficient light absorption, photodiodes are usually the most radiation sensitive component of currently used optoelectronic systems [Ref. 15]. This is especially true for infrared optical communications systems where radiation induced attenuation for 1.3 micrometer wavelength is low for optical fibers.

If a hypothetical optoelectronic system utilized an optical signal junction between the InGaAsP LED and the InGaAs photodiode studied in this investigation, the LED would be the most electron radiation sensitive component. At a fluence of $10^{14} e/cm^2$, the InGaAsP LED displayed a 63% decrease in the intensity of the emitted light while the InGaAs photodiode displayed a 36% decrease in responsivity. Futhermore, the dark current of the InGaAs photodiode is not significant after a fluence of $2x10^{14} e/cm^2$ when compared to the signal current transferred between the LED and photodiode in this system. Before irradiation, the responsitvity of the InGaAs photodiode was 0.6 amperes/watt and the average optical power output of the InGaAsP LEDs at 1.2 volts bias was 137 microwatts. Therefore, using the % performance degradation values given in Tables six and ten, the

transfered signal of this system after a fluence of $2x10^{14}$ e/cm^2 was 2.1 microamperes. Since the average dark current of photodiodes number seven, eight and ten (after an irradiation of $3x10^{14}$e/cm^2) was 56 nanoamperes, the signal to dark current ratio of this system would be greater than 37 to one. (In many optoelectronic applications a signal to noise ratio of greater than 1.0 is acceptible [Ref.25].)

The result that light output intensity of the InGaAsP LED and the responsivity of the InGaAs photodiode degrades at a much lower rate for fluences greater than $2x10^{13}$e/cm^2 is significant. By compensating for the large initial intensity degradation by using LEDs which have twice the light output required for a given application, this system would perform properly for fluences greater than $7.5x10^{13}$e/cm^2. Also, the lack of change in the peak responsivity wavelength of both the photodiode and the LED indicates that this system would be very useful in applications where constant wavelength is important.

The results presented in Chapter four indicate that the manner in which the InGaAsP LED and the InGaAs photodiode are operated has a significant impact on their radiation susceptibility. Table six and eight show that the radiation damage to the LEDs was generally greater when no bias was applied during irradiation. Table 11 shows that the decrease in the photocurrent was greater when the photodiode was irradiated in a completely darkened target chamber. Table 12 shows that when the photodiodes were irradiated in a darkened target chamber, the dark current increased more than 60 times greater than

the dark current increased when the target chamber was illuminated. However, no significant difference in the annealing of the LEDs or the photodiodes was observed. Barnes [Ref.2] provides a detailed discription of the mechanism which reduces the effect of radiation when the target device has a bias applied or is operated during irradiation.

Depending on the application, this optoelectronic system may operate satisfactorily in environments of large electron fluences despite a 50% or larger reduction in device performance. Additionally, requiring that the before irradiation intensity or responsivity of the LED and photodiode be twice as large as actually needed would compensate for the large effect that the initial radiation had on both devices.

VI. CONCLUSIONS AND RECOMMENDATIONS FOR FUTURE WORK

A. CONCLUSIONS

When exposed to 30 Mev irradiations of $10^{14} e/cm^2$ the light output of the InGaAsP LEDs deteriorated by an average of 63%. The total current increased by an average of 8%. During irradiation, most of the effects of electron radiation on the total current and the light output occurred at fluences less than $2x10^{13} e/cm^2$. The effect of temperature on the total current output was determined not to be significant in this investigation. The wavelength of the peak intensity of emitted light, 1310 nanometers, did not change during irradiation. The effect of irradiation fluences up to $10^{15} e/cm^2$ did not affect the transmission of infrared light through the glass caps that covered the LEDs and photodiodes used in this investigation. An average annealing of 14% of the change in the light output and an average annealing of 13% of the change in the total current output indicated that the dominant permanent radiation damage was Frenkel defect sites in the crystal lattice of the LED.

The average lifetime-damage constant product of $t_o K = 1.5x10^{-14}$ $cm^2/e\text{-sec}$ was calculated for the InGaAsP LEDs studied in this investigation. This $t_o K$ is the same order of magnitude as $t_o K$ exhibited by LEDs manufactured from GaAsP and other III-V compounds in previous research. However, the reliability of these lifetime-damage

constant products is dependent on the appropriateness of the assumptions inherent in the use of radiation damage constants. Difficulty in determining the dominant total current controlling mechanism was a major problem in calculating the $t_o K$ of the InGaAsP LEDs. When the high initial radiance of the InGaAsP LED is compared to the less efficient LEDs that have a $t_o K$ indicating superior radiation hardness, the InGaAsP LED could be the most appropriate LED for certain applications in electron radiation environments.

The responsivity of the InGaAs photodiode exhibited less sensitivity to electron radiation than the light output of the InGaAsP LED. Little degradation of responsivity was recorded for fluences below 10^{12} e/cm^2. An average reduction in responsivity of 42% was recorded for fluences of 10^{14} e/cm^2. Complete responsivity degradation occurred at 1.5×10^{15} e/cm^2. Most of the effects of irradiation occurred at fluences between 10^{13} and 2×10^{14} e/cm^2. Additionally, the wavelengths of the region of peak responsivity, between 1330 and 1340 nanometers, did not change after being irradiated with a fluence of 10^{14} e/cm^2.

The increase in the dark current of the InGaAs photodiodes during irradiation was significant. The dark current increased by more than 84 times after an electron fluence of 3×10^{14} e/cm^2. However, when irradiated in a darkened target chamber, the dark current increased by more than 140 times at 3×10^{14} e/cm^2. The increase in the dark current

was the most sensitive parameter of either the InGaAsP LED or the InGaAs photodiode.

The difficulty in determining the exact position of the target devices within the cross-sectional profile of the LINAC's electron beam was considered the primary source of error in this investigation. Cross-sectional plots of beam intensity revealed that the fluence of electrons was not uniform; therefore, the actual intensity of the radiation received by an LED or photodiode was dependent on the location of the device inside the beam. Improvements in the methods used in determining beam area supported Foley's [Ref.20] suspicions of possible errors of up to 30% in the calculation of fluence at the NPSAL LINAC.

B. RECOMMENDATIONS FOR FUTURE WORK

In order to improve the results of similar investigations in the future, a more accurate method of determining the fluence of an irradiation must be developed. Defocusing the beam would result in the uniform irradiation of a device with a small surface area (and make the exact location of the device in the beam's cross-section less critical). This would also make the random movement of the beam during irradiation a less significant error. However, the sensitivity of the current integrators presently utilized at the NPSAL LINAC cannot detect radiation induced current signals for beams with cross-sectional areas larger than one square centimeter. Additionally, if

the cross hair wires used to profile the beam were moved through the beam at a very slow speed, a better current integration would occur. This would result in a greater resolution of the plot of the electron beam's cross-sectional fluence intensity profile. To achieve this, ladder assemblies with incremental stepping motors and precision gearing of crosshair support arms should be constructed.

Additional insight into the effects of electron radiation on these LEDs and photodiodes could be gained by irradiating the devices at different forward biases and with electrons of different kinetic energies. Improvements in methods used to determine the radiative current controlling mechanisms in InGaAsP LEDs would greatly improve the reliability and use of lifetime-damage constant products. Measurement of the effects of radiation on LEDs and photodiodes operated in an alternating current or alternating signal mode would provide information on the response time, charge storage and noise problems encountered with the exposure of these devices to ionizing radiation. Additionally, the measurement of the dark current of the photodiodes at incremental fluences would allow a more accurate characterization of the radiation hardness of the InGaAs photodiodes. Finally, an infrared illumination source which allowed the wavelength and intensity of the illuminating light to be precisely controlled would allow improved insight into the effects of radiation on photodiodes during electron radiation exposure.

APPENDIX A

MEASUREMENT OF RADIATION EFFECTS ON THE GLASS CAP

LEDs and photodiodes are usually manufactured with a protective glass cap. All the experiments in this thesis were performed using LEDs and photodiodes with their glass caps attached. In order to determine the effect that electron radiation had on the transmission of these glass caps, four Corning 7052 glass caps were irradiated. This glass was utilized in the manufacture of the InGaAsP LED and is widely used as a standard glass cap in the optoelectronics industry. Each cap was 0.1034 inches thick and had an index of refraction of 1.487.

The percentage of light transmitted through the glass was measured before and after each irradiation using an Hitachi 330 spectrophotometer. This spectrophotometer passes light through the glass at continuously increasing wavelengths between 0.9 and 2.0 micrometers. The glass cap had a polarizing effect on the reference beam of the spectrophotometer, therefore, each cap was rotated to a different position in order to identify any dependence of radiation effects on the polarizing angle.

Four glass caps were irradiated at 10^{12}, 10^{13}, 10^{14} and 10^{15} e/cm^2. The results of the before and after irradiation measurements are shown in Figure A-1. The different angles of rotation of the caps in the

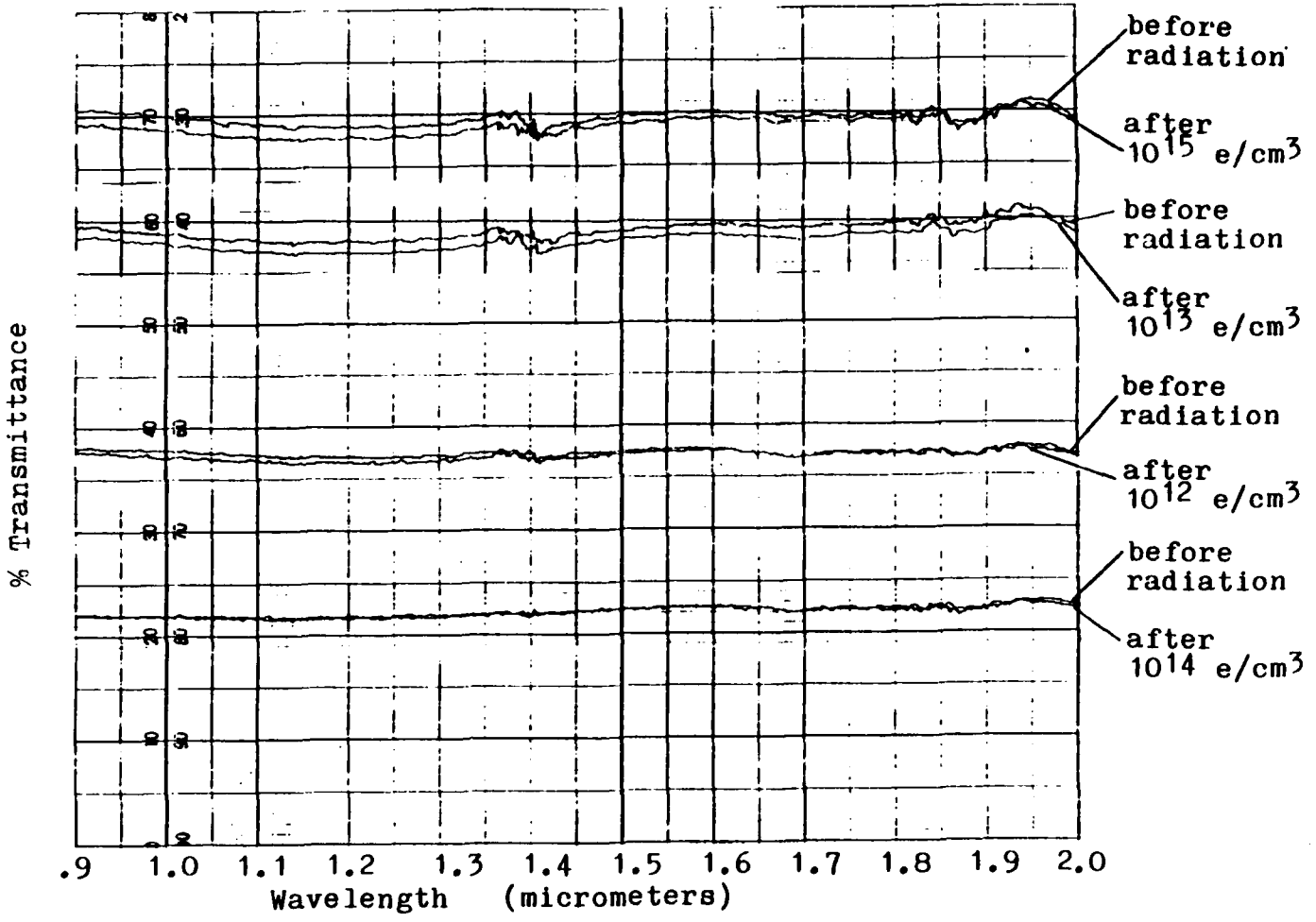

Figure A-1. Glass Cap Transmittance Versus Wavelength

spectrophotometer accounts for their difference in the percentage of transmission. No dependence of the radiation effects on the polarization angle was found. Since the spectrophotometer is 2% accurate in the near infrared wavelength region, it is evident that the radiation effect on the glass is insignificant for fluences up to $10^{15} e/cm^2$. However, the lenses appeared to darken after irradiation of fluences greater than $10^{16} e/cm^2$.

The efecty of radiation on the caps was also investigated by comparing the effects of radiation on two visible LEDs with the glass caps removed to two LEDs with the glass caps still mounted. Hewlett Packard high intensity red LEDs (Part number HPIN6092) were irradiated. Table A-1 shows the results of these measurements.

TABLE A-1: RADIATION EFFECTS ON LED PERFORMANCE

LED Number:	1*	2	3*	4
Fluence (e/cm^2):	10^{12}	10^{12}	10^{14}	10^{14}
Current Output: **				
Before irradiation:	99 ma	98 ma	102 ma	98 ma
After irradiation:	79 ma	81 ma	58 ma	57 ma
% Decrease:	20 %	17 %	43 %	42 %
Light Output: **				
Before irradiation:	48 µw	58 µw	47 µw	58 µw
After irradiation:	8 µw	11 µw	0	0
% Decrease:	83 %	81 %	100 %	100 %
Peak wavelength of emitted light:				
Before irradiation:	640 nm	639 nm	643 nm	638 nm
After irradiation:	640 nm	640 nm	642 nm	638 nm

* Glass cap removed prior to irradiation
** Measured at 2.0 volts forward bias

The current, the light output and the peak intensity wavelength were measured using the procedures described in Chapter three. Since the before irradiation measurements revealed that the LEDs were not identical, only a limited amount of information can be derived from these measaurements. For comparison purposes, the percent change as well as the actual values are listed in Table A-1. It should be noted that the electron beam had to be turned off each time a different LED was placed in front of it. Therefore, the required refocusing of the beam slightly changed the intensity of the beam before and after each irradiation. Due to the small number of LEDs measured and the previously mentioned inaccuracies, the results of the exact effect of the glass cap are inconclusive. However, it should be noted that there was less than a 3% effect on any of the measured parameters. These effects are small when compared to the other experimental errors discussed in Appendix B.

APPENDIX B

RESULTS OF MEASURING THE ELECTRON BEAM FLUENCE

The calculation of the electron fluence during irradiations and the nonuniform before irradiation performance characteristics of the devices were the major sources of error in this investigation. This appendix considers the former error. The primary causes of this error were inaccurate measurements of the electron beam's cross-sectional area, the nonuniform distribution of the electron fluence, the noncentered position of the device in the beam, inaccurate current measurements made by the secondary emissions monitor (SEM) and power fluctuations in the circuits of the electron gun and focusing magnets. Each of these topics will be discussed in the order presented above.

The method used to measure the cross-sectional area of the beam was described in section III.E. Several problems existed with this method. The slow speed of the EASYMOVER remote control moving stage allowed the vertical dimension and the vertical fluence distribution to be plotted to one micrometer accuracy (see Figure 18). However, the motor used to move the vertical wire would not move slowly enough for the plotter to plot the current integrator's output data. Therefore, the horizontal fluence distribution had to be manually read from the current meter at one millimeter increments across the beam.

A second problem in calculating the beam area was determining the shape of the cross-sectional area. Since only the vertical and horizontal dimensions of the beam were known, knowledge of the shape of the beam was critical to the accurate calculation of the cross-sectional area. The general shape of the beam was seen on the phosphorous target screen prior to moving a target device in front of the beam. The beam could not be focused into an exact circle, square, or ellipse. Since the area of a circle is 21% smaller than a square whose sides are twice the radius of the circle, it was estimated that a maximum error of 20% in the calculation of the beam's cross-sectional area (due to inaccurate beam shape) was possible. A slight change in the shape of the beam was observed during irradiations of fluences greater than 10^{15} e/cm^2. The need to turn the beam off while the phosphorous screen was replaced by the target device contributed to a slight change in the beam shape. Since replacing the phosphorous screen after irradiation required the beam to be turned off a second time, the exact shape of the beam during irradiation was not known.

After estimating the error in measuring the area of the beam, the effect of this error on the fluence calculation was determined. Equation 43 (repeated here),

$$\Phi = cv/.026qA \qquad (43)$$

shows the dependance of the fluence (Φ) on the area (A). A first order error approximation was made by taking the derivative of this

equation with respect to the area and multiplying the expression by the uncertainty of the area:

$$\Delta\Phi=(.20)cv/.026qA^2 = (.20)\Phi/A. \qquad (60)$$

(Typically, A ranged from 0.25 cm^2 to 0.7 cm^2.)

Next, equation 43 was multiplied by an intensity term to account for the nonuniform distribution of the electron fluence. This analysis is simplified by the assumption that the electron distribution is radially symmetric across the beam's cross-section. Therefore, the intensity term (I(r)) has only radial dependence and Equation 43 becomes:

$$d\Phi(r)=(I(r)/h)cv/.026qA \qquad (61)$$

where h is the relative fluence of electrons when a uniform electron distribution was approximated. To derive I(r), a typical electron distribution curve was selected from 24 plotted curves (see Figure B-1). The area on or under the curve was divided into 1,419 equal squares. The number of vertical squares from the bottom of the figure is the variable z and the number of horizontal squares from the peak of the curve is the variable r. Foley approximated the distribution curve by an inverted parabola. However, Figure B-2 shows that

$$I(r)=I_o\exp(-0.00826r^2), \qquad (62)$$

where I_o is the intensity at the center of the beam, is a more accurate approximation. The 0.00826 was derived from the average radial distance from the center to the e^{-1} points on the original

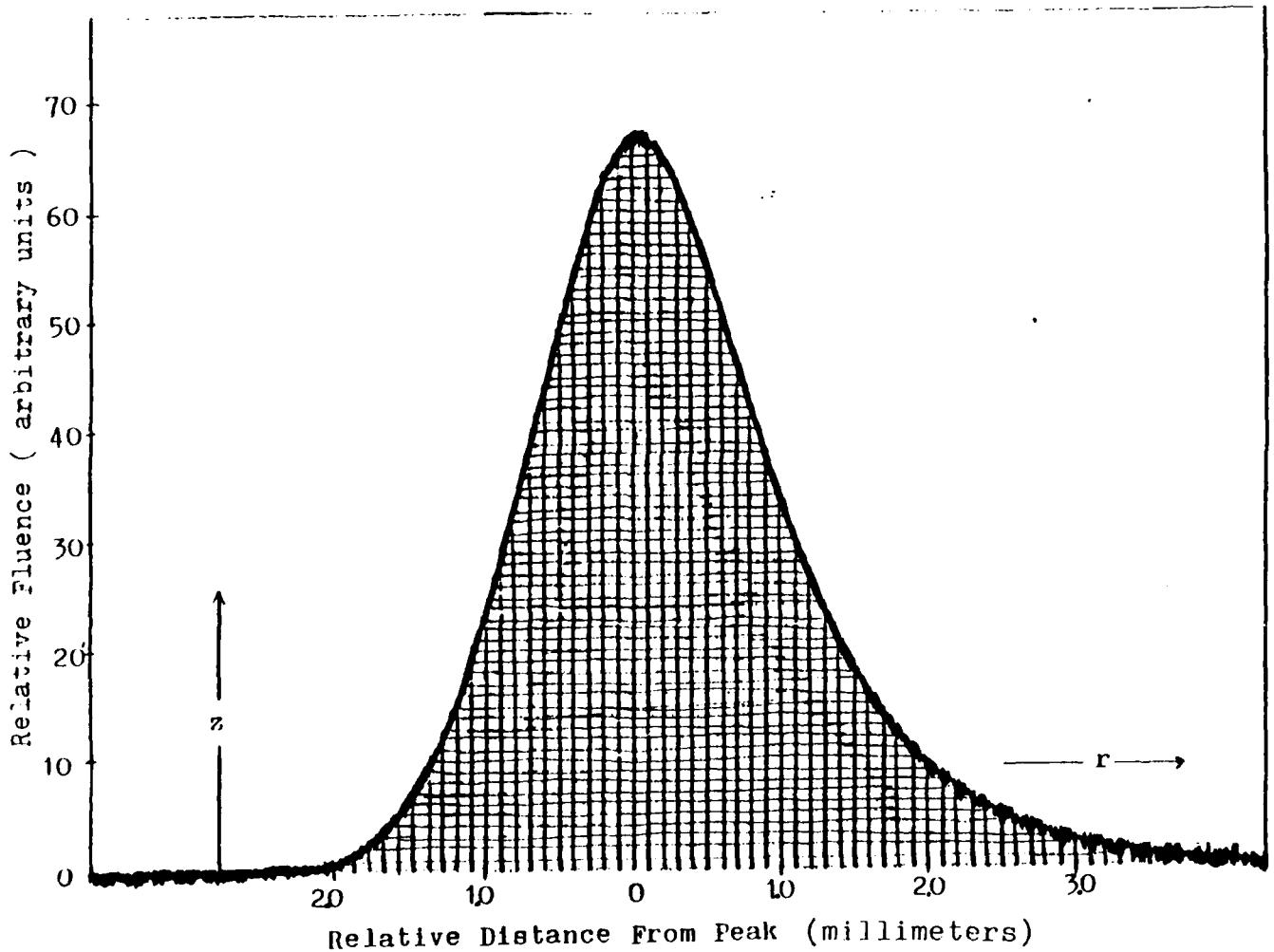

Figure B-1. Typical Electron Fluence Distribution

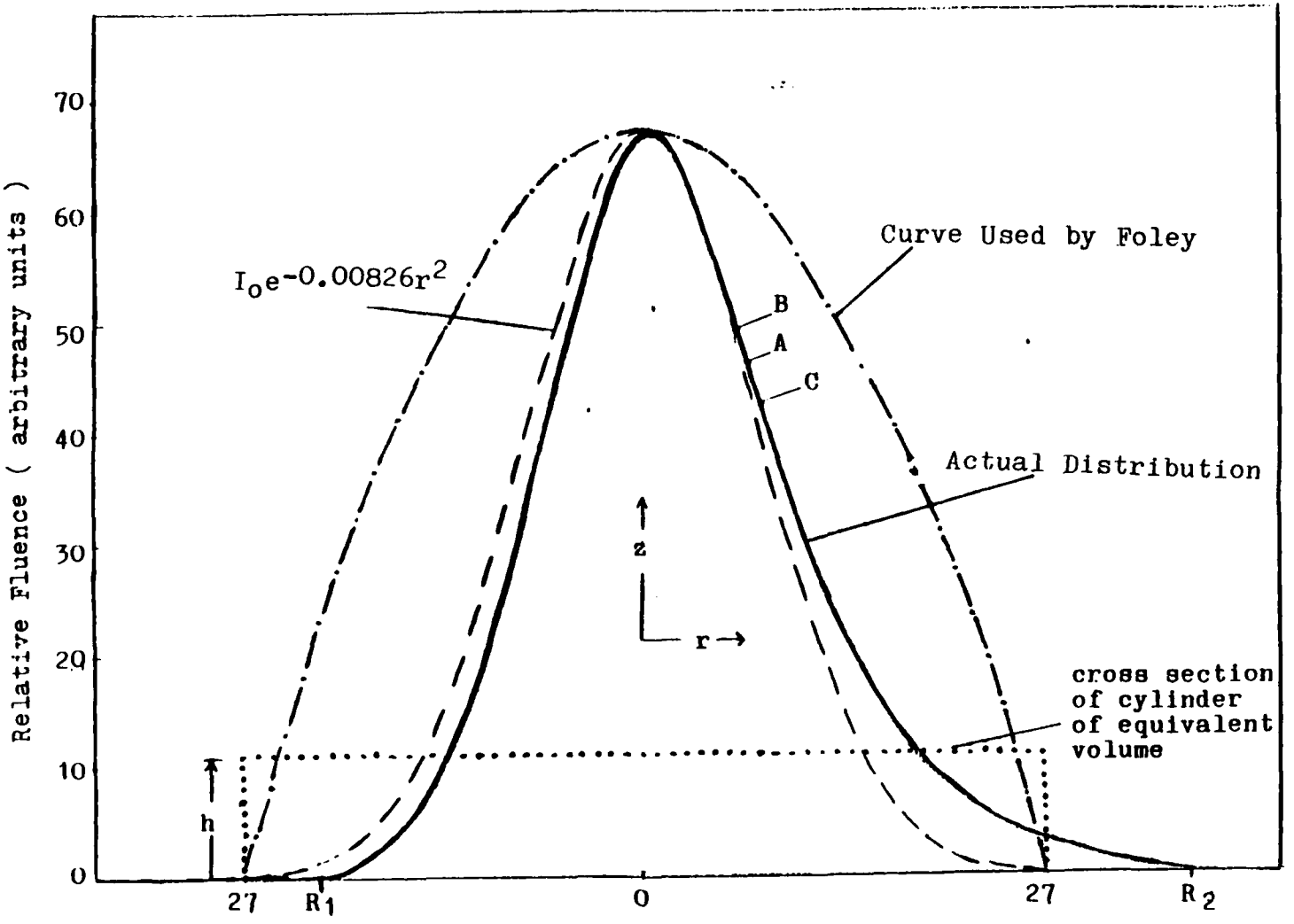

Figure B-2. Approximated Electron Fluence Distribution

curve. Numerical integration of this function revealed that it represents 97.8% of the area under the original distribution curve. Therefore, this function was considered a good approximation of the actual fluence distribution.

A three dimensional electron fluence distribution was derived by calculating the volume (V) under the I(r) curve rotated about it's verticle axis of symmetry. Integrating over cylindrical coordinates results in

$$V=2\pi\int_{o}^{Z_{max}} I(r)rdr \qquad (63)$$

or

$$V=134\pi\int_{o}^{27} \exp(-.00826r)rdr. \qquad (64)$$

Changing the variable of integration to $u=.00826r^2$ results in

$$V=2.547\times10^{4}\int_{o}^{6.02} \exp(-u)du \qquad (65)$$

$$=2.54\times10^{4} \text{ cubic units.}$$

(Since Figure B-1 was considered a typical electron distribution, the numerical values calculated in this section were considered to be representative of all the irradiations.) The relative fluence of electrons when a uniform distribution was assumed was found by calculating the height (h) of a right circular cylinder with a volume equal to V (see Figure B-2). The value of h was 11.1. By comparing h to the value of I(r) at a specific location, the relative difference between the actual fluence and the fluence of the uniform electron distribution was approximated. At the peak of the electron

distribution, the actual fluence is six times greater than the uniform fluence estimation.

To determine I(r) for a device, the location of the target device inside the electron beam must be known. The device location was determined by observing the uniform phosphorescence of a phosphorous ring painted around the device. This indicated that the target device was at the center of the beam's cross-section. Figure B-2 shows that the actual distribution curve was not symmetric. The center between the edges of the phosphous ring (shown as R_1 and R_2) locates the target device at point A on the actual curve in Figure B-2. The fluence at position A is 4.2 times greater than the uniform fluence estimation. Any beam movement less than 20% of the width of the LED or the photodiode (both devices were encased in a 0.5 cm can) could not be detected. A 20% error in the radial position places the target device at positions B or C where the fluence is 4.7 or 3.5 times greater than the uniform fluence estimation. Therefore, the intensity term of equation 61 was approximated to be $I=4.2 \pm 0.5$ for the irradiations performed in this investigation. The width of the active area of the LED and photodiode was small (17.5 and 10 micrometers respectively) compared to the average width of the electron beam (5 millimeters). Thus, it was assumed that the electron distribution was uniform across the area of the target device.

A fourth source of error in fluence calculations was the inacccuracy of the SEM. When the beam was turned off, the SEM

continued to measure an electron current. This current was termed the "leakage current". The leakage current was only noticeable when fluences of 10^{12} e/cm^2 or less were measured. The source of the leakage current was not de'ermined. However, during fluence measurements, this error was compensated for by subtracting the leakage current from SEM measurements. The leakage current was determined by operating the SEM with the beam off for the same amount of time as the actual irradiation. The current indicated by the SEM was then subtracted from the current measured during the irradiation.

Power fluctuation in the circuits of the electron gun and beam focusing magnets was the fith source of error in measuring fluence. It is essential that six vacuum pumps located in the accelerator sections and the target chamber operate during irradiations. Independent monitors automatically turn each pump on when the vacuum drops below 10^{-5} Torr. Figure B-3 shows the effect of the circuit breaker switching when a pump starts. The discontinuities in the curve of Figure B-3.a shows the decrease in fluence when two small pumps started. These reductions in fluence lasted from one to ten seconds depending on the size of the pumps. Figure B-3.b shows the reduction in fluence when one of the three large pumps started. Figure B-3.c shows reduction in fluence when two small and two large pumps started during a fifteen second interval. The reductions in fluence were not periodic or consistent enough to develop a logical method to account for their effects. Unsuccessful attempts were made

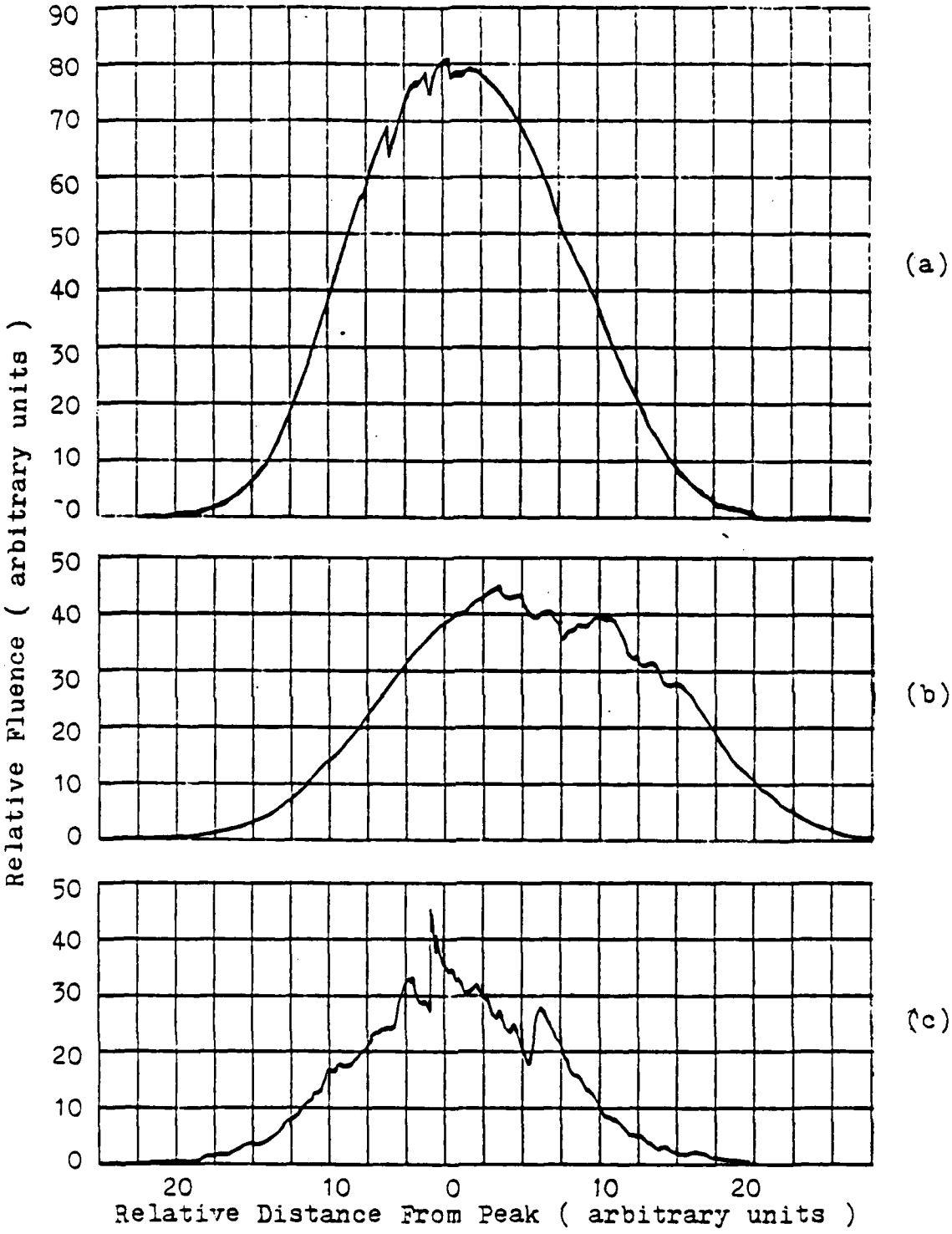

Figure B-3. Deteriorated Electron Fluence Distribution

to perform irradiations between the operating cycles of the large pumps. The longer the irradiation, the less affect the power reductions had on the total fluence. For fluences of 10^{14} e/cm^2 or greater, the pumps were not operating more than 10% of the time of irradiation and were usually on less than 5% of the time of irradiation .

To illustrate the order of magnitude of these errors, the error for a typical fluence measurement is calculated below. The fluence equation when the area and nonuniform distribution errors are considered is

$$\Phi = I(r)cv/.026qA \pm \Delta A I(r)cv/.026qA \pm \Delta I(r)cv/.026qA. \quad (66)$$

For a typical irradiation c=0.1 $\pm$ 0.001 microfarads, v=1.1 volts, $q=1.6\times10^{-19}$ coulombs, A=.27 centimeters and I(r)=4.2 $\pm$ .3. Therefore the fluence was

$$\Phi=4.0\times10^{14} \pm 8.2\times10^{13} \pm 4.9\times10^{13} \text{ e/cm}^2. \quad (67)$$

This value is a good approximation since the leakage current error is negligible and the pumps were usually on less than 5% of the time for fluences of 10^{14} e/cm^2.

APPENDIX C

COMPUTER PROGRAM USED FOR LED CURRENT AND LIGHT OUTPUT VERSUS FORWARD BIAS MEASUREMENTS

The following program measured the LED current and light output while stepping the applied voltage in 0.02 volt increments. The data was then plotted and stored. This program operated the Hewlett Packard HP 86 computer, HP 3478A multimeter, HP-6002A power supply, HP 7090 Plotter, and the Fiberoptics 550 powermeter.

```
10  ! ******************************   MEASURE2I   ******************************
31 OUTPUT 706 USING "#,4A" ; "1002"
20 MASS STORAGE IS ":D701"
30 OUTPUT 705 ;"IN"
40 BEEP
50 DISP "Press continue after conneting LED to power supply."
60 PAUSE
70 PRINTER IS 705
80 DISP "This program measures before and after irradiation light output and"
90 DISP "current versus voltage (from 0.50 to 1.30 v : 0.02v increments) of "
100 DISP "infrared LEDs."
110 DISP "Enter date,LED#" ! format: IR13
120 INPUT DAY,LED$
130 OPTION BASE 1
140 DIM I(41),LT(41),V(41),DB(41) ! I-current,LT-light,V-voltage,DB-lt. reading

150 CLEAR 723
160 OUTPUT 723 ;"F5,Z0,R-1,N5,D1"
170 OUTPUT 705 ;"RO 90"
180 FOR N=1 TO 41 STEP 1 ! Initializes variables
190     I(N)=0
200     LT(N)=0
210     V(N)=0
220     DB(N)=0
230 NEXT N
240 DISP "Enter 1 for before irradiation or 2 for after irradiation"
250 INPUT A
260 IF A=1 THEN 290 ELSE 270
270 DISP "Enter power of fluence."
280 INPUT F
290 IF A=1 THEN LO$="BLT_" ELSE LO$="ALT_"
300 IF A=1 THEN I$="BI_" ELSE I$="AI_"
```

```
310 LNAME$=LOS&LED$
320 INAME$=IS&LED$
330 CREATE LNAME$&":0701",1,8400
340 CREATE INAME$&":0701",1,13400
350 ASSIGN# 1 TO  LNAME$&":0701"
360 ASSIGN# 2 TO  INAME$&":0701"
370 DISP "Measurements will now be taken"
380     BEEP 400,50
390     BEEP
400     DISP "********************  NOTICE  ********************************"
410     DISP "Set light meter to microdecible range."
420     FOR N=1 TO 41
430     V(N)=N/50+.48
440     I=49+N*2
450     Z$=VAL$ (1000+I)
460     OUTPUT 706 USING "#,4A" ; Z$
470     IF N=21 THEN 480 ELSE 510
480     BEEP 400,50
490     DISP "********************  NOTICE  ********************************"
500     DISP "Set light meter range to millidecibels."
510     DISP "Bias is ";V(N);"volts. Enter light output reading ."
520     INPUT DB
530     DB(N)=DB
540     X=DB/10
550     OUTPUT 723 ;"T3"
560     IF N>20 THEN 570 ELSE 590
570     LT(N)=10^X*1000
580     GOTO 600
590     LT(N)=10^X ! LT is in units of microwatts.
600     WAIT 100
610     ENTER 723 ; I(N)
620     NEXT N
630 DISP "Measurements are completed."
640 OUTPUT 706 USING "#,4A" ; "100!"
650 GOSUB Plot_area
660 GOSUB Grid_
670 GOSUB Plot_I
680 GOSUB Plot_areaLT
690 GOSUB Plot_LT
700 DISP "Is data correct? Enter 1 if no, 2 if yes."
710 INPUT D
720 IF D=1 THEN 730 ELSE 740
730 GOSUB Correct
740 GOSUB Annotate
750 CLEAR
760 DISP "Do you want a second copy of the graph? Enter 1-yes, 2-no."
770 INPUT G
780 IF G=1 THEN 790 ELSE 820
790 DISP "Press continue after inserting new paper in plotter."
800 PAUSE
8 0 GOTO 650
820 PRINT# 1 ; LT()
830 PRINT# 1 ; LED$,DAY
840 PRINT# 2 ; I()
850 PRINT# 2 ; LED$,DAY
860 ASSIGN# 1 TO  *
870 ASSIGN# 2 TO  *
```

```
880 PRINTER IS 701
890 OUTPUT 705 ;"SP;"
900 MASS STORAGE IS ":D700"
910 DISP "Light data was stored on ";LNAME$;".DATA3 ,current data was stored"
920 DISP "on ";INAME$;".DATA3."
930 DISP "This program is completed."
940 !
950 END
960 !
970 ! ************************   SUBROUTINES   ******************************

980 Plot_area:
990           OUTPUT 705 ;"IP1670,1450,7100,8300;"
1000          OUTPUT 705 ;"IZ1670,1450,7100,8300;"
1010          RETURN
1020          !
1030 Grid_:
1040          OUTPUT 705 ;"SP6;"
1050          OUTPUT 705 ;"GL8,7;"
1060          OUTPUT 705 ;"DG;"
1070          RETURN
1080          !
1090 Plot_I:
1100          OUTPUT 705 ;"IW1670,1450,7100,8300;"
1110          OUTPUT 705 ;"SC1,41,0,1000;"
1120          OUTPUT 705 ;"SP 3"
1130          FOR N=1 TO 41
1140          IF N=1 THEN OUTPUT 705 ;"PUPA";N;I(N)*5714
1150          OUTPUT 705 ;"PDPA";N;I(N)*5714
1160          NEXT N
1170          OUTPUT 705 ;"SC;IW;"
1180          RETURN
1190          !
1200 Plot_areaLT:
1210          OUTPUT 705 ;"IP1670,1450,7100,8300;"
1220          OUTPUT 705 ;"IZ1670,1450,7100,8300;"
1230          RETURN
1240          !
1250 Plot_LT:
1260          OUTPUT 705 ;"IW1670,1450,7100,8300;SP5"
1270          OUTPUT 705 ;"SC1,41,0,1000;"
1280          FOR N=1 TO 41
1290          IF N=1 THEN OUTPUT 705 ;"PUPA";N;LT(N)*5.71
1300          OUTPUT 705 ;"PDPA";N;LT(N)*5.71
1310          NEXT N
1320          OUTPUT 705 ;"SC;IW;SP"
1330          RETURN
1340          !
1350 Annotate:
1360          OUTPUT 705 ;"IP1670,1450,7100,8300;SP5"
1370          OUTPUT 705 ;"SC0,80,0,175;"
1380          OUTPUT 705 ;"SP5;PUPA0,0;"
1390          OUTPUT 705 ;"LO4;SI.2,.3;"
```

```
1400            FOR X=0 TO 80 STEP 10
1410            Z=X+.01+.5
1420            OUTPUT 705 USING "K" ; "PA";X;",-5.25;LB";Z;CHR$ (3)
1430            NEXT X
1440            OUTPUT 705 ;"PA40,-14;LBForward Bias  (Volts)";CHR$ (3)
1450            FOR Y=0 TO 175 STEP 25
1460            OUTPUT 705 ;"SP5;"
1470            OUTPUT 705 USING "K" ; "PA-3.36,";Y;";LB";Y;CHR$ (3)
1480            NEXT Y
1490            OUTPUT 705 ;"SP5;LO4;PA-8,68;DI0,1;LBMicrowatts";CHR$ (3)
1500            OUTPUT 705 ;"SP3; PA-8,110;LB(Milliamperes)";CHR$ (3)
1510            OUTPUT 705 ;"SP5;LO2;PA2.2,180;SI.2,.3;DI 1,0;LBLight output :___
_";CHR$ (3)
1520            WAIT 100
1530            OUTPUT 705 ;"SP3;PA42.2,180;LBCurrent output :____";CHR$ (3)
1540            WAIT 100
1550            OUTPUT 705 ;"SP5;PA49.1,187;LBDate:";DAY;CHR$ (3)
1560            WAIT 1000
1570            IF A=1 THEN 1610 ELSE 1580
1580            A$="After"
1590            OUTPUT 705 ;"PA2.2,187;LB";A$;" 10E";F;"(e/sq cm)";CHR$ (3)
1600            GOTO 1630
1610            A$="Before"
1620            OUTPUT 705 ;"PA2.2,187;LB";A$;" irradiation of LED";CHR$ (3)
1630            OUTPUT 705 ;"PA-4.8,196;SI.3,.4;LBLED# ";LED$;" LIGHT AND CURRENT
 OUTPUT ";CHR$ (3)
1640            RETURN
1650 Correct:
1660            CLEAR
1670            DISP "Do you want to review the data? 1-yes, 2-no"
1680            INPUT H
1690            IF H=1 THEN 1700 ELSE 1900
1700            DISP "subscript, bias, light data, microwatts, current data"
1710            WAIT 2000
1720            FOR I=1 TO 14
1730            Z=I/50+.48
1740            DISP I;Z;DB(I);LT(I);I(I)
1750            NEXT I
1760            DISP "Press continue when ready."
1770            PAUSE
1780            FOR I=15 TO 30
1790            Z=I/50+.48
1800            DISP I;Z;DB(I);LT(I);I(I)
1810            NEXT I
1820            DISP "Press continue when ready."
1830            PAUSE
1840            FOR I=31 TO 41
1850            Z=I/50+.48
1860            DISP I;Z;DB(I);LT(I);I(I)
1870            NEXT I
1880            DISP "Press continue when ready."
1890            PAUSE
1900             CLEAR
1910            DISP "Enter incorrect subscript."
1920            INPUT N
```

```
1930            I=49+N*2
1940            Z$=VAL$ (1000+I)
1950            OUTPUT 706 USING "#,4A" ; Z$
1960            DISP "Enter 1 if light data is wrong. Enter 2 if current"
1970            DISP "data is wrong."
1980            INPUT E
1990            IF E=1 THEN 2000 ELSE 2150
2000            BEEP 400,50
2010            DISP "********************  NOTICE  *************************"
2020            IF N>20 THEN 2030 ELSE 2050
2030            DISP "Set light meter to millidecibel range."
2040            GOTO 2060
2050            DISP "Set light meter to microdecible range."
2060            V(N)=N/50+.48
2070            DISP "Bias is ";V(N);". Enter correct light output reading."
2080            INPUT LB
2090            V=LB/10
2100            IF N>20 THEN 2110 ELSE 2130
2110            LT(N)=10^V*1000
2120            GOTO 2180
2130             LT(N)=10^V
2140             GOTO 2180
2150             OUTPUT 723 ;"T3"
2160             WAIT 100
2170             ENTER 723 ; I(N)
2180             CLEAR
2190             DISP "Light is ";LT(N);"and current is ";I(N);" for ";V(N);" vol
ts."
2200             DISP "Enter 1 if there is more bad data or if the rest of the da
ta is good enter 2."
2210             INPUT C
2220             IF C=1 THEN 1660 ELSE 2230
2230             CLEAR
2240             DISP "Press continue after inserting new paper in plotter."
2250             PAUSE
2260             GOTO 650
```

APPENDIX D

COMPUTR PROGRAM USED FOR LED CURRENT AND LIGHT OUTPUT VERSUS FLUENCE MEASUREMENTS

This program measured LED current and light output versus time (during irradiations). The data was then stored and plotted on current and light versus fluence graphs. This program operated the Hewlett Packard HP 86 computer, two HP 3478A multimeters, HP 6002A power supply and a HP 7090 plotter.

```
10 ! ************************  MEASURE11  ********************************

20 OUTPUT 706 USING "#,4A" ; "1000"
30 MASS STORAGE IS ":D701"
40 PRINTER IS 705
50 DISP "This program measures light output, current and forward bias versus tim
e"
60 DISP "during irradiation of infrared LEDs."
70 DISP "Enter date,LED#-run#" ! format: IR13-R3
80 INPUT DAY,LED$
90 DISP "Enter SEM capacitance (microfarads), area of beam(sq cm)"
100 INPUT SCAP,AREA
110 DISP "Enter fluence power (e/sq cm), applied forward bias (volts)"
120 INPUT FLU,BIAS
130 OPTION BASE 1
140 DIM CHN1(1000),I(500) ! 1-light,2-current
150 FOR M=1 TO 1000 STEP 1 ! Initializes variables
160    CHN1(M)=0
170 NEXT M
180 FOR N=1 TO 500 STEP 1
190    I(N)=0
200 NEXT N
210 LO$="LT_"
220 I$="I_"
230 LNAME$=LO$&LED$
240 INAME$=I$&LED$
250 CREATE LNAME$&":D701",1,8400
260 CREATE INAME$&":D701",1,7000
270 ASSIGN# 1 TO  LNAME$&":D701"
280 ASSIGN# 2 TO  INAME$&":D701"
```

```
290 OUTPUT 705 ;"IN;IR.1" ! Sets range for channel 1
300 OUTPUT 705 ;"TB100,0;" ! Total time is 100 sec.
310 OUTPUT 705 ;"TM0;" ! Sets trigger mode to manual.
320 CLEAR 723
330 OUTPUT 723 ;"F5,Z0,R-1,N3,D1"
340 A=0
350 DISP "Press continue to turn on LED."
360 PAUSE
370 OUTPUT 706 USING "#,4A" ; "1121"
380 DISP "Press continue to start measurements."
400 DISP "Press continue when measurements are complete."
410 OUTPUT 705 ;"MS1;" ! Sarts buffered recording measurements.
420 ON TIMER# 1,200 GOTO 430
430 OUTPUT 723 ;"T3"
440 A=A+1
450 IF A=501 THEN 490
460 ENTER 723 ; I(A)
470 WAIT 15
480 GOTO 480
490 OFF TIMER# 1
491 OUTPUT 706 USING "#,4A" ; "1000"
500 PAUSE
510 DISP "Enter total time for irradiation ( seconds )"
520 INPUT T
530 WAIT .5
540 GOSUB Data_out
550 PRINT# 1 ; CHN1( )
560 PRINT# 1 ; LED$,DAY,AREA,SCAP,BIAS,FLU,T
570 PRINT# 2 ; I( )
580 PRINT# 2 ; LED$,DAY,AREA,SCAP,BIAS,FLU,T
590 ASSIGN# 1 TO *
600 ASSIGN# 2 TO *
610 GOSUB Plot_area1
620 GOSUB Grid_1
630 GOSUB Plot_1
640 GOSUB Plot_area2
650 GOSUB Grid_2
660 GOSUB Plot_2
670 GOSUB Annotate1
680 GOSUB Annotate2
690 GOSUB Title
700 GOSUB Info
710 OUTPUT 705 ;"SP;"
720 DISP "Do you want another copy? 1-yes ,2-no"
730 INPUT P
740 IF P=1 THEN 750 ELSE 780
750 DISP "Press continue after inserting new plotter paper."
760 PAUSE
770 GOTO 610
780 DISP "This program is completed."
790 PRINTER IS 701
800 END
810 ! ************************   SUBROUTINES   ****************************
820 Data_out:
830           OUTPUT 705 ;"DO1,1000,0,0;"
```

```
840             OUTPUT 705 ;"QI;"
850             DISP "TRANSFERRING DATA"
860             FOR N=1 TO 1000
870             ENTER 705 USING "#,K" ; CHN1(N)
880             NEXT N
890             DISP "DATA TRANSFER  COMPLETE"
900             RETURN
910 Plot_area1:
920             OUTPUT 705 ;"IP1000,1000,9000,3000;"
930             OUTPUT 705 ;"IZ1000,1000,9000,3000;"
940             RETURN
950             !
960 Grid_1:
970             OUTPUT 705 ;"SP5;"
980             OUTPUT 705 ;"GL20,20;"
990             OUTPUT 705 ;"DG;"
1000             RETURN
1010             !
1020 Grid_2:
1030             OUTPUT 705 ;"GL20,20;"
1040             OUTPUT 705 ;"DG;"
1050             RETURN
1060             !
1070 Plot_1:
1080             OUTPUT 705 ;"IW1000,1000,9000,3000;"
1090             OUTPUT 705 ;"SC1,1000,0,1000;SP3;"
1100             FOR N=1 TO 1000
1110             IF N=1 THEN OUTPUT 705 ;"PUPA";N;CHN1(N)*20000
1120             OUTPUT 705 ;"PDPA";N;CHN1(N)*20000
1130             NEXT N
1131             OUTPUT 705 ;"SP5"
1140             RETURN
1150             !
1160 Plot_area2:
1170             OUTPUT 705 ;"IP1000,3250,9000,7250;"
1180             OUTPUT 705 ;"IZ1000,3250,9000,7250;"
1190             RETURN
1200             !
1210 Plot_2:
1220             OUTPUT 705 ;"IW1000,3250,9000,7250;"
1230             OUTPUT 705 ;"SC1,500,0,1000;SP3;"
1240             FOR N=1 TO 500
1250             IF N=1 THEN OUTPUT 705 ;"PUPA";N;I(N)*10000
1260             OUTPUT 705 ;"PDPA";N;I(N)*10000
1270             NEXT N
1280             OUTPUT 705 ;"SC;IW;SP5;"
1290             RETURN
1300             !
1310 Annotate1:
1320             OUTPUT 705 ;"IP1000,1000,9000,3000;"
1330             OUTPUT 705 ;"SC0,100,0,100;"
1340             OUTPUT 705 ;"SP5;PUPA0,0;"
1350             OUTPUT 705 ;"LO4;SI.2,.3;"
1360             FOR X=0 TO 100 STEP 10
```

```
1370            OUTPUT 705 USING "K" ; "PA";X;",-15;LB";X;CHR$ (3)
1380            NEXT X
1390            OUTPUT 705 ;"PA47,-25;LBTime (seconds)";CHR$ (3)
1400            OUTPUT 705 ;"PA0,0;LO18;"
1410            FOR Y=0 TO 100 STEP 10
1420            OUTPUT 705 USING "K" ; "PA-1,";Y;";LB";Y;CHR$ (3)
1430            NEXT Y
1440            OUTPUT 705 ;"LO4;PA-8,50;DI0,1;LBLight output";CHR$ (3)
1450            OUTPUT 705 ;"DI1,0;SC;LO;"
1460            RETURN
1470            !
1480 Annotate2:
1490            OUTPUT 705 ;"IP1000,3250,9000,7250;"
1500            OUTPUT 705 ;"SC0,100,0,100;"
1510            OUTPUT 705 ;"PA0,0;LO18;"
1520            FOR Y=0 TO 100 STEP 10
1530            OUTPUT 705 USING "K" ; "PA-.5,";Y;";LB";Y;CHR$ (3)
1540            NEXT Y
1550            OUTPUT 705 ;"LO4;PA-8,37;DI0,1;LBMilliamperes";CHR$ (3)
1560            OUTPUT 705 ;"DI1,0;SC;LO;"
1570            RETURN
1580 Title:
1590            OUTPUT 705 ;"IP1000,7250,9000,7750;"
1600            OUTPUT 705 ;"SC0,10,0,5;"
1610            OUTPUT 705 ;"PA2,2;LO2;DI1,0;"
1620            OUTPUT 705 ;"LBLIGHT and CURRENT OUTPUT DURING RADIATION";CHR$ (3
)
1630            RETURN
1640 Info:
1650            OUTPUT 705 ;"IP1000,0,9000,1000;"
1660            OUTPUT 705 ;"SC0,20,0,5;"
1670            OUTPUT 705 ;"PA-1,2;LO2;DI1,0;"
1680            OUTPUT 705 ;"LBLED#";LED$;" , Date:";DAY;" , Beam area (sq cm):";
AREA;" , Radiation time (sec):";T;CHR$ (3)
1690            OUTPUT 705 ;"PA-1,1;LBCapacitance (microfarads):";SCAP;" , Bias
(Volts):";BIAS;" , Fluence (e/sq cm): 10E";FLU;CHR$ (3)
1700            RETURN
```

APPENDIX E

COMPUTER PROGRAM USED FOR PHOTODIODE CURRENT VERSUS FORWARD BIAS MEASUREMENTS

This program measured current versus applied bias for the photodiodes. The applied bias was stepped in 0.02 volt increments. This program operated a Hewlett Packard HP 86 computer, a HP 3478A multimeter, and a HP 7090 plotter.

```
10  ! ******************************   MEASURE3I   ***************************
20 MASS STORAGE IS ":D701"
30 OUTPUT 705 ;"IN;RO90;"
40 OUTPUT 706 USING "#,4A" ; "1000"
50 BEEP
60 DISP "Press cont. after conneting detector and insterting plotter paper."
70 PAUSE
80 PRINTER IS 705
90 DISP "This program measures before and after irradiation "
100 DISP "current versus voltage (from 0.00 to 1.30 v : 0.02v increments) of "
110 DISP "infrared photodectors."
120 DISP "Enter date,DET#" ! format: 4-1
130 INPUT DAY,PET$
140 OPTION BASE 1
150 SHORT I(66),V(66),LI(66) ! I-current,V-voltage,LI-log of I
160 CLEAR 723
170 OUTPUT 723 ;"F5,Z0,R-1,N5,D1"
180 OUTPUT 705 ;"RO 90"
190 FOR N=1 TO 66 STEP 1 ! Initializes variables
200     I(N)=0
210     V(N)=0
220 NEXT N
230 DISP "Enter 1 for before irradiation or 2 for after irradiation"
240 INPUT A
250 IF A=1 THEN 280 ELSE 260
260 DISP "Enter power of fluence."
270 INPUT F
280 IF A=1 THEN I$="BI_" ELSE I$="AI_"
290 DNAME$=I$&PET$
300 CREATE DNAME$&":D701",1,21600
310 ASSIGN# 1 TO  DNAME$&":D701"
320 DISP "Measurements will now be taken"
330      BEEP 400,50
```

```
340      FOR N=1 TO 66
350      V(N)=(N-1)*.02
360      I=(N-1)*2
370      Z$=VAL$ (1000+I)
380      OUTPUT 706 USING "#,4A" ; Z$
390      WAIT 100
400      OUTPUT 723 ;"T3"
410      WAIT 200
420      ENTER 723 ; I(N)
430      NEXT N
440 DISP "Measurements are completed."
450 OUTPUT 706 USING "#,4A" ; "1000"
460 GOSUB Plot_area
470 GOSUB TICKS
480 GOSUB Plot_I
490 GOSUB Annotate
500 OUTPUT 705 ;"SP;"
510 PRINTER IS 701
520 GOSUB PRINT_
530 PRINT# 1 ; I()
540 PRINT# 1 ; PET$,DAY
550 ASSIGN# 1 TO  *
560 MASS STORAGE IS ":D700"
570 DISP "Current data was stored on ";ONAME$;".DATA8."
580 BEEP
590 DISP "This program is completed."
600 END
610 !
620 ! ************************  SUBROUTINES  ********************************

630 Plot_area:
640           OUTPUT 705 ;"SP5;IP1670,2550,7100,9400;"
650           OUTPUT 705 ;"IW 900,1750,8000,10900;"
660          OUTPUT 705 ;"SC1,66,0,1000;"
670          OUTPUT 705 ;"PU1,0;PD1,1000,66,1000,66,0,1,0;PU;"
680          RETURN
690          !
700 TICKS:
710          T(1)=.3
720          T(2)=.48
730          T(3)=.6
740          T(4)=.7
750          T(5)=.78
760          T(6)=.85
770          T(7)=.9
780          T(8)=.95
790          OUTPUT 705 ;"SI.2,.3;PA 1,0;LO18;LB10E-3";CHR$ (3)
800          OUTPUT 705 ;"SI.2,.3;PA 1,200;LO18;LB10E-2";CHR$ (3)
810          OUTPUT 705 ;"SI.2,.3;PA 1,400;LO18;LB10E-1";CHR$ (3)
820          OUTPUT 705 ;"SI.2,.3;PA 1,600;LO18;LB1";CHR$ (3)
830          OUTPUT 705 ;"SI.2,.3;PA 1,800;LO18;LB10E1";CHR$ (3)
840          OUTPUT 705 ;"SI.2,.3;PA 1,1000;LO18;LB10E2";CHR$ (3)
850          FOR J=0 TO 4
860          M=J*200
870          P=J+1
```

```
880           N=P*200
890           FOR K=1 TO 8
900           Z=T(K)*200+M
910           OUTPUT 705 USING "K" ; "TL3;PA1,";Z;";YT;"
920           WAIT 50
930           NEXT K
940           OUTPUT 705 USING "K" ; "TL6;PA1,";N;";YT;"
950           WAIT 100
960           NEXT J
970           FOR X=1 TO 66 STEP 5
980           Z=(X-1)*.02
990           OUTPUT 705 USING "K" ; "TL4;PA";X;",0;XT;"
1000           OUTPUT 705 USING "K" ; "LO4;PA";X;",-30;LB";Z;CHR$ (3)
1010           WAIT 50
1020           NEXT X
1030           OUTPUT 705 USING "K" ; "SC;IW"
1040           RETURN
1050 Plot_I:
1060           OUTPUT 705 ;"IP1670,2550,7100,9400;"
1070           OUTPUT 705 ;"IW1670,2550,7100,9400;"
1080           OUTPUT 705 ;"SC1,66,0,1000;"
1090           FOR N=1 TO 66
1100           IF I(N)<.000001 THEN AI=.000001 ELSE AI=I(N)
1110           LI(N)=LGT (AI)+6
1120           IF N=1 THEN OUTPUT 705 ;"PUPA";N;LI(N)*200
1130           OUTPUT 705 ;"PDPA";N;LI(N)*200
1140           NEXT N
1150           OUTPUT 705 ;"SC;IW;"
1160           RETURN
1170           !
1180 Annotate:
1190           OUTPUT 705 ;"IP1670,2550,7100,9400;"
1200           OUTPUT 705 ;"SC1,41,0,1000;"
1210           OUTPUT 705 ;"PUPA0,0;"
1220           OUTPUT 705 ;"LO4;PA20,-80;LBForward Bias (Volts)";CHR$ (3)
1230           OUTPUT 705 ;"DI0,1;PA-3,550;LBmilliamperes";CHR$ (3)
1240           WAIT 100
1250           IF A=1 THEN 1260 ELSE 1280
1260           OUTPUT 705 ;"DI1,0;LO5;SI.17,.27;PA20,-120;LBBefore irradiation ";
CHR$ (3)
1270           GOTO 1290
1280           OUTPUT 705 ;"DI1,0;LO5;SI.17,.27;PA20,-120;LBAfter irradiation of"
;F;"e/sq cm";CHR$ (3)
1290           OUTPUT 705 ;"LO2;PA-3,-160;SI.23,.34;LBDet.# ";PET$;" Current vs.
Voltage Characteristics";CHR$ (3)
1300           RETURN
1310           !
1320 PRINT_:
1330           PRINT DNAME$
1340           PRINT "INDEX,BIAS,        CURRENT (Amperes)"
1350           WAIT 20
1360           FOR N=1 TO 66 STEP 2
1370           PRINT N;V(N),I(N)
1380           WAIT 30
1390           NEXT N
1400           PRINT 66;V(66),I(66)
1410           RETURN
```

APPENDIX F

COMPUTER PROGRAM USED FOR PHOTODIODE CURRENT VERSUS FLUENCE MEASUREMENTS

This program measured photodiode current versus time (during irradiations). The data was then stored and plotted. This program operated a Hewlett Packard HP 86 computer, a HP 3478A multimeter and a HP 7090 plotter.

```
10 ! ************************   MEASURE3   ***********************************
20 MASS STORAGE IS ":D701"
30 PRINTER IS 705
40 OUTPUT 705 ;"IN;RO90;"
50 DISP "This program measures voltage output versus time."
60 DISP "during irradiation of infrared light detectors."
70 DISP "Enter date,DET#-run#" ! format: D13-1
80 INPUT DAY,DT$
90 DISP "Enter SEM capacitance (microfarads), area of beam(sq cm)"
100 INPUT SCAP,AREA
110 DISP "Enter fluence power (e/sq cm)"
120 INPUT FLU
130 OPTION BASE 1
140 DIM V(100)
150 FOR N=1 TO 100 STEP 1
160     V(N)=0
170 NEXT N
180 V$="V_"
190 VNAME$=V$&DT$
200 CREATE VNAME$&":D701",1,1500
210 ASSIGN# 1 TO  VNAME$&":D701"
220 CLEAR 723
230 OUTPUT 723 ;"F1,Z1,R1,N5,D1"
240 A=0
250 DISP "Enter estimated time of irradiation (100 sec. increments)."
260 INPUT L
270 J=CEIL (L*.01) ! The time multiplication factor is J.
280 DISP "Press continue to start measurements."
290 PAUSE
300 ON TIMER# 1,J*1000 GOTO 310
```

```
310 OUTPUT 723 ;"T3"
320 A=A+1
330 IF A=101 THEN 380
340 WAIT 700
350 ENTER 723 ; V(A)
360 WAIT 175
370 GOTO 370
380 OFF TIMER# 1
390 BEEP
400 CLEAR
410 DISP "Measurement is completed."
420 DISP "Enter total time for irradiation ( seconds )"
430 INPUT T
440 WAIT .5
450 PRINT# 1 ; V( )
460 PRINT# 1 ; DT$,DAY,AREA,SCAP,FLU,T
470 ASSIGN# 1 TO  *
480 GOSUB Plot_area1
490 GOSUB Plot_V
500 GOSUB Annotate
510 OUTPUT 705 ;"SP;RO;"
520 DISP "Do you want another copy? 1-yes ,2-no"
530 INPUT P
540 IF P=1 THEN 550 ELSE 580
550 DISP "Press continue after inserting new plotter paper."
560 PAUSE
570 GOTO 480
580 DISP "Voltage data was stored on ";VNAME$;":D701 ."
600 DISP "This program is completed."
610 PRINTER IS 701
620 END
630 ! ************************  SUBROUTINES  ****************************
640 Plot_area1:
650             OUTPUT 705 ;"IP1670,1450,7100,8300;"
660             OUTPUT 705 ;"IZ1670,1450,7100,8300;"
670             OUTPUT 705 ;"SP5;"
680             OUTPUT 705 ;"GL20,24;"
690             OUTPUT 705 ;"DG;"
700             RETURN
710             !
720 Plot_V:
730             OUTPUT 705 ;"IW1670,1450,7100,8300;"
740             OUTPUT 705 ;"SC1,100,0,1000;"
750             FOR N=1 TO 100
760             IF V(N)<0 THEN V(N)=.0001
770             IF N=1 THEN OUTPUT 705 ;"PUPA";N;V(N)*166.67
780             OUTPUT 705 ;"PDPA";N;V(N)*166.67
790             NEXT N
800             OUTPUT 705 ;"IW;"
810             RETURN
820             !
830 Annotate:
840             OUTPUT 705 ;"IP1670,1450,7100,8300;"
850             OUTPUT 705 ;"SC0,100,0,300;"
860             OUTPUT 705 ;"PUPA0,0;LO4;SI.2,.3;"
```

```
870           FOR X=0 TO 100 STEP 10
880           OUTPUT 705 USING "K" ; "PA";X;",-9;LB";X*J;CHR$ (3)
890           NEXT X
900           OUTPUT 705 ;"PA50,-24;LBTime (seconds)";CHR$ (3)
910           FOR Y=0 TO 300 STEP 25
920           OUTPUT 705 USING "K" ; "PA-4.2,";Y;"LB";Y*.02;CHR$ (3)
930           NEXT Y
940           WAIT 100
950           OUTPUT 705 ;"PA-13,150;DI0,1;LBAmplifier Output (volts)";CHR$ (3)
960           WAIT 100
970           OUTPUT 705 ;"LO2,DI1,0;PA2.75,308;LBBeam area:";AREA;"sq cm , Radi
ation time:";T;"sec.";CHR$ (3)
980           WAIT 100
990           OUTPUT 705 ;"PA0,320;LBDate:";DAY;", Cap.:";SCAP;"uf , Fluence:";F
LU;"e/sq cm";CHR$ (3)
1000           WAIT 100
1010           OUTPUT 705 ;"PA-6,335;LBDETECTOR$ ";DT$;" VOLTAGE vs. TIME DURING
 IRRADIATION";CHR$ (3)
1020           RETURN
1030           !
```

LIST OF REFERENCES

1. Bergh, A. A. and Dean, P. J., Light Emitting Diodes, Oxford University Press, 1976.

2. Sandia National Laboratories Report AFWL-TR-83-114, Radiation Effects In Optoelectronic Devices, by C. E. Barnes and J. J. Wiczer, June 1984.

3. Sze, S. M., Physics of Semiconductor Devices, John Wiley & Sons, Inc., 1981.

4. Rudie, N. J., Principals and Techniques of Radiation Hardening, Western Periodicals Company, 1980.

5. Barnes, C. E.,"Radiation Eeffects in 1.06-um InGaAs LED's and Si Photodiodes," J. Applied Phys., v. 50(8), pp. 5242-5250, August 1979.

6. Grover, J. E., Tutorial Short Course at IEEE 1981 Annual Conference on Nuclear and Space Radiation Effects, I-31, 1981.

7. Enge, H., Introduction to Nuclear Physics,Addison-Wesley, Inc., 1966.

8. Aukermana, L., Song, Y., Vernon, F., "Radiation Effects on Semiconductor Optical Devices For Space Communications", Proceedings of the International Society of Optical Engineers Conference, V. 328, pp. 56-65, 1982.

9. Haymes, R. C., Introduction to Space Science, John Wiley & Sons, Inc., 1969.

10. Garrett, H., Pike, C., Space Systems and Their Interactions With The Earth's Space Environment, American Institute of Aeronautics and Astronautics, 1980.

11. Glasstone, S., Dolan, P., The Effects of Nuclear Weapons, United States Department of Defense, 1977.

12. Aukerman, L.W., Millea, M.F., McColl, M., Effects of Radiation Damage On The Behavior of GaAs p-n Junctions,IEEE Trans. Nucl. Sci. , V. NS-13(6) , pp. 174-180, December 1966.

13. Stanley, A.G., "Comparison of Light Emitting Diodes in a Space Radiation Environment, IEEE Trans. Nucl. Sci., Vol. NS-17(3), p. 239, 1970.

14. Mitchell, Kim W., "Optimizing Photodetectors For Radiation Environments", IEEE Trans. Nucl. Sci, V. 24(6), pp. 2294-2297, December 1977.

15. Hardwick, W. H., Kalma, A. H., "Effects of Low-Dose-Rate Radiation on Opto-Electronic Components and the Consequences Upon Fiber Optic Data Link Performance", IEE Trans. Nucl. Sci., V. NS-26(6), pp. 4808-4813, December 1979.

16. Wiczer, J. J., Dawson, L. R., Barnes, C. E., "Transient Effects Of Ionizing Radiation In Photodiodes", IEE Trans. Nucl. Sci., V. N-28(6), pp. 4397-4402, December 1981.

17. Rose, B. H., Barnes, C. E., "Proton Damage Effects On Light Emitting Diodes", J. Appl. Phys., V. 53(3), pp. 1772-1780, March 1982.

18. Wiczer, J. J., Dawson, L. R., Osborn, G. C., and Barnes, C. E., "Permanent Damage Effects In SI And AlGaAs/GaAs Photodiodes", IEEE Trans. Nucl. Sci., V. NS-29(6), pp. 1539-1544, December 1982.

19. Ness, C. Q., Electron Irradiation Of Light Emitting Diodes, Master's Thesis, Naval Postgraduate School, Monterey, California, December 1984.

20. Foley, J. K., 30 Mev Electron Beam Irradiation Effects On GaAsP LEDs, Master's Thesis, Naval Postgraduate School, Monterey, California, June 1985.

21. Campbell, J. C., Fiber and Integrated Optics, V. 5(1), pp. 1-21, 1984.

22. Naval Ocean Systems Center Report ERC41025.15FR, Fiber Optic Light Emitting Diode, by P. D. Dapkus, pp. 1-30, August 1980.

23. Muller, R. S., Kamins, T. I., Device Electronics For Integrated Circuits, John Wiley & Sons, Inc., 1977.

24. Larin, F., Radiation Effects In Semiconductor Devices, John Wiley & Sons, Inc., 1968.

25. Wilson, J., Hawkes, J., Optoelectronics: An Introduction, Prentice-Hall International Inc., 1983.

26. Gage, S., Hodapp M., Evans, D., Sorensen, H., Optoelectronics Applications Manual, McGraw-Hill Book Company, 1977.

27. RCA Laboratories Report RADC-TR-81-199, Fabrication of Hetero-junction LEDs For Operation At 13 Micrometers, by G. H. Olsen et. al, September 1981.

28. Wiczer, J., Banes, C., Dawson, L., "Transient Effects Of Ionizing Radiaation In Si, InGaAsP, GaAL56, and Ge Photodiodes", Proceedings of The Fiber Optics In The Nuclear Environmenet, pp. 209-222, March 1980.

29. Chaffin, R.J., Microwave Semiconductor Devices, John Wiley & Sons, 1973.

30. Private communication and attached advertisements from Stephen Klunk, Product Line Manager, M/A-COM Laser Diode, Inc., September 1985.

31. Barnett, M. T., Cunneen, W. J., Design And Performance Of The Electron Linear Accelerator At The U. S. Naval Postgraduate School, Master's Thesis; Naval Postgraduate School, Monterey, California, May 1966.

32. Private communication with Stanley Gage of Epitaxx, Inc., September 1985.

INITIAL DISTRIBUTION LIST

		No. Copies
1.	Defense Technical Information Center Cameron Station Alexandria, Virginia 22302-6145	2
2.	Library, Code 0142 Naval Postgraduate School Monterey, California 93943-5000	2
3.	Dr. K. C. Dimiduk c/o Mr. & Mrs. Richard Conway 425 Lansing Station Road Lansing, New York 14882	10
4.	Professor K. Woehler, Code 61Wh Department of Physics Naval Postgraduate School Monterey, California 93943-5000	1
5.	CPT P. O'Reilly 29 Kendall Dr. New City, New York 10956	3
6.	Dr. J. Lee Divison 6433 Sandia National Laboratories Albuquerque, New Mexico 87115	1
7.	Andy, Smith, H-23 Naval Surface Weapons Center White Oak Laboratory Silver Spring, Maryland 20903-5000	1
8.	D. Snyder, Code 61 Department of Physics Naval Postgraduate School Monterey, California 93943-5000	2

END

12-86

DTIC